Modeling Coupled THM Processes and Brine Migration in Salt at High Temperatures

Fuel Cycle Research & Development

Prepared for

U.S. Department of Energy
Used Fuel Disposition Campaign

Jonny Rutqvist
Laura Blanco-Martín
Mengsu Hu
Sergi Molins
David Trebotich
Jens Birkholzer

Lawrence Berkeley National Laboratory

September 2016

FCRD-UFD-2016-000439
LBNL-1006308

Revision 2
12/20/2012

APPENDIX E

FCT DOCUMENT COVER SHEET [1]

Name/Title of Deliverable/Milestone/Revision No.	Modeling Coupled THM Processes and Brine Migration in Salt at High Temperatures
Work Package Title and Number	DR Salt R&D - LBNL FT-16LB08030902
Work Package WBS Number	1.02.08.03.09
Responsible Work Package Manager	Jens Birkholzer (signature on file) (Name/Signature)

Date Submitted 9/19/2016

Quality Rigor Level for Deliverable/Milestone[2]	☒ QRL-3	☐ QRL-2	☐ QRL-1 ☐ Nuclear Data	☐ Lab/Participant QA Program (no additional FCT QA requirements)

This deliverable was prepared in accordance with Lawrence Berkeley National Laboratory
(Participant/National Laboratory Name)

QA program which meets the requirements of
☒ DOE Order 414.1 ☐ NQA-1-2000 ☐ Other

This Deliverable was subjected to:

☒ Technical Review ☐ Peer Review

Technical Review (TR)

Review Documentation Provided
- ☐ Signed TR Report or,
- ☐ Signed TR Concurrence Sheet or,
- ☐ Signature of TR Reviewer(s) below

Name and Signature of Reviewers

Kunhwi Kim (signature on file)

Peer Review (PR)

Review Documentation Provided
- ☐ Signed PR Report or,
- ☐ Signed PR Concurrence Sheet or,
- ☐ Signature of PR Reviewer(s) below

NOTE 1: *Appendix E should be filled out and submitted with the deliverable. Or, if the PICS:NE system permits, completely enter all applicable information in the PICS:NE Deliverable Form. The requirement is to ensure that all applicable information is entered either in the PICS:NE system or by using the FCT Document Cover Sheet.*

NOTE 2: *In some cases there may be a milestone where an item is being fabricated, maintenance is being performed on a facility, or a document is being issued through a formal document control process where it specifically calls out a formal review of the document. In these cases, documentation (e.g., inspection report, maintenance request, work planning package documentation or the documented review of the issued document through the document control process) of the completion of the activity along with the Document Cover Sheet is sufficient to demonstrate achieving the milestone. If QRL 1, 2, or 3 is not assigned, then the Lab/Participant QA Program (no additional FCT QA requirements) box must be checked, and the work is understood to be performed, and any deliverable developed, in conformance with the respective National Laboratory/Participant, DOE- or NNSA-approved QA Program.*

Intentionally Left Blank

TABLE OF CONTENTS

Intentionally Left Blank

LIST OF TABLES

Intentionally Left Blank

ACRONYMS

DOE	Department of Energy
DRZ	Disturbed Rock Zone
EDZ	Excavation Damaged Zone
EOS	Equation-of-State
EWASG	Water, Salt, Gas
FEPs	Features, Events and Processes
LANL	Los Alamos National Laboratory
LBNL	Lawrence Berkeley National Laboratory
NCG	Non-condensable Gas
PA	Performance Assessment
R&D	Research & Development
THM	Thermal-Hydrological-Mechanical
THMC	Thermal-Hydrological-Mechanical-Chemical
TM	Thermal-Mechanical
TSDE	Thermal Simulation for Drift Emplacement
TUC	Clausthal University of Technology, Germany
UFD	Used Fuel Disposition
UFDC	Used Fuel Disposition Campaign
WASG	WAter-Salt-Gas
WIPP	Waste Isolation Pilot Plant

1. INTRODUCTION

Within the Natural Barrier System group of the Used Fuel Disposition (UFD) Campaign at Department of Energy's (DOE) Office of Nuclear Energy, Lawrence Berkeley National Laboratory's (LBNL) Salt Research and Development (R&D) activities are focused on understanding and modeling coupled processes and impacts of the Excavation Damaged Zone (EDZ) and high-temperature on parameters and processes relevant to performance of a salt repository, including potential brine migration. These activities address key Features, Events and Processes (FEPs), which have been ranked in importance from medium to high, as listed in Table 7 of the Used Fuel Disposition Campaign Disposal Research and Development Roadmap (FCR&D-USED-2011-000065 REV0) (Nutt 2011). Specifically, they address FEP 2.2.01, Excavation Disturbed Zone, for salt, by investigating how coupled processes affect EDZ evolution; FEP 2.2.05, Flow and Transport Pathways; FEP 2.2.08, Hydrologic Processes; and FEP 2.2.07, Mechanical Processes by studying near-field coupled THM processes in salt repositories. The activities documented in this report also address a number of research topics identified in R&D Plan for Used Fuel Disposition Campaign (UFDC) Natural System Evaluation and Tool Development (Wang 2011), including Topics S3, Disposal system modeling – Natural system; P14, Technical basis for thermal loading limits; and P15 Modeling of disturbed rock zone (DRZ) evolution (salt repository).

This report documents LBNL's FY2016 Salt R&D Milestone M3FT-16LB080309022, related to modeling of coupled thermal-hydrological-mechanical (THM) processes in salt and their effect on brine migration at high temperatures. This report not only presents the progress made in FY2016, but also provides a summary of LBNL's THM modeling work over the past four years, including findings related coupled processes and their importance to the long-term performance of a potential waste repository. This is done in the light of a shift of the UFD Salt R&D program in FY2017 towards a field testing program that is intended to bring together current UFD Salt R&D activities at Sandia, Los Alamos, and Lawrence Berkeley National Laboratories.

In Section 2 of this report, we briefly introduce coupled processes in salt and then in Section 3 provide an overview of LBNL's work within the UFD Salt R&D program during FY2012-FY2016. In Section 4, we report on the status of the TOUGH-FLAC simulator for modeling salt coupled processes. In Section 5, we present important findings from our coupled THM modeling over the past four years related to some key coupled processes in the light of the future field testing program. Section 6 presents pore-scale modeling of brine inclusion movements and Section 7 we discuss a new continuum model of brine inclusion movements that will be implemented into our coupled THM modeling framework. Finally, in Section 8 we summarize key coupled processes and relevance to long-term waste isolation as well as links to Performance Assessment (PA) and then conclude with proposed work for FY2017.

Intentionally Left Blank

2. COUPLED PROCESSES AND WATER FLOW ASSOCIATED WITH RADIOACTIVE WASTE DISPOSAL IN SALT

For modeling of salt coupled processes and water flow, we have to define the general requirements of such a model based on the current state of knowledge. It is clear that disposal in salt formations differs in an essential way from other host rock options, e.g., clay and crystalline. Rock salt in the undisturbed state typically has an extremely low permeability (~10^{-21} m^2) and low water content (<1%), which are significant positive attributes for disposal of radioactive waste. For undisturbed rock salt, numerous examples demonstrate the ability of such a rock mass to behave as a nearly impermeable barrier to fluid flow over geologic time periods. A significant challenge for radioactive waste disposal in salt is to preserve these positive attributes under repository conditions where effects such as drift-wall convergence, thermo-mechanically induced stress redistribution, and local damage can alter rock properties (Minkley and Popp 2010).

Although salt has very low permeability in undisturbed conditions, many laboratory experiments and field tests have shown that given sufficient deviatoric stress, or alternatively, sufficient pore pressure, salt rock will enter a dilatant regime in which microfractures develop along grain boundaries, as shown in Figure 2-1 (Popp et al. 2001; Minkley and Popp 2010). Such stress conditions are present in the disturbed rock zone around excavations in salt. The microfracturing leads to large increases in permeability compared to the undisturbed condition. As shown in laboratory experiments, the permeability can increase by several orders of magnitude after a few percent of axial strain under increasing deviatoric (shear) stress, as shown in Figure 2-2 (Popp et al. 2001).

Heat released from the waste package will trigger strongly coupled Thermal-Hydrological-Mechanical-Chemical (THMC) processes that may be relatively short lived, but could potentially induce permanent changes to the system that could impact the long-term performance of a nuclear waste repository. Moreover, brine volumes can move either up or down a gradient, depending upon its occurrence, e.g., if present in intercrystalline pore space or intracrystalline inclusions. Therefore, despite the basic impermeability of salt rock, brine may still reach the waste packages and compromise their performance under repository-induced conditions (Kelly 1985). Given the complexity of these inter-related processes and the time scales that need to be considered (typically, thousands or even millions of years for heat-generating nuclear waste), the performance assessment of an underground repository requires that numerical modeling based on suitable tools as well as on state-of-the-art and physically-based knowledge be performed. Figure 2-3 summarizes some of the coupled processes that may be significant for the long-term waste isolation and will have to be predicted with numerical modeling validated against laboratory and field data for uncertainty reduction.

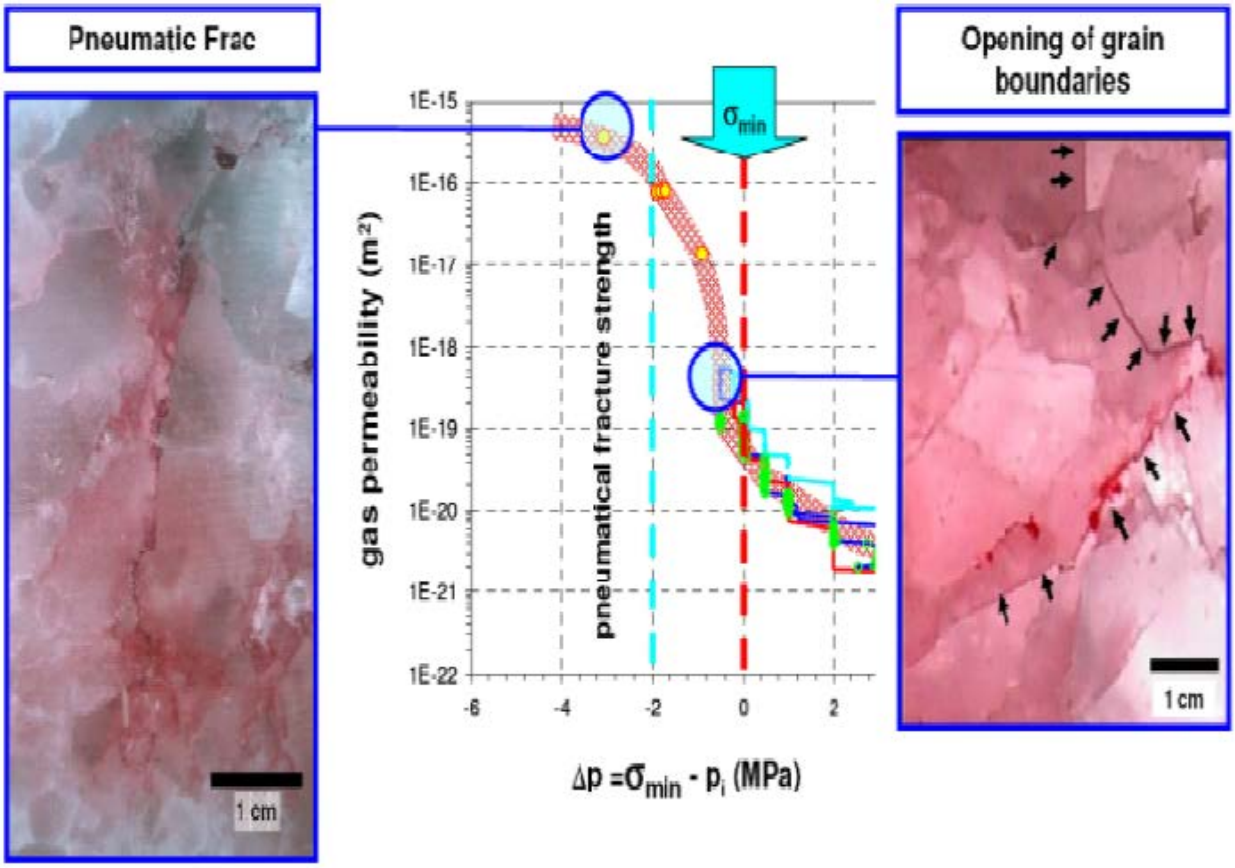

Figure 2-1. Microstructural observations on samples subjected to various injection pressures (Popp and Minkley 2010).

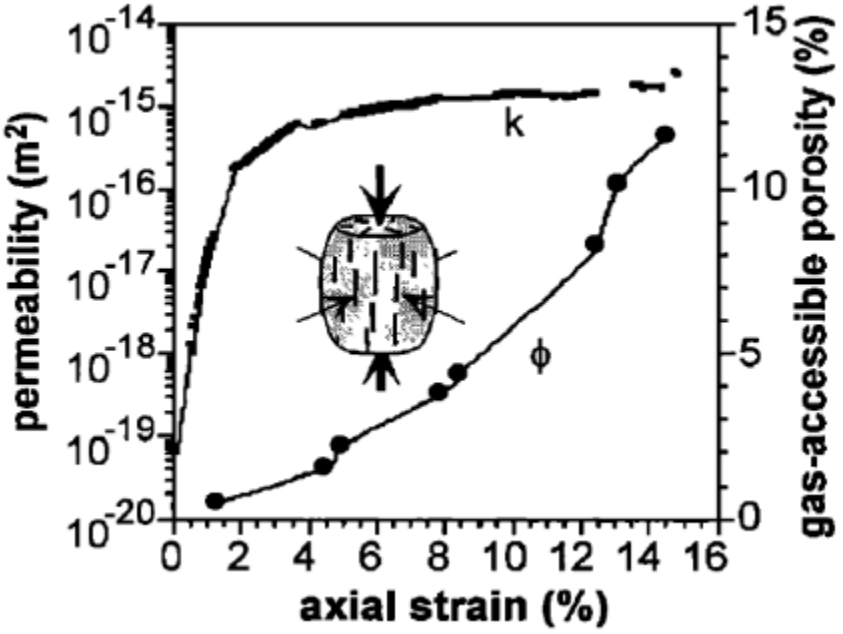

Figure 2-2. Experimental results on the evolution of permeability and gas accessible porosity versus strain (Popp et al. 2001).

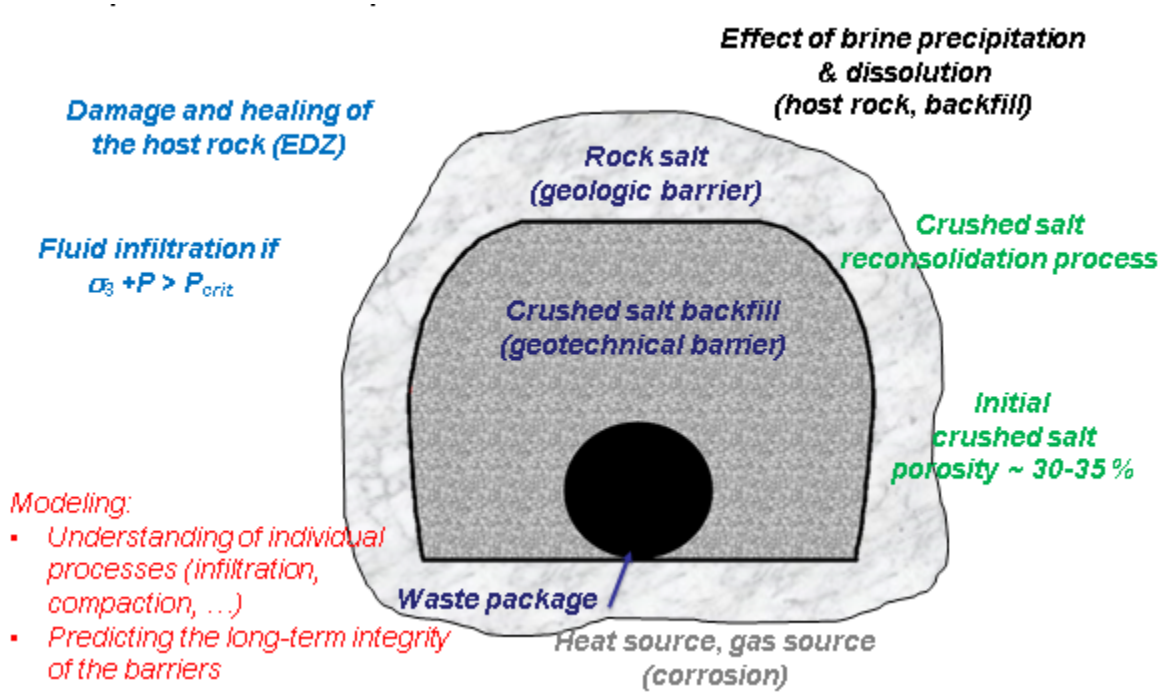

Figure 2-3. Coupled THMC processes around a nuclear waste emplacement drift in salt.

Intentionally Left Blank

3. OVERVIEW OF LBNL'S SALT R&D PROGRESS FY2012-FY2016

LBNL's work on the modeling of coupled THMC processes in salt was initiated in FY2012, focusing on exploring and demonstrating the capabilities of an existing LBNL modeling tool (TOUGH-FLAC) for simulating temperature-driven coupled flow and geomechanical processes in salt. The TOUGH-FLAC simulator (Rutqvist 2011), is based on linking the TOUGH2 multiphase flow and heat transport simulator (Pruess et al. 2012) with the FLAC^{3D} geomechanical simulator (Itasca 2011). In this approach, TOUGH2 (Pruess et al. 2012) is used for solving multiphase flow and heat transport equations, whereas FLAC^{3D} (Itasca 2011) is used for solving geomechanical stress-strain equations. In FY2012, TOUGH-FLAC was considered promising for modeling coupled THM processes associated with spent nuclear fuel in salt formations as TOUGH-FLAC had previously been applied for modeling high-temperature multiphase flow processes coupled with geomechanics associated with nuclear waste disposal in other geological media, and the geomechanical components in FLAC^{3D} had been applied for modeling salt geomechanics, including creep.

An important component in this code development and applications is LBNL's collaboration with a research group led by Professor Lux at Clausthal University of Technology (TUC) in Germany, a world-leading research institution in salt geomechanics. The DOE UFD campaign and LBNL greatly benefit from TUC's experience in salt geomechanics and modeling of salt thermal-mechanical (TM) processes using FLAC^{3D}. Similarly, TUC benefits from LBNL's expertise in modeling multiphase and heat transport processes at high temperature with TOUGH2 as well as LBNL's experience with the TOUGH-FLAC simulator for the modeling coupled THM processes in nuclear waste isolation. By leveraging on existing complementary capabilities of the LBNL and TUC, we have within a few years been able to develop and validate an advanced state-of-the-art numerical simulation tool for modeling of coupled THM processes in salt and have demonstrated its applicability to nuclear waste isolation. After the initiation in FY2012, this work has been possible through continuous close collaboration between LBNL and TUC during FY2013 to FY2016 as detailed below.

In FY2013, the work was focused on implementation and testing of constitutive models for salt host rocks and crushed salt. In particular, we implemented the *Lux/Wolters* model for modeling of creep, damage, sealing, and healing of the salt as a function of stress, temperature, and pore pressure. Moreover, we used the TOUGH-FLAC code with this newly implemented model together with other constitutive models for crushed salt backfill, and for the first time successfully completed model simulations of a generic salt-based repository over 100,000 years of simulation time. We also developed and tested alternative ways for modeling hydraulic and mechanical coupling under large strain necessary for modeling compaction of crushed salt.

In FY2014 LBNL's work was focused on continued testing, application, and improvement of TOUGH-FLAC relevant to spend fuel disposal in salt. This included improvements to the TOUGH-FLAC simulator related to implemented constitutive models for both solid rock salt and crushed salt, as well as related to the use of a Voronoi discretization for improved accuracy in the flow sub-problem. Based on these model improvements, updated simulations of long-term THM behavior of a generic repository were performed and we conducted code benchmarking in collaboration with the TUC research team. This code benchmarking consisted of comparing simulation results with LBNL's TOUGH-FLAC simulator with TUC's FLAC-TOUGH

simulator, which is based the same basic codes (TOUGH2 and FLAC^{3D}), but the numerical schemes for linking the two codes are different.

In FY2015 we conducted further verification, validation, and application of the TOUGH-FLAC model. We conducted the first full 3D (86,000 elements) TOUGH-FLAC modeling of a salt repository (heater experiment); the Thermal Simulation for Drift Emplacement (TSDE) test in Asse Mine, Germany, and extended TOUGH-FLAC for considering salt precipitation and dissolution, i.e., coupled THMC. The following two journal papers were published in FY2015:

- Blanco-Martín et al. (2015a) "Long-term modelling of the thermal-hydraulic-mechanical response of a generic salt repository for heat-generating nuclear waste" in Engineering Geology.
- Blanco-Martín et al. (2015b) "Comparison of two simulators to investigate thermal-hydraulic-mechanical processes related to nuclear waste isolation in saliniferous formations" in Computers and Geotechnics.

The above mentioned long-term modeling included updated two phase flow properties, capillary pressure curves, which are generally not available for natural salt, and improved modeling of water filtration induced at high pore-pressure. In addition, in FY2015 LBNL initiated pore-scale (or micro-) modeling of salt inclusion migration to be linked with laboratory experiments conducted at LANL.

In FY2016, we continued to focus on verification, validation, application, and publications. We completed the code validation against the Asse Mine TSDE experiment, and published the results in a peer-reviewed journal paper:

- Blanco-Martín et al. (2016) "Thermal–hydraulic–mechanical modeling of a large-scale heater test to investigate rock salt and crushed salt behavior under repository conditions for heat-generating nuclear waste" in Computers and Geotechnics.

The modeling of the TSDE resulted in updated creep deformation parameters for salt rock, parameters that are difficult to determine in laboratory. Using these parameters, we updated the long-term THM modeling investigating the effect on the drift closure and sealing.

In FY2016, we also conducted model validation against a 1980s in situ brine-release experiment at *Waste Isolation Pilot Plant* (WIPP), New Mexico, Room A1, as well as new model verification against analytical solutions. We further have completed the pore-scale modeling of salt inclusion migration with comparison to laboratory experiments of Los Alamos National Laboratory (LANL). Finally, a modeling approach for continuum modeling of brine inclusion movements have been developed and tested. With addition of brine inclusion modeling into the continuum framework of TOUGH-FLAC, a complete and comprehensive state-of-the-art numerical model will be available for coupled THM modeling in the planned salt field test campaign.

4. STATUS OF TOUGH-FLAC SIMULATOR FOR SALT COUPLED PROCESSES

The TOUGH-FLAC simulator (Rutqvist et al. 2002; Rutqvist, 2011), has within the UFD Salt R&D, been adapted for modeling salt coupled THM processes and brine migration. As mentioned, an important component in this work is LBNL's international collaboration with Clausthal University of Technology (TUC) in Germany. Through the collaboration with TUC, we have implemented an advanced constitutive model for salt geomechanics, the *Lux/Wolters* model and we have closely collaborated on improving the TOUGH-FLAC simulator along with model verifications, validations and application related to the short and long-term performance of nuclear waste disposal in salt formations. In the following subsections we present more details on the status of the TOUGH-FLAC, including the status of the numerical framework for coupled THM modeling and salt geomechanics constitutive models, followed by a list of completed verification and validation examples as well as new verifications against analytical solutions.

4.1 TOUGH-FLAC COUPLED THM FRAMEWORK

Figure 4-1 shows a schematic on the linking of TOUGH2 and FLAC^{3D}, whereas Figure 4-2 shows the scheme for the sequential coupling scheme of the two codes. The main advantages with such a sequential coupling scheme include the use of existing robust and well-established simulators for each subproblem, the resolution of smaller systems of equations, the use of different time-stepping algorithms, and the possibility to study different domains in each subproblem (Dean et al. 2006). The coupling scheme between TOUGH2 and FLAC^{3D} is based on the fixed stress-split method (Kim et al. 2011). In this method, the flow problem is solved first (with an explicit evaluation of the volumetric total stress), and the pore pressure and temperature are prescribed during the geomechanical calculation, which therefore requires drained rock-mechanical properties.

In order to accommodate the large strains and time-dependent processes associated with saliniferous materials (creep, mesh distortions, crushed salt reconsolidation, etc.), TOUGH-FLAC required some updates. Indeed, FLAC^{3D} has the capability to deal with large strains, but TOUGH2 does not. In FY2013, we developed an algorithm to update the mesh in the flow subproblem as the geomechanics mesh deforms (Rutqvist et al. 2013), and we implemented formulation of coupled geomechanics and multiphase fluid and heat flows developed by Kim et al. (2011). This analytical formulation is an extension of the classic thermodynamic approach implemented in TOUGH2 and includes a porosity correction term that accounts for the geomechanical effect (via the volumetric component of the total stress tensor).

In FY2014, we reformulated the balance equations solved in TOUGH2 to account for geometrical changes and ensure mass conservation. This way, after every FLAC^{3D} call, mass is conserved, but density is not. The geometrical update is made at the first iteration of the TOUGH2 Newton-Raphson process (Pruess et al. 2012). In this iteration, the primary variables (pore pressure, temperature, and saturation) and porosity remain equal to those at the end of the previous time step (only geometrical data are different), and we check whether the system continues to be in thermodynamic equilibrium for a new time increment and new geometry. If the maximum residual exceeds a preset convergence tolerance, an iterative process is carried out. In this process, the geometry is kept unchanged (i.e., the geometry is updated in TOUGH2 after

every FLAC^{3D} call, but is constant during each TOUGH2 run) and consistency in the balance equations is ensured through the porosity-variation formulation, adapted from (Kim et al. 2012). The balance equations for a grid block *n* read:

$$\frac{d\left(M_n^{\kappa} V_n\right)}{dt} = \sum_m A_{nm} F_{nm}^{\kappa} + q_n^{\kappa} \rightarrow \frac{dM_n^{\kappa}}{dt} + M_n^{\kappa} \frac{dV_n}{Vdt} = \frac{1}{V_n}\left(\sum_m A_{nm} F_{nm}^{\kappa} + q_n^{\kappa}\right) \tag{4.1}$$

for κ=1, *NK* (*NK* is the total number of fluid components [air, water, etc.]). In Equation (4.1), M_n^{κ} is the accumulation term, V_n is the volume of the grid block (new volume after FLAC^{3D} call), q_n^{κ} represents the sink/sources, and F_{nm}^{κ} is the flow of component κ across surface A_{nm} (new value after FLAC^{3D} call). We note that for second and further iterations, the term $M_n^{\kappa} \frac{dV_n}{Vdt}$ is not computed. The accumulation terms read

$$M_n^{\kappa} = \phi \sum_{\beta} S_{\beta} \rho_{\beta} \chi_{\beta}^{\kappa} \tag{4.2}$$

where ϕ is porosity, S_β is the phase saturation, ρ_β is the density of phase β, and χ_β^{κ} is the mass fraction of component κ in phase β. Porosity changes during a time step (for second and further iterations) are calculated adding a porosity variation $d\phi$, which includes a correction term, $\Delta\phi$, from geomechanics (therefore, it includes volume changes). This term is constant for a given time step. This way, the geometrical data used during the iterations of a time step are consistent, and mass conservation is ensured. The porosity variation has the form

$$d\phi = A(\alpha, \phi, K)dP + B(\alpha_{th})dT + \Delta\phi \tag{4.3}$$

where α [-] is the Biot coefficient, α_{th} [K^{-1}] is the linear thermal expansion coefficient, K [MPa] is the drained bulk modulus, and $\Delta\phi$ is the porosity correction from geomechanics. A detailed explanation of this formulation can be found in Kim et al. (2012). The Biot coefficient is defined as the ratio of the fluid-volume variation in a material element to the volume change of that element. It gives an indication of the grain compressibility with respect to the bulk compressibility, and of the coupling strength. It can take the values $\alpha \in [0,1]$; a Biot coefficient close to 1 describes a high poromechanical effect (the grains are not compressible, so the pores take an important role), whereas a low value indicates that the poromechanical effect is low (the response of the grains and the bulk material is similar, so the coupling strength is low).

Currently, the modeling sequence is as follows: TOUGH2 moves the simulation forward and FLAC^{3D} is executed once within a TOUGH2 time step, just before the Newton-Raphson iteration process to solve the residual nonlinear equations (Figure 4-2). The pressure, P^n, temperature, T^n, liquid saturation, $S_l{}^n$, and porosity, ϕ^n, of each grid block computed at the end of the previous time step (from t^{n-1} to t^n) are transferred to FLAC^{3D}. Note that the pressure transferred depends on the definition of pore pressure (Coussy 2004; Kim et al. 2013).

From flow to geomechanics, the pore-pressure change, $\Delta P = P^n - P^{n-1}$, and the temperature change, $\Delta T = T^n - T^{n-1}$, corresponding to two successive TOUGH2 time steps are accounted for as a correction to the total stress tensor, σ_{ij} (direct coupling). These changes are computed internally

in FLAC^{3D} once the new values P^n and T^n are transferred. The corrected total stress tensor, σ_{ij}^c, has the form

$$\sigma_{ij}^c = \sigma_{ij} - \alpha \Delta P \delta_{ij} - 3\alpha_{th} K \Delta T \delta_{ij} \tag{4.4}$$

where δ_{ij} [-] is the Kronecker delta. Compressive stresses are defined negative here. From Equation (4.4), it can be inferred that the coupling from flow to geomechanics (TOUGH2 to FLAC^{3D}) affects only the volumetric component of the stress tensor. Porosity and liquid saturation are used to update the body forces in the quasi-static governing equations of the geomechanical analysis (Kim et al. 2012). Note that these equations account for the thermal strains that result from the temperature change ΔT.

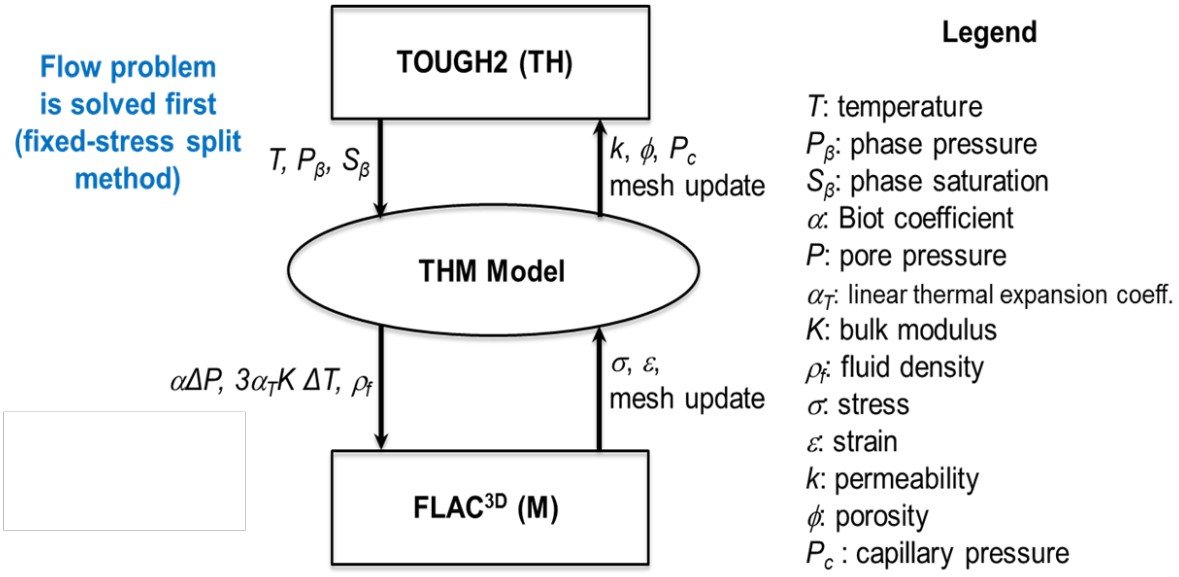

Figure 4-1. Linking of TOUGH2 multiphase and heat transport simulator with FLAC^{3D} geomechanical simulator for modelling coupled.

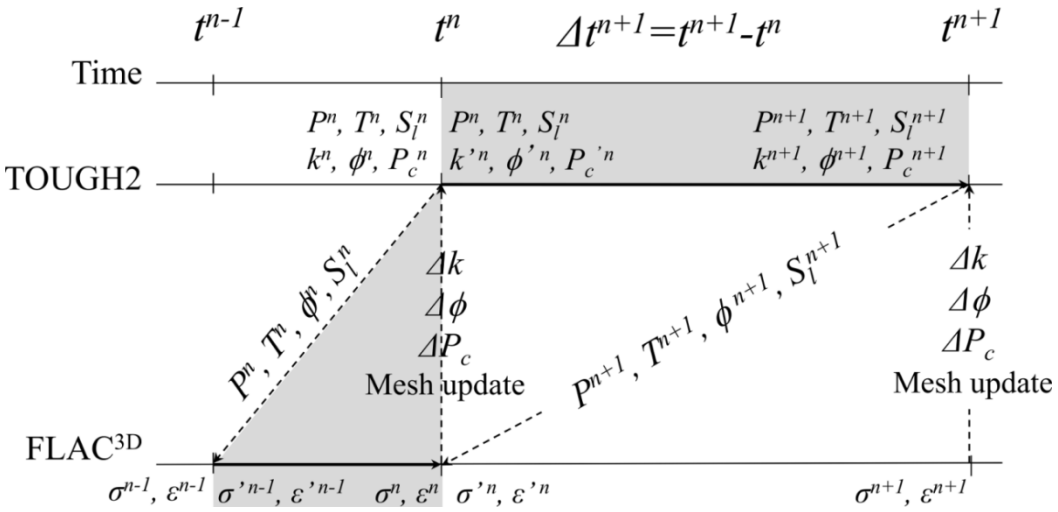

Figure 4-2. Explicit sequential THM analysis scheme (adapted from Rutqvist et al. 2002). The highlighted zones correspond to the time step between time tn and tn+1.

Once all the updates are made, FLAC^{3D} runs in creep and large strain modes from time t^{n-1} to time t^n. A new equilibrium mechanical state is obtained at time t^n (stresses σ^n and strains ε^n in Figure 4-2). Recall that during the mechanical calculation, the flow data (P^n, T^n, $S_l{}^n$, and ϕ^n) remain constant. In FLAC^{3D} the new static equilibrium is established internally through a dynamic-solution approach, solving the equation of motion in which the inertial terms are used as numerical means to reach the equilibrium state of the system under consideration. The established new static equilibrium brings about a new strain tensor and a new effective stress tensor (i.e., a new mechanical state).

From geomechanics to flow, geometrical changes are first incorporated. The geometrical data updated in TOUGH2 are: volume of the elements, distances of the centroids of two connected elements to their common interface, common interface area, and cosine of the angle between the gravitational acceleration vector and the line between the centroids of two connected elements. Also, as explained before, in the first Newton-Raphson iteration, the accumulation terms in the balance equations are updated to account for possible volume changes.

Additionally, the new mechanical state obtained at t^n is used through several coupling functions to compute mechanically induced changes in permeability and capillary pressure (Δk and ΔP_c in Figure 4-2). The coupling functions depend on each material (and the phenomena it goes through) and should be based on specific laboratory and theoretical results. The mechanically modified flow properties (k'^n, ϕ'^n and $P_c'^n$ in Figure 4-2) are used to solve the residual equations of the flow problem. Within a time step, the Newton-Raphson iteration process is continued until the residuals are reduced below a preset convergence tolerance. At the end of the current time step (time t^{n+1} in Figure 4-2), a new set of primary thermodynamic variables (P^{n+1}, T^{n+1} and $S_l{}^{n+1}$ in Figure 4-2) and new flow properties (k^{n+1}, ϕ^{n+1} and $P_c{}^{n+1}$ in the figure) are obtained.

Another improvement incorporated into TOUGH-FLAC during FY2014 is the use of a Voronoi discretization in the flow subproblem, even when the mesh deforms over time due to the creep and the large strains associated with the mechanical behavior of saliniferous materials. Since the

resolution method used in TOUGH2 is based on the Voronoi partition (Pruess et al. 2012), more accurate solutions will be obtained when the discretization of the flow subproblem conforms to this technique. If the domain under study deforms over time, the partition used in the flow subproblem should still comply with the resolution method of the code. Bearing this in mind, we use the software library Voro++ (Rycroft 2009) to ensure that the mesh used in TOUGH2 conforms to the principles of the Voronoi tessellation.

As the mesh deforms in the geomechanics subproblem, Voro++ is executed to compute the corresponding Voronoi tessellation. This operation is performed every time the mesh deforms with respect to strains a preset value, typically 2–5 % (Benz 2007). In the current approach, the centroids of the deformed geomechanical mesh are transferred to Voro++, which computes the corresponding Voronoi discretization. Geometrical data of the new Voronoi mesh (volumes, common interface area between two adjacent grid blocks, etc.) are then transferred to TOUGH2.

Figure 4-3 shows a detail of two grids (flow and geomechanics) used in a THM simulation (initial mesh and deformed mesh after 20 years). As can be seen, the flow subproblem uses Voronoi cells, both in the initial and the deformed configurations. The grid blocks at the boundary between two different domains (waste package, backfill, and host rock) are slim and have the same thickness (Figure 4-3). This way, Voro++ will conserve the volume of each domain even when the mesh deforms (the generators of the Voronoi mesh are the centroids of the mesh used in FLAC^{3D}).

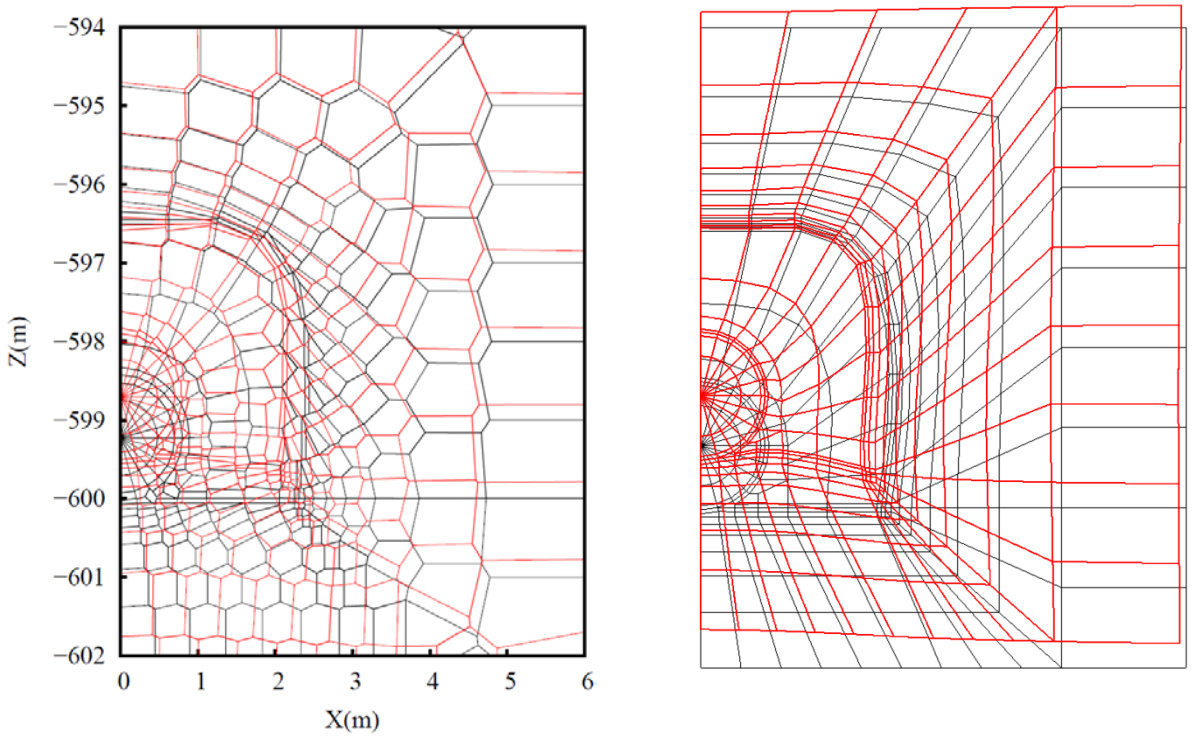

Figure 4-3. Mesh update in large strain mode. Example of initial and deformed discretizations in the (left) flow sub-problem and (right) geomechanics sub-problem.

In FY2015 we dedicated a substantial effort to enhance TOUGH-FLAC for the modeling of coupled processes in saliferous media by considering the flow of brine and Halite dissolution/precipitation effects. This means that we consider three components in the flow sub-problem: water, air, and halite. The liquid phase is not composed of water with dissolved air, but by brine (solution of halite in water) with dissolved air. Halite (sodium chloride, NaCl) is very soluble in water, and solubility increases with temperature. However, if the mass fraction of halite in the liquid phase exceeds the solubility limit (which is a function of temperature), precipitation of solid halite will occur. Conversely, dissolution of solid salt will occur if the mass fraction of halite in the liquid phase is lower than the solubility limit at the current temperature. Halite solubility constraints introduce a new phase into the flow sub-problem, so that in addition to the gas and liquid phases, a solid phase is also possible. Salt dissolution

The enhancement in TOUGH-FLAC to consider flow of brine and halite dissolution/precipitation was accomplished by the use EWASG (Water, Salt, Gas), an equation-of-state (EOS) module of TOUGH2 (Pruess et al. 2012; Battistelli 2012) that effectively accounts for the thermo-physical properties of fluids of variable salinity. EWASG was developed for the modeling of hydrothermal systems containing salt and a non-condensable gas (NCG), such as air. The standard version of this EOS fluid property module has been recently improved to overcome some limitations (Battistelli 2012); some of these limitations are related to the correlations used for brine and halite, which were derived from different sources (with a potential risk for limited internal coherence). Additionally, the effects of NCG were evaluated with an approach limited to low partial pressures.

From a mechanical point of view, the solid phase within the pores is able to bear load, since it is considered to be regular rock salt. The relationship between the effective and the total porosity reads

$$\phi_{eff} = \phi(1 - S_s) \tag{4.5}$$

where ϕ_{eff} [-] is the effective porosity, ϕ [-] is the total porosity and S_s [-] is the solid saturation. We note that flow properties that depend on saturation, such as capillary pressure and relative permeability of the rock salt.

Currently, the TOUGH-FLAC numerical THM framework includes the most relevant coupled THM processes, including multiphase fluid flow (Darcy flow and diffusion), heat transfer (advective and conductive), and non-linear geomechanics. One potential important process currently not included is the migration of brine through the movements of small brine-filled inclusions within sand crystals. In Section 7 we present the development of continuum model related to brine-inclusion movements that will be implemented and tested in the TOUGH-FLAC numerical THM framework. First, in the next two sub-sections we present the status of THM constitutive models for natural and crush salt, which are critical for the prediction of damage and long-term sealing and healing of the salt rock when exposed to high temperatures.

4.2 Status of THM constitutive model for natural salt

The behavior of the natural salt is modeled in TOUGH-FLAC using the *Lux/Wolters* constitutive model, developed at (TUC). This model has been under development and improvement since the 1980s (Hou 2003; Hou and Lux 2000, 1999, 1998; Hou et al. 1998; Lux 1984; Wolters et al. 2012). Based on continuum damage mechanics, it has been established using a series of laboratory investigations designed to study, from a macroscopic viewpoint, the mechanisms involved in the short- and long-term responses of rock salt. This model was validated against field- and laboratory-scale data (Hou 2003) and implemented as a plug-in (user-defined model) in FLAC^{3D}.

Versions of the *Lux/Wolters* model have been detailed previously (Rutqvist et al. 2013; Wolters et al. 2012), whereas a complete description of the current version was provided in the recent journal paper by Blanco-Martin et al. (2016). In brief, the *Lux/Wolters* model integrates the effects of a range of different deformation mechanisms (diffusion, dislocation, consolidation, strain hardening, fabric damage, and healing). Different creep rates resulting from different deformation mechanisms are combined by superposition, yielding an overall strain rate tensor, $\dot{\varepsilon}_{ij}$ [s^{-1}], that reads

$$\dot{\varepsilon}_{ij} = \dot{\varepsilon}^{e}_{ij} + \dot{\varepsilon}^{ie}_{ij} = \dot{\varepsilon}^{e}_{ij} + \dot{\varepsilon}^{vp}_{ij} + \dot{\varepsilon}^{d}_{ij} + \dot{\varepsilon}^{h}_{ij} \tag{4.6}$$

where $\dot{\varepsilon}^{e}_{ij}$ [s^{-1}] is the elastic strain rate tensor, $\dot{\varepsilon}^{ie}_{ij}$ [s^{-1}] is the inelastic strain rate tensor, $\dot{\varepsilon}^{vp}_{ij}$ [s^{-1}] is the viscoplastic (i.e., transient and stationary) strain rate tensor, $\dot{\varepsilon}^{d}_{ij}$ [s^{-1}] is the thermomechanically-induced damage strain rate tensor, and $\dot{\varepsilon}^{h}_{ij}$ [s^{-1}] is the thermomechanically-induced damage reduction (i.e., healing) strain rate tensor. All the components of the strain rate tensor in Equation (4.6) take a damage-induced reduction of the load-bearing cross-sectional area into account, in accordance with a previous study (Kachanov 1986). (This way, the load-bearing cross-sectional area is the original area multiplied by 1-*D*, where *D* [-] is a damage parameter.) A current description of the constitutive model *Lux/Wolters* is given in Blanco-Martin et al. (2016), including the influence of temperature on the rock salt creep deformation, and also damage/dilatancy processes, healing/sealing, and yield and potential functions of constitutive terms.

The elastic strain rate tensor, $\dot{\varepsilon}^{e}_{ij}$ [s^{-1}], is described by Hooke's constitutive model, whereas viscoplastic strain rate tensor, $\dot{\varepsilon}^{vp}_{ij}$ [s^{-1}], is described by a modified version of the constitutive model *Lubby2* (Lux 1984), including the damage-induced reduction of the load-bearing cross-sectional area, by means of the damage parameter *D* [-].

Within the constitutive model *Lux/Wolters*, the damage process involves the creation of micro-fissures in the rock salt material accompanied by an increase of its volume (i.e., dilatancy). The damage process can be induced by stress states exceeding the dilatancy boundary, or by fluid pressure exceeding the minimum principal stress. If the dilatancy boundary is exceeded, an additional damage-induced strain rate tensor $\dot{\varepsilon}^{d}_{ij}$ occurs. However, the damage of rock salt may be sealed or even healed if the stress state falls below the sealing/healing boundary.

The thermomechanically-induced creation of micro-fissures is accompanied by the generation of a secondary permeability. Finally, if the fluid pressure gets higher than the minimum (i.e., least) compressive principal stress, a hydraulically-induced damage process starts. This process is mainly characterized by the creation of a secondary permeability due to the opening of formerly closed grain boundaries, resulting in a flow of the fluid through these open grain boundaries. Therefore, this process is also called pressure-driven fluid infiltration.

The physical modelling and numerical simulation of sealing/healing processes need the consideration of micro-fissure orientation resulting from the former stress state evolution in which only stresses perpendicular to the micro-fissures are able to close the micro-fissures. The closure of micro-fissures is modelled with an additional sealing/healing-induced strain rate tensor, $\dot{\varepsilon}_{ij}^{h}$, and the damage parameter is reduced. According to laboratory observations, in the *Lux/Wolters* model, the recovery of damage is faster at the beginning of the healing process (due to a rapid volume contraction), while in a second stage, slower mechanisms such as re-crystallisation or diffusion dominate (Hou 2003).

In FY2015 we introduced some further improvements to the *Lux/Wolters* model, as provided by Professor Lux's team. The main improvement concerns the damage dependence of the Biot coefficient (recall that the Biot coefficient controls the strength of the coupling effects between flow and geomechanics). In the undisturbed state, the Biot coefficient of rock salt is very close to zero (Hou 2003), but increases as damage takes place. From the interpretation of laboratory-scale results, the evolution of the Biot coefficient is described by

$$\alpha_{salt} = \max\left(\frac{D}{D_{\alpha}},\ 1-\exp\left(\frac{\sigma_v\, m\, D}{D-D_{\alpha}}\right)\right) \tag{4.7}$$

where D [-] is a damage parameter (Wolters et al. 2012), D_{α}=0.1 [-] is a constant, σ_v [MPa] is von Mises equivalent stress and m<0 [MPa^{-1}] is a parameter that enhances Maxwell viscosity. Note that healing can restore the initial Biot coefficient.

With this addition to the constitutive model, the modeling of dilatancy, damage and healing can be performed much more accurately especially related to long-term performance of nuclear waste repository in salt host rocks. In total, the *Lux/Wolters* constitutive model needs 34 parameters. However, the number of parameters used in a simulation may be reduced depending on the phenomena under investigation.

4.3 Status of THM constitutive model for crushed salt

The *cwipp* model available in FLAC^{3D} to model the reconsolidation process of granular salt is based on previous studies on crushed salt compaction (Callahan and DeVries 1991; Sjaardema and Krieg 1987) and on the *wipp* model for natural salt, also implemented in FLAC^{3D} (Itasca 2011).

The main characteristic of the *cwipp* model is that it allows modeling volumetric strain changes associated with creep processes (classically, viscoplasticity occurs at constant volume). The total strain rate tensor, $\dot{\varepsilon}_{ij}$, comprises a nonlinear elastic component, a viscous compaction component

and a viscous shear contribution. The latter is adapted from the *wipp* model and is purely deviatoric. The total strain rate tensor reads

$$\dot{\varepsilon}_{ij} = \dot{\varepsilon}^{e}_{ij} + \dot{\varepsilon}^{vc}_{ij} + \dot{\varepsilon}^{vs}_{ij} \tag{4.8}$$

where superscripts *e*, *vc* and *vs* stand for elastic, viscous compaction, and viscous shear, respectively. As reconsolidation occurs, density increases towards that of the natural salt. In the *cwipp* model density is a monotonic function. The nonlinear compaction density rate is derived from experimental results (Callahan and DeVries 1991; Sjaardema and Krieg 1987). The viscous compaction term in the model accounts for the density evolution during compaction. This term is only active if the mean effective stress is compressive and if the monotonic density has not yet reached the intact salt density (i.e., there is no further compaction beyond the intact salt density). During compaction, the elastic properties (shear, *G*, and bulk, *K*, moduli) increase as the monotonic density increases according to a nonlinear empirical expression of the form

$$a = a_{salt} \exp\left(a_1 \left[\rho - \rho_{salt}\right]\right) \tag{4.9}$$

where $a=\{K,G\}$. Variables ρ and ρ_{salt} stand for the drained densities of the crushed salt and the natural salt, respectively. Parameter a_1 [$kg^{-1}m^3$] is obtained from the condition that the moduli take their initial value at the initial value of density. When $\rho=\rho_{salt}$, the elastic moduli are those of the natural salt, $K=K_{salt}$ and $G=G_{salt}$. In total, the *cwipp* model is characterized by 17 parameters.

In FY2014, we made some important improvement of the *cwipp* model for our purpose. Indeed, in the original *cwipp* model, density is monotonic, and therefore cannot increase even if the mean compressive stress increases. To avoid this limitation, we developed a modified version in which density honors the volumetric strain evolution, but keeping other features of the original *cwipp* model.

As the bulk modulus increases towards that of the intact salt, the Biot coefficient decreases from almost 1 to the Biot coefficient of the host rock; therefore, the poromechanical effects within the backfill will be stronger before substantial compaction occurs The Biot coefficient is calculated using

$$\alpha_{crushed\ salt} = 1 - \frac{K}{K_s} \tag{4.10}$$

where K is the drained bulk modulus, and K_s is the bulk modulus of the solid material.

It is important to highlight that the long-term mechanical responses predicted by the *cwipp* and the *Lux/Wolters* models are similar: due to the creep over time, the stresses tend toward the isotropic state and therefore the deviatoric components of both models tend to zero. For the crushed salt, the compaction component vanishes after full reconsolidation, and for the natural salt, damage and healing counteract each other. Consequently, only the elastic components

prevail. Given that after reconsolidation the elastic moduli of the crushed salt are equal to those of the natural salt, the modeled long-term response of the two materials is similar.

A shortcoming of the current crushed salt constitutive model is that it does not consider the effects of temperature on compaction rate. Such temperature dependency should be included once additional data on temperature effects on the crushed salt compaction are available from new laboratory testing.

4.4 List of completed verifications and validations

The coupled THM processes in salt are complex but can be analyzed using coupled numerical modeling with adequate constitutive models, verified and validated against laboratory and field tests. Such validation is also important for uncertainty reduction related to long-term model predictions. Below we list completed verifications and validations of TOUGH-FLAC related to salt coupled processes and references were those activities are documented.

- Brine infiltration laboratory experiments validating implementation of Lux/Wolter's model in TOUGH-FLAC for brine infiltration (Rutqvist et al. 2012; Blanco-Martin et al. 2015a)

- Triaxial compression test to validate TOUGH-FLAC with Lux/Wolter's model regarding mechanical behavior under shear stress and strain (Rutqvist et al. 2013)

- Modeling of Terzaghi's 1D consolidation problem, Mandel's poro-elastic problem, and Booker and Savvidou's thermos-poro-elastic problem with comparison to analytic solution to verify TOUGH-FLAC hydraulic and mechanical sequential coupling algorithm (this report)

- Modeling TSDE experiment validating THM model including drift closure and crushed salt compaction at a realistic scale (Rutqvist et al. 2015; Blanco-Martin et al. 2016)

- Modeling WIPP Room A1 THM-induced brine-migration experiment (this report)

- Modeling salt dissolution/precipitation laboratory experiment under thermal gradient (Rutqvist et al. 2015)

- Code-to-code verification between TOUGH-FLAC and FLAC-TOUGH for various benchmark examples, including long-term repository behavior and TSDE experiment (Blanco-Martin et al. 2015b; 2016). Recall that TUC's FLAC-TOUGH simulator is based the same basic codes (TOUGH2 and FLAC3D), but the numerical schemes for linking the two codes are different from that in TOUGH-FLAC.

Note, the above verifications and validations are associated with testing of TOUGH-FLAC and the implementation of constitutive models in TOUGH-FLAC. In addition, there are numerous validations of the *Lux/Wolters* constitutive model conduced at TUC, of the *cwipp* crushed salt model documented in FLAC^{3D} manual (Itasca 2011), as well as numerous verifications and validations of the respective codes TOUGH2 (Pruess et al. 2012) and FLAC^{3D} (Itasca 2011). Such extensive testing over a wide range of applications and conditions provides additional confidence in the TOUGH-FLAC simulator.

4.5 New Verifications of TOUGH-FLAC Sequential HM and THM Couplings

In this section we document new verifications for strong HM and THM couplings, related to poroelasticity and thermoporoelasticity. These verification examples are relevant for verifying the approach for the sequencing between the two simulators (TOUGH2 and FLAC^{3D}) considering the sequential solution technique employed in TOUGH-FLAC.

4.5.1 Mandel's problem

Mandel's problem (Mandel 1953) is commonly used to test the validity of numerical codes of poroelasticity. The problem considers a porous specimen at single-phase conditions with rectangular cross-section and infinite length along the third direction is sandwiched at the top and the bottom by two stiff, frictionless plates (Figure 4-4a). Laterally, the specimen is not mechanically constrained, and drainage is possible (no drainage at the top and bottom). The specimen is initially in equilibrium. At t = 0, a compressive force is applied normal to the plates, and we seek to determine the evolution of pore pressure, as well as relevant displacements, strains and stresses within the sample.

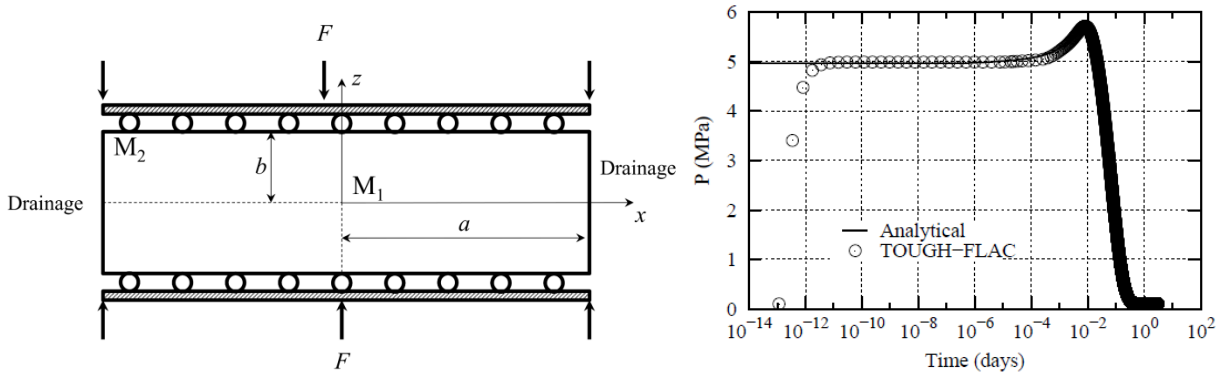

(a) (b)

Figure 4-4. (a) Schematic representation of Mandel's problem, and (b) comparison between analytical and modeling results for (a) pore pressure at M1.

Mandel's problem has been modeled with TOUGH-FLAC. We have assumed a sample with a = 5 m, b = 1.25 m, E = 450 MPa, and ν = 0. The initial stress field is 0.1 MPa (compressive), and we apply 10 MPa normal to the plates. The initial porosity is ϕ_0 = 42.5% and the permeability of the sample is k = 6.51 10^{-15} m^2. The sample is saturated with water, having T = 25 °C (constant) and p_0 = 0.1 MPa. Given that TOUGH2 accounts for fluid compressibility changes (in this case due to pressure changes), we have compared our modeling results with the analytical solution proposed by Abousleiman et al. (1996).

The plots in Figure 4-4b compare analytical and modeling results of pore pressure evolution at the center of the sample. As the figure shows, the comparisons are very satisfactory (note that the analytical solution assumes instantaneous changes when the load is applied). Other results not

shown here include stress and displacement which also were in good agreement. These results help verify the validity of TOUGH-FLAC to solve coupled flow and geomechanics problems.

4.5.2 Booker and Savvidou's problem

Booker and Savvidou (1985) proposed an analytical solution for a problem involving a point heat source buried in a saturated medium. In this problem, a saturated, infinite medium is initially in equilibrium. At t = 0, a heat load is applied in the center of the medium. Over time, as temperature increases both the pore water and the solid skeleton expand. Since in general the thermal expansion of water is greater than that of the solid medium, the pore pressure increases, leading to a reduction in effective stresses (THM coupling). The pore pressure increase gradually dissipates as the medium is allowed to consolidate.

Figure 4-5a shows the axisymmetric model prepared to benchmark TOUGH-FLAC against the analytical solutions in Booker and Savvidou (1985). We note that, in order to reproduce an infinite medium, Dirichlet boundary conditions (i.e., constant pore pressure and temperature) are imposed at the outer boundaries of the model (R = Z = 200 m in Figure 4-5a). The heat source is applied in a small element at r = z = 0. The medium is linear elastic with E = 650 MPa and ν = 0.24. The initial stress field is 0.1 MPa (compressive), equal to the initial pore pressure. The sample is saturated with water. The initial temperature is T_0 = 25 °C, and we apply a heat source of 15.6 W. The initial porosity of the sample is ϕ_0 = 45%, its permeability is $k = 6.51\times10^{-18}$ m^2, its thermal conductivity is λ = 1.2 W/m/K, and the coefficient of linear thermal expansion is $\alpha_{th} = 7\times10^{-6}$ K^{-1}. Solid density is ρ = 2500 kg/m^3 and the specific heat of the solid skeleton is C_p = 1000 J/kg/K. Gravity is neglected.

Figure 4-5b and c compares analytical and modeling results for pore pressure evolution at three locations along the radial axis of the model. As the figures show, results from TOUGH-FLAC compare quite well with the analytical solutions, with the largest errors at shorter distances from the heat source (in TOUGH-FLAC, the heat load is applied to a small-volume element rather than to a point).

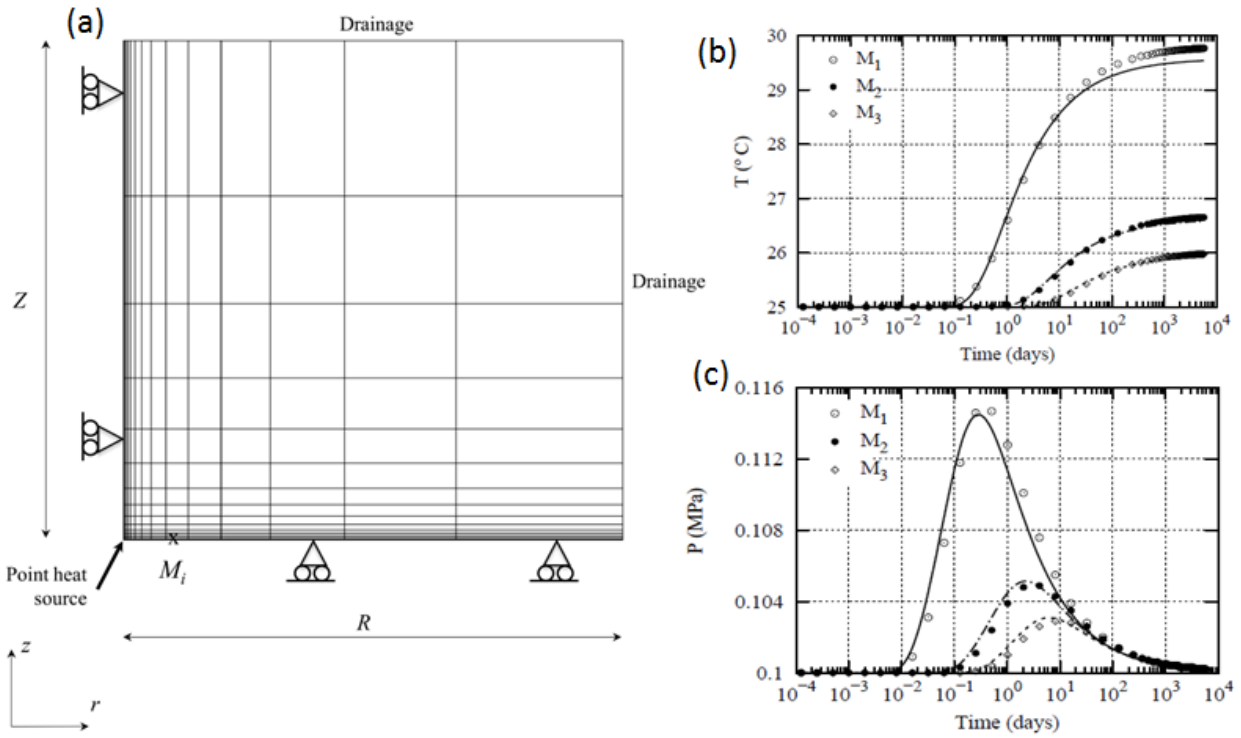

Figure 4-5. (a) Schematic representation of Booker and Savvidou's problem with monitoring points (Mi) indicated (they are all located along the radial axis). Comparison between analytical (lines) and modeling (symbols) results for (b) temperature, and (c) pore pressure at locations M1 = 0.22 m, M2 = 0.63 m, and M3 = 1 m.

4.5.3 Terzaghi's problem

Terzaghi's (Terzaghi 1943) classical consolidation problem: a confined soil sample, surrounded by a circular ring, and placed in a container filled with water. The sample is loaded by a constant vertical stress at its upper surface, and its deformation is measured (Figure 4-6a). The lower boundary is impermeable, and the upper boundary is fully drained. As the fluid flows out of the sample and the pore pressure decreases, there is a load transfer between the fluid and the solid, so that the effective stresses increase. We note that in Terzaghi's problem the pore pressure decreases monotonically after the initial rise, and therefore the Mandel-Cryer effect, distinctive feature of the coupled consolidation theory, is not observed.

Terzaghi's problem has been modeled with TOUGH-FLAC, using L = 31 m, E = 600 MPa, and ν = 0.15. Initially, the sample is in equilibrium under a compressive stress of 10 MPa (the initial pore pressure is also 10 MPa). The initial porosity is ϕ_0 = 42.5% and the permeability of the sample is $k = 6.5\times10^{-15}$ m^2. The sample is saturated with water, having T = 25 °C (constant). At t=0, the applied load increases by 10 MPa.

The plot in Figure 4-6b shows a comparison between analytical and modeling results for the evolution of pore pressure at the monitoring point (0.5 m from the bottom). In the results shown

in Figure 4-6b, the standard fluid compressibility in TOUGH2 was used which means the pressure increases to about 1 MPa less than the applied load. The pressure dissipation over time is very well captured by TOUGH-FLAC. Moreover, the approach implemented in TOUGH-FLAC is coupled and able to model the whole process (pressure rise and pressure dissipation), using the sequential coupling technique.

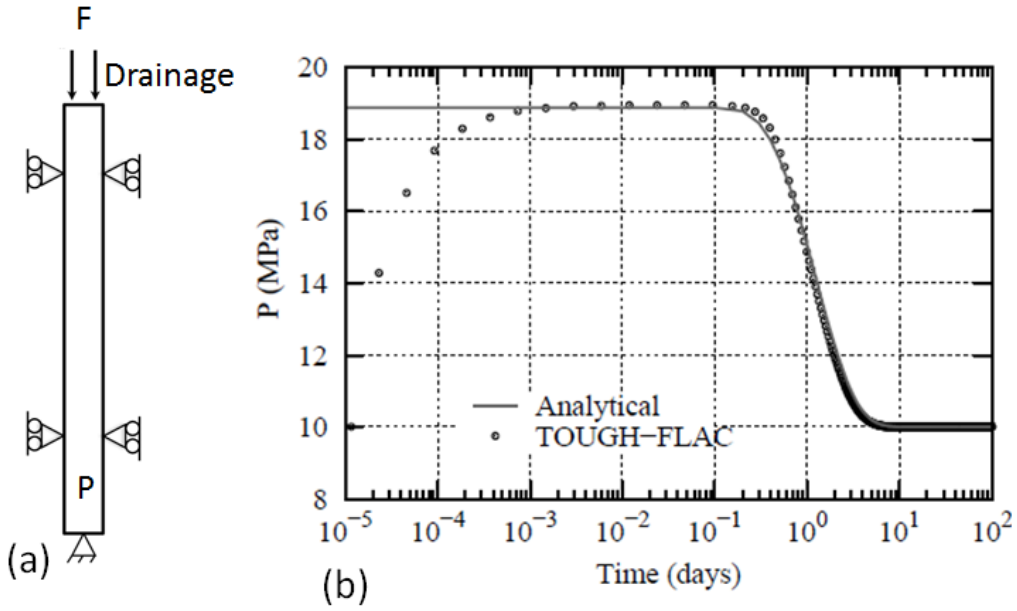

Figure 4-6. (a) Schematic representation of Terzaghi's problem, and (b) comparison between analytical and modeled pore pressure evolution at a monitoring point located 5 m from the bottom

5. FINDINGS FROM THM MODELING AND RELEVANCE TO LONG-TERM PERFORMANCE

In this section we present some findings from our coupled THM Salt R&D modeling over the past four years and discuss potential relevance to the long-term repository performance. We characterize the following subsections into topics of (5.1) drift compaction and sealing, (5.2) brine-release and migration, (5.3) temperature-induced brine-release and migration, and (5.4) pressure-induced dilatant fluid percolation, and halite precipitation and dissolution.

5.1 Drift Compaction and Sealing

The TOUGH-FLAC coupled THM modeling framework and associated constitutive models for salt host rock creep deformations and crushed salt compaction allow us to conduct detailed simulations of drift compaction and sealing, which are key processes for waste isolation in salt. This section first summarizes modeling results from the Thermal Simulation for Drift Emplacement (TSDE) experiment, including parameters for the rate of compaction and sealing, which is then applied for new analysis of the closure and sealing of a repository drift.

5.1.1 MODELLING TSDE EXPERIMENT AT ASSE MINE

Our TOUGH-FLAC modeling of the TSDE experiment was initiated in FY2014 and has now been completed with final results published in a peer-reviewed journal paper (Blanco-Martin et al. 2016). The modeling has included a number of aspects, including inverse modeling and parameter estimation of backfill properties and calibration of creep properties for the host rock, as well as sensitivity studies. Most of the modeling activities related to the TSDE test has been performed in collaboration with TUC, Germany. In addition to beneficial scientific exchanges, this fruitful collaboration has allowed us to benchmark two simulators for coupled flow and geomechanics processes, TOUGH-FLAC and FLAC-TOUGH. At LBNL, the updated TOUGH-FLAC simulator for large strains and creep processes is used. The details of the TSDE experiment and TOUGH-FLAC modeling are described in the FY2015 milestone report (Rutqvist et al. 2015), and also in the recent journal paper by Blanco-Martin et al. (2016).

The experiment was conducted in two parallel drifts, drilled for the purposes of this test, at a depth of 800 m, in the North-Eastern part of the salt dome (Figure 5-1). These drifts are both about 76 m long and lay 10 m apart. In each of the drifts, three electrical heaters were emplaced, each of them releasing a constant power of 6.4 kW. The heaters were 5.5 m long and placed in the central part of the drifts, at a constant distance of 3 m. The heaters were emplaced 1.4 years after the excavation of the drifts, parallel to the drifts' axis. The open space was subsequently backfilled with crushed salt, with an initial porosity of 35%. A significant amount of data was measured in 20 monitoring cross sections: temperature, stress changes, displacement, convergence and porosity of crushed salt, among others. These data could be used to validate the large-scale applicability of models developed from laboratory data, and also to calibrate some model parameters whose identification is difficult at the laboratory scale (Bechthold et al. 1999; 2004).

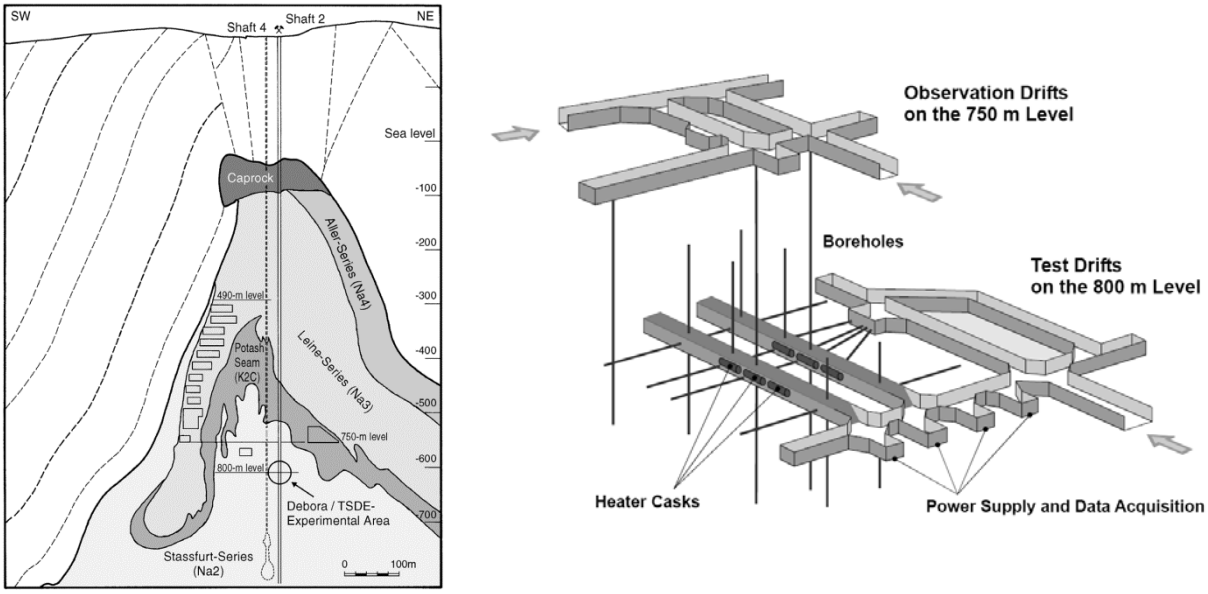

(a) (b)

Figure 5-1. TSDE test: (a): cross-section of the Asse salt mine, indicating the location of the TSDE experiment; (b): schematic representation of the test area (Blanco-Martin et al. 2016).

The model domain was a three-dimensional model of half of one drift, with two symmetry planes: one at X=0 (across the pillar between the two test drifts) and one at Y=0 (across the central cross-section of the drifts) (Figure 5-2). All external planes are no-flow boundaries. Additionally, the displacement is blocked in the normal direction to those planes. The mesh has 85,870 elements. Our TOUGH-FLAC THM simulations of the TSDE include full two-phase flow of water and air, both by diffusion and advection, and heat flow occurs by conduction and convection. The simulations account for material-specific characteristics of salt rock mass and crushed salt backfill and salt host rock, included transient, damage and healing processes.

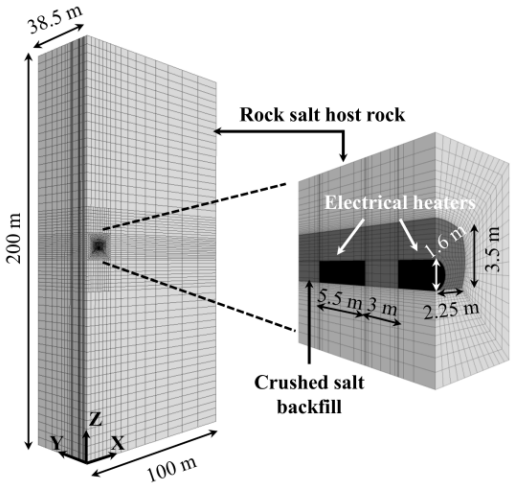

Figure 5-2. TSDE test: views of the initial mesh used in the geomechanics sub-problem. The main dimensions of the model are also shown (Blanco-Martin et al. 2016).

Table 5-1 lists the final flow and mechanical parameters of the host rock and the crushed salt. In addition, a number of parameters evolve during the simulation, such as grain density, the linear thermal expansion coefficient, relative permeability parameters, and thermal conductivity (Blanco-Martin et al. 2016).

Table 5-1. Mechanical and flow properties of the crushed salt and the natural salt.

Property [unit]	Crushed salt	Rock salt
Bulk modulus, K [MPa]	150[a]	17,390[b]
Shear modulus, G [MPa]	70[a]	9450[b]
Initial Biot coefficient, α[-]	1[a]	0.003[b]
Porosity [-]	0.35[a]	0.002[b]
Permeability, k [m^2]	$5.8 \cdot 10^{-13}$ [a]	0[b]
Initial thermal conductivity (36.4 °C) [$W \cdot m^{-1} \cdot K^{-1}$]	0.8[a]	5.36[c]
Initial heat capacity (36.4 °C) [$J \cdot kg^{-1} \cdot K^{-1}$]	860[c]	860[c]
Initial liquid saturation, S_l [-]	0.02	0.5
Grain density, ρ [$kg \cdot m^{-3}$]	2154	2154
Linear thermal expansion coeff., α_T [K^{-1}]	$4.2 \cdot 10^{-5}$	$4.2 \cdot 10^{-5}$
Relative permeability functions	Corey	Corey
Residual liquid saturation, S_{lr} [-]	0.05	0.05
Residual gas saturation, S_{gr} [-]	0	0

[a] non-constant value (changes during reconsolidation);
[b] damage- and healing- dependent value;
[c] temperature-dependent property

From the mechanical point of view, the time-dependent response of the natural salt is described using the *Lux/Wolters* constitutive model describe in Section 4.2. For the crushed salt, we used a modified version of the *cwipp* model described in Section 4.3. For our simulations, we initially used parameters available in the literature (DBE 2001; Itasca, 2011). Then, in order to achieve a better prediction, the parameters of the compaction part were recalibrated as explained in Blanco-Martin et al. (2016).

Detailed results for the difference phases of excavation, 1.4 years of open drift, and over 8 years of heating are presented in Blanco-Martin et al. (2016). Here we present selected results to show the main findings from the THM modeling, in particular related to compaction and sealing. First the results showed that the transient creep of the natural salt host rock finishes during the 1.4 years of open drift. Moreover, due to the stress redistribution induced by the excavation, the dilatancy boundary (Hou 2003; Popp et al. 2001; Wolters et al. 2012) is exceeded and an excavation damaged zone (EDZ) develops around the drift. It extends about 1.5 m below the drift floor (flat floor), 0.8 m above the roof, and 0.75 m beyond the sidewalls. Experimental evidence from the TSDE experiment (Bechthold et al. 2004) is in agreement with these EDZ characteristics. In the EDZ, permeability increases up to four orders of magnitude, and porosity reaches values as high as 0.7%.

During the eight years of heating, the temperature at the heater cask reached 210°C five months after the beginning of heating, and it decreased thereafter as the thermal conductivity of the backfill increased (due to compaction) (Figure 5-3). After about five years, temperatures in the heater cask area reached a steady state (160-180 °C at the heater surface), while they continued to increase within the backfill at farther distances from the heater (Figure 5-3a). The backfill porosity evolution is displayed in Figure 5-3b, for the heated and non-heated areas. The changes in backfill porosity were calculated from horizontal and vertical convergence data. The simulation showed that the closure rate in the heated area increased significantly (factor of about 12) once heating started. The closure rate decreases progressively over time due to the compaction and stiffening of the backfill.

Overall, the numerical modeling results are in very good agreement with measurement of temperature and compaction rates. The large difference in compaction rate between heated and non-heated areas is well captured in the modeling. Note though that the numerical closure rate displayed in Figure 5-3 was obtained after the recalibration of three parameters that control the stationary creep of the natural salt host rock (recall that the transient creep finishes during the open drift phase). Two of the stationary creep parameters control the effect of the von Mises equivalent stress on Maxwell viscosity, and the other controls the effect of temperature on the viscosity. These two effects are strongly nonlinear, and therefore results are very sensitive to them. In addition, the three parameters adjusted are very difficult to measure at laboratory-scale, because they require very small deviatoric stresses, which translate into very small strain rates (about 10^{-10} s^{-1}), and therefore, exceedingly long test durations. Consequently, modeling a large-scale monitored experiment is a useful means for their determination.

Related to the evolution of the EDZ, the modeling showed that porosity increases further during heating, particularly in the heated area, and decreases over time as compaction takes place. This involves development of mechanical support against the drift wall, and subsequent healing/sealing within the host rock. Since compaction is faster in the heated area, in this zone,

host rock porosity at the end of the test has decreased more than in the non-heated area (Figure 5-4).

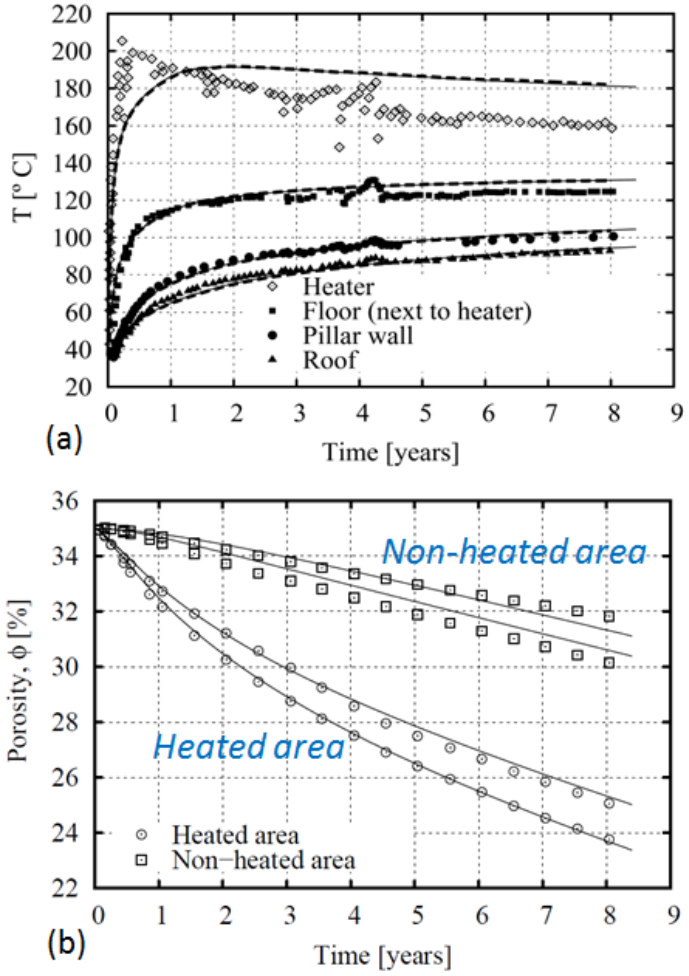

Figure 5-3. TSDE test: backfill porosity in the heated area (section G1) and in the non-heated area (section E2). Points represent measurements, solid lines correspond to TOUGH-FLAC and dashed lines correspond to FLAC-TOUGH.

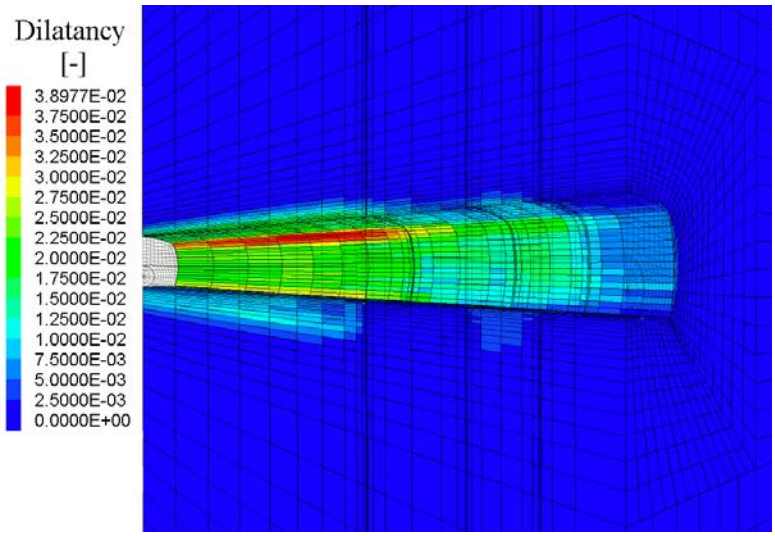

Figure 5-4. Calculated host rock porosity around the drift area after 8 years.

In the TOUGH-FLAC TSDE simulations, the crushed salt time-dependent compaction was modeled using a modified version of the *cwipp* constitutive model, with a parameter set adapted from previous studies (DBE 2001; Itasca 2011). Using this parameter set, numerical predictions of the backfill stress evolution during the TSDE experiment were not satisfactory, since they yielded very small values as compared to the experimental ones. Experimental backfill stress was measured using hydraulic pressure cells, both in the hot and cold areas of the drifts (Bechthold et al. 1999).

In an attempt to reproduce the measured backfill stress more accurately, we performed a parameter estimation using the inverse modeling theory as described in detail in Blanco-Martin et al. (2016). Some parameters related to the initial stiffness of the backfill were updated to achieve a much better agreement to measured backfill stress. Figure 5-5 shows the comparison of calculated and measured stress in the backfill. The agreement is generally good, but with some difference of 0.8 MPa near the roof (D1 roof). In order to validate these parameter set, we modeled Oedometer test of the same material cored from one of the TSDE drifts (dismantling phase). Some discrepancies between model and experiments can be observed in Figure 5-6.

The disagreement between model and data could be due to the need to model compaction as a function of temperature (in the *cwipp* model, compaction is temperature-independent). This indicates the need for improved constitutive models on compaction of crushed salt under elevated temperatures, i.e., a model in which compaction rate depends on temperature.

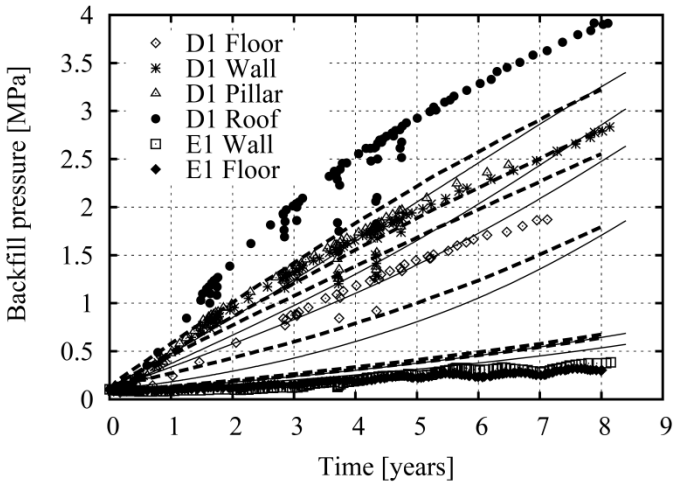

Figure 5-5. TSDE test: backfill stress increase in the heated area (section D1) and in the non-heated area (section E1). In the non-heated area, the oscillations in the experimental data are due to seasonal changes. Points represent measurements, solid lines correspond to TOUGH-FLAC and dashed lines correspond to FLAC-TOUGH (Blanco-Martin et al. 2016).

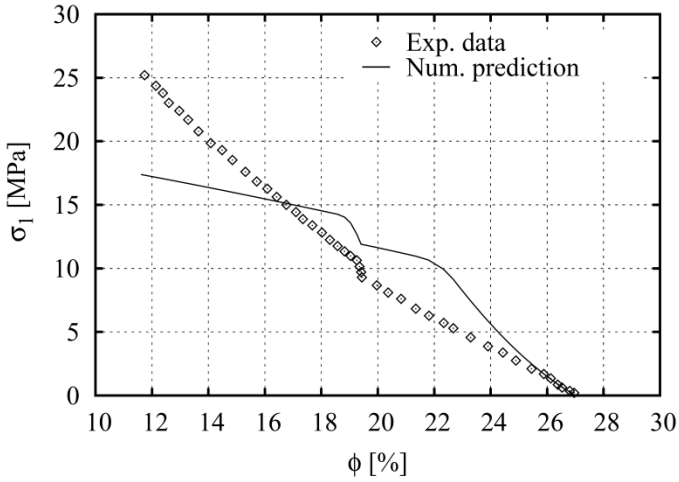

Figure 5-6. TSDE test: prediction of an oedometer test conducted on a crushed salt sample taken from one of the TSDE drifts (Blanco-Martin et al. 2016).

5.1.2 Long-term THM modeling with TSDE model parameters

During the past few years, along with the model developments and validations, we have also conducted model simulations of the long-term repository behavior. The first successive TOUGH-FLAC simulation over 100,000 years of post-closure was conducted in FY2013. Based on significant TOUGH-FLAC model developments in FY2014, we then in FY2015, presented new simulations of the long-term repository performance including those that were presented in two journal papers (Blanco-Martín et al. 2015a,b). In FY2016, we again updated the long-term repository performance simulation using the new parameter set for the crushed salt backfill and for the host rock parameters back-calculated from the modeling of the TSDE test as summarized in the previous section. This includes the recalibration of the creep parameters of the host rock under low deviatoric stress.

Figure 5-7 shows the model geometry and main dimensions, with an enlarged view of the area near the drift (same model as in FY2015). The model extends 1200 m in the vertical direction and starts at the ground surface. The repository is located in the middle of a 400 m thick salt layer, at a depth of 600 m. The drifts are 4.5 m wide and 3.5 m high. The cylindrical metallic waste canisters are 5.5 m long, have a diameter of 1.6 m and are separated by 3 m along the drift axis. We consider a two-dimensional plane-strain assumption. Symmetry allows modeling just half of one drift. In the *X* direction, the drifts are 50 m apart. A geothermal gradient of 0.03 $K \cdot m^{-1}$ is initially applied to the model. This corresponds to about 28ºC at the repository level assuming a ground surface temperature of 10ºC. The initial mechanical condition is isotropic stress, equal to the lithostatic stress magnitude (overburden); this corresponds to about -14 MPa at Z=-600 m (compression is negative). As in previous years, the heat released by each waste package is consistent with the expected nuclear waste characteristics in the U.S. Department of Energy Used Fuel Disposition Campaign (Carter et al. 2011). It is assumed that each waste package comprises ten pressurized water reactor (PWR) assemblies and that the packages are emplaced underground after 20 years of interim storage. Under these conditions, and taking the size and distance between canisters into account, the average heat load per meter of drift is approximately 1000W at the time of emplacement (Blanco-Martin et al. 2015a).

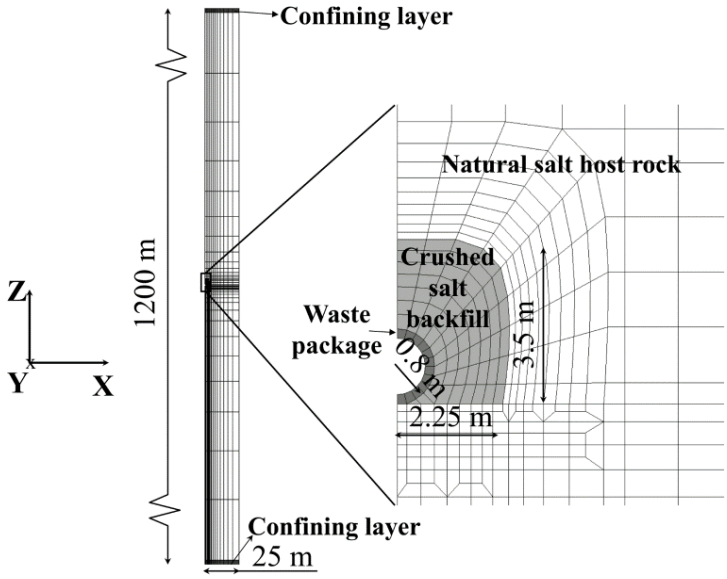

Figure 5-7. Generic Salt Repository in 2D: geometry of the generic salt repository studied and detailed view of the drift area.

Table 5-2 lists parameters used for the crushed salt, the host rock and the confining layers. These are also the same as used in FY2015 modeling. We note that some of these parameters have been adopted from previous research (Bechthold et al. 2004; Camphouse et al. 2012; Jové-Colón et al. 2012; Olivella et al. 2011). Moreover, in the absence of sufficient experimental data on capillary effects in natural halite, we have used an extrapolation of capillary pressure data corresponding to granular salt (Olivella et al. 2011), using a Leverett factor (Cinar et al. 2006; Leverett 1941). The van Genuchten function (van Genuchten 1980) is used for all materials. The *Lux/Wolters* model parameters used for the host rock have been obtained from interpretation of experimental results (Lerche 2012). Regarding the cwipp model for the crushed salt, the values were initially adapted from available experimental data (DBE 2001; Itasca 2011). Initial flow parameters are listed in Table 5-2 are also the same as in FY2015 modeling.

Table 5-2. Mechanical and flow properties of the crushed salt, natural salt and confining layers.

Property [unit]	Crushed salt	Rock salt	Confining rock
Grain density, ρ [kg·m^{-3}]	2200	2200	2600
K [MPa]	150[a]	16,650[b]	37,900
G [MPa]	70[a]	7690[b]	19,500
α_T [K^{-1}]	$4\cdot10^{-5}$	$4\cdot10^{-5}$	10^{-5}
α [-]	1[a]	0.003[b]	1
Relative permeability functions	Corey	Corey	van Genuchten (liquid), Corey (gas)
Residual liquid saturation, S_{lr} [-]	0.1	0.1	0.02
Residual gas saturation, S_{gr} [-]	0	0	0.01
van Genuchten's λ [-]	0.6	0.6	0.6
van Genuchten's P_0 [MPa]	0.0004[c]	5.7[c]	3.6
van Genuchten's S_{lr} [-]	0.01	0.01	0.01

[a]: non-constant value
[b]: values are damage- and healing- dependent
[c]: non-constant value

Table 5-3. Initial flow parameters of the crushed salt, natural salt, and confining layers.

Parameter [unit]	Crushed salt	Rock salt	Confining rock
S_l [-]	0.015	1	1
ϕ [-]	30 %	0.2 %	12 %
k [m^2]	$3\cdot10^{-13}$	10^{-22}	10^{-17a}
C [J·kg^{-1}·K^{-1}]	860	860	900[a]
λ [W·m^{-1}·K^{-1}]	0.9	4	1.8[a]

[a]: constant values

Figure 5-8 displays the temperature evolution at different positions in the repository over the simulated 100 000 years of post-closure phase, which is identical to that obtained in FY2015. The temperature at the waste package surface peaks slightly below 200 °C after about one year. The nearby crushed salt and host rock also show an initial temperature peak. This local peak is due to the low thermal conductivity of the backfill before significant compaction takes place. After 25 years, a temperature peak of about 160 ºC is obtained in the drift area. The temperature 25 m away from the drift peaks at about 108 ºC after 80 years, reflecting progressive heat propagation through the natural salt host rock. Crushed salt reconsolidation occurs in a similar fashion as well (see Figure 5-9). As noted already in our FY2015 study, the predicted duration of the reconsolidation process may be too short indicating the uncertainties in laboratory determined parameters.

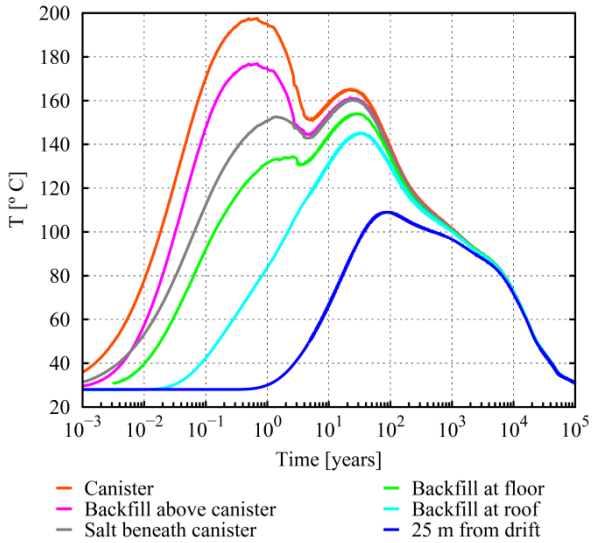

Figure 5-8. Generic Salt Repository in 2D: temperature evolution during the post-closure phase, at six locations within the repository.

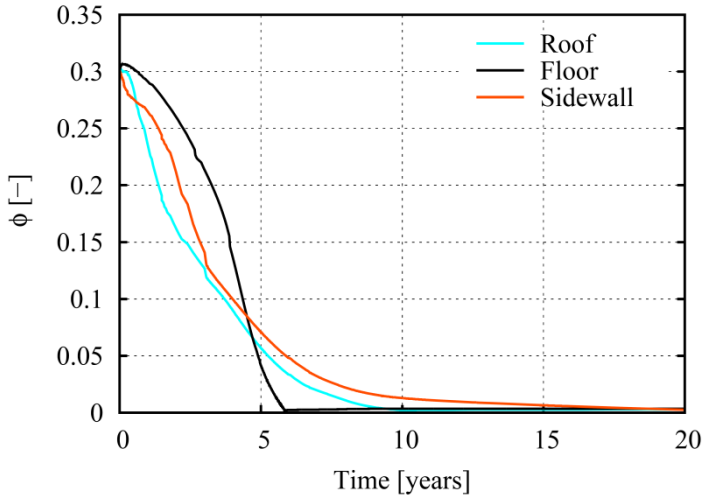

Figure 5-9. Generic Salt Repository in 2D: porosity evolution within the crushed salt, during the first 20 years of post-closure phase.

We have in FY2016 updated the simulations now using parameters back-calculated from the modelling of the TSDE experiment. Recall that we conducted recalibration of three parameters of the *Lux/Wolters* model, which control the stationary creep of the natural salt host rock. Also we calibrated the parameters for the crush salt model, leading to higher stress changes and therefore should result in larger resistance during external compaction load. In Figure 5-10, we compare the compaction of the crushed backfill for original and updated (TSDE calibrated) parameters. Also note that based on the observations at the TSDE, the initial porosity in the backfill is 0.35 rather than 0.3 in the original data set. We see that the time to complete closure and sealing has increased from about 10 years toward 100 years.

The most important changes in material parameters as a result of the recalibration against the TSDE closure data are the stationary creep parameters for the salt host rock, which determine how fast the drift can close. The stationary creep parameters that were recalibrated against TSDE closure data include two effects on the creep behaviour: (1) the effect of the von Mises equivalent stress on Maxwell viscosity, and (2) the effect of temperature on the viscosity. These two effects are strongly nonlinear, and therefore the results are very sensitive to changes in these creep parameters. In addition, the three parameters adjusted are very difficult to measure at laboratory-scale, because they require measurements at very small deviatoric stresses. Small deviatoric stresses translate into very small strain rates (about 10^{-10} s^{-1}), and therefore, require exceedingly long test durations. Consequently, modeling a large-scale monitored experiment such as the TSDE is useful for determination of these creep parameters.

The parameters for the crushed salt backfill can play a bigger role once the backfill is compacted sufficiently and its elastic modulus has increased sufficiently. However, there are considerable uncertainties in the crushed salt backfill parameters because experimental data for porosities smaller than 5-10% are scarce. Moreover, the current crush salt constitutive model (*CWIPP*) does not consider temperature effects on the compaction.

Predictions of the compaction of the backfill and sealing are very important for the long-term performance assessment, therefore *in situ* experiments addressing creep at low deviatoric stress gradient and backfill compaction properties at high temperature would be very useful for reducing the uncertainties of such predictions.

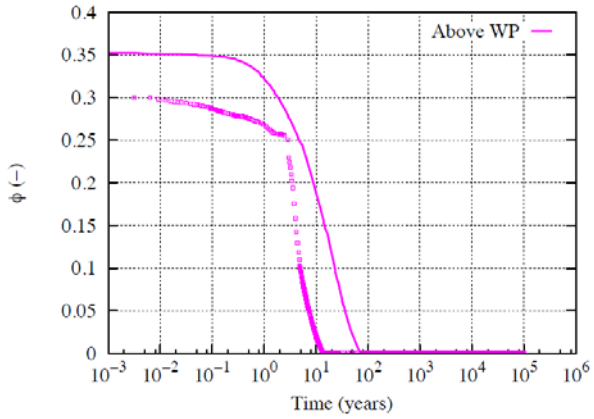

(a)

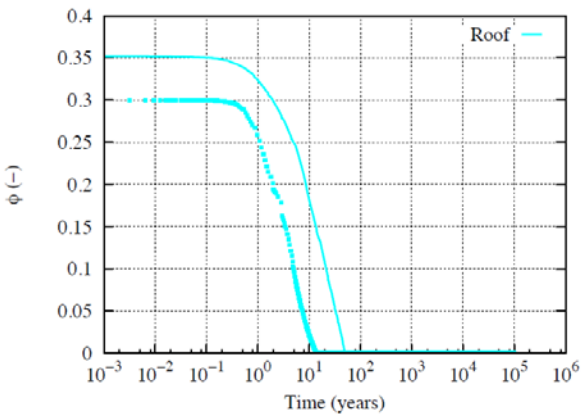

(b)

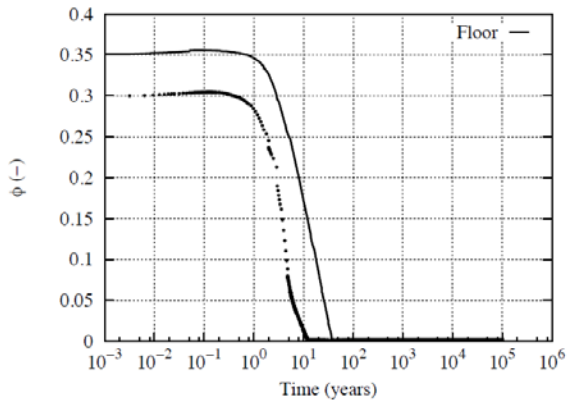

(c)

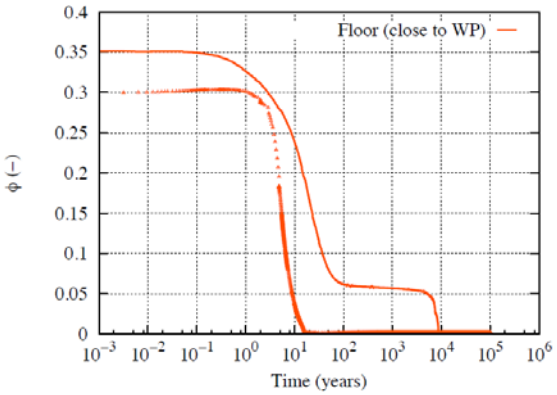

(d)

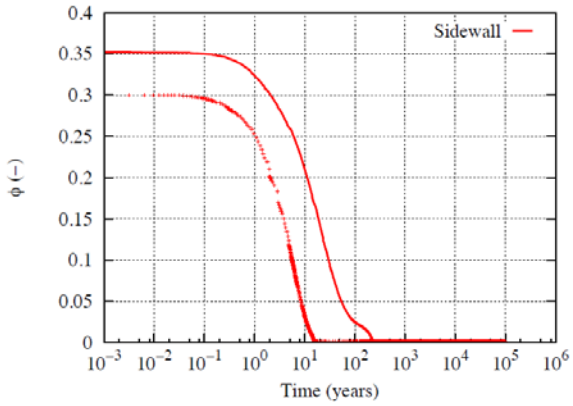

(e)

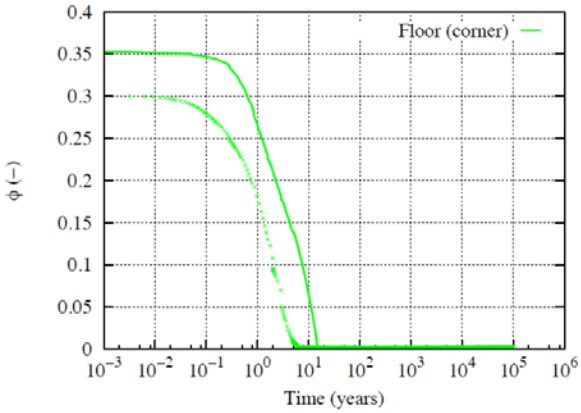

(f)

Figure 5-10. Generic Salt Repository in 2D: comparison of porosity evolution within the crushed salt previous (symbols) and updated (lines) simulations. In the updated simulations, the properties of host rock and crush salt backfill have been updated by model calibrations against TSDE data.

5.1.3 Summary and Relevance to Long-term Isolation

Our modeling of TSDE experiment showed that previously laboratory calibrated parameters of creep parameters are not valid for very low deviatoric stress that prevails *in situ* and therefore the time required for complete backfill compaction and sealing could be underestimated. Using creep parameters calibrated against the TSDE *in situ* convergence data, the time to complete compaction and sealing of the backfill in a generic repository extended from tens of years to hundreds of years. Further, our modeling of backfill compaction indicated some deviations in the calculated and measured stress evolution within the backfill. This may be due to that the constitutive model for backfill is not adequate to accurately capture the stress evolution, especially at high temperatures. Predictions of the compaction of the backfill and sealing are very important for the long-term performance assessment and therefore *in situ* experiments addressing creep at low deviatoric stress gradient and backfill compaction properties at high temperature would be very useful for reducing the uncertainties of such predictions.

5.2 Thermally induced brine-release and migration:

Using TOUGH-FLAC we are able to model thermally-induced fluid flow as has been demonstrated in many of the generic repository simulations and in the TSDE simulation. The basic mechanism is that a temperature increase and fluid thermal expansion in a low permeability porous media causes a pressure increase that might lead to increased damage and permeability enhancement that in turns allows for fluid percolation within the salt host rock. Here we present model simulations of brine-migration experiments around heated boreholes that were conducted at the WIPP site in the 1980s. A good understanding of thermally induced brine-release and migration are very important for the long-term performance as water and brine migrating to waste container can accelerate the corrosion of container materials.

5.2.1 Modeling Brine-Release and Inflow at WIPP Room A1

Heated brine inflow experiments were carried out in WIPP Rooms A1 and B in the mid-1980s, involving four vertical heated borehole experiments without backfill between the heaters and the borehole wall. Figure 5-11 shows a schematic of the experimental setup at each borehole experiment. Annular space was flushed with dry nitrogen and passed through periodically weighed downstream desiccant canisters to measure borehole brine inflow.

The experiments in Room A1 corresponded to a reference design, with 470-W heaters set in vertical boreholes to produce the heat load expected from a design defense high-level waste repository. Room B was an overtest design, with 1500-W heaters in similar vertical boreholes. All 4 test boreholes produced brine under isothermal conditions at 5 to 15 g/day, prior to the start of heating (Nowak 1986). After early transient effects, the 470-W heater boreholes in Room A1 produced brine at approximately 8 g/day per borehole, while the 1500-W heater boreholes in Room B produced brine at 50 and 80 g/day per borehole once transient effects had died down (Nowak and McTigue 1987a). In total the measured inflow per borehole was about 2 liters over 160 days in the Room A1 experiment and more than 20 liters in Room B experiment.

The quantity of collected brine in the experiments in Rooms A1 and B were much larger than laboratory tests and preliminary models had predicted. Those preliminary models considered the mechanisms of brine inclusion migration, thermally-induced stress-gradient transport, and vapor phase transport. Nowak and McTigue (1987b) showed that intergranular Darcy flow would be a

promising mechanism to explain the inflow rates observed at Rooms A1 and B. The increased inflow when turning on the heater would be explained by thermal pressurization due to thermal expansion of brine and salt that would create an increased pressure gradient and hence and increased inflow. Nowak and McTigue (1987b) used simplified one-dimensional analytic solutions to achieve order of magnitude agreement with field data, but still achieved qualitative difference attributed simplification such as one-dimensional analysis of the three-dimensional problem.

Here we present a TOUGH-FLAC numerical analysis of the Room A1 heater experiment, including THM coupled processes. We constructed an axisymmetric model of the heated borehole and surround bedded salt. We applied the specified heat load of 470-W. Figure 5-12 shows the calculated and measured evolutions of temperature at the mid-height of the borehole, inflow rate, and tangential strain at four locations along the borehole wall. An excellent agreement shown between calculated and measured temperature evolution is a results of a model calibration of the heat source to match the measured temperature evolution. The measured inflow and tangential strain are reasonably well matched by the modeling. Both calculated and measured flow rate increases sharply as soon as the heater is turned on, though the flow peak is much higher in the calculation (Figure 5-12b). After this early transient effect, both the calculated and measured rate stabilizes at an inflow rate of about 8 g/day. The plots of the tangential strains show gradual circumferential (horizontal) contraction on the borehole wall at each of the four equally spaced locations from the top to the bottom of the heater. Thus, no rapid strain changes were apparent immediately after heater turn-on.

Overall the WIPP heated borehole experiments highlighted a significant difference in flow rates obtained in bedded salt at WIPP and flow rates obtained at similar experiments in domal salt at ASSE Mine, Germany. Our modeling confirmed previous findings in Nowak and McTigue (1987b) that the measured inflow could be explained by Darcy flow in a connected inter-crystalline pore network. The experiments inflow into heated boreholes at WIPP (Room A1 and B) in bedded salt showed that the inflow rate depends on the heat load by roughly increasing the rate of inflow by one order of magnitude when wall temperature increases from maximum of 50°C to maximum above 100°C. Over less than a 1 year of heating at Room B with wall borehole finally approaching 120°C, a total inflow volume of 22 liters was recorded. Our numerical modeling of Room A1 indicated that the inflow could be explained by release of brine adjacent to the borehole flowing through increased permeability in the disturbed zone. Although the inflow could be explained by Darcy flow and not by transport of fluid inclusions, the movement of fluid inclusions to grain boundaries might contribute as a source of brine that is released upon heating. Further studies of the simulation results of the Room A1 experiment will be conducted to investigate the role of thermal pressurization and pressure-induced percolation.

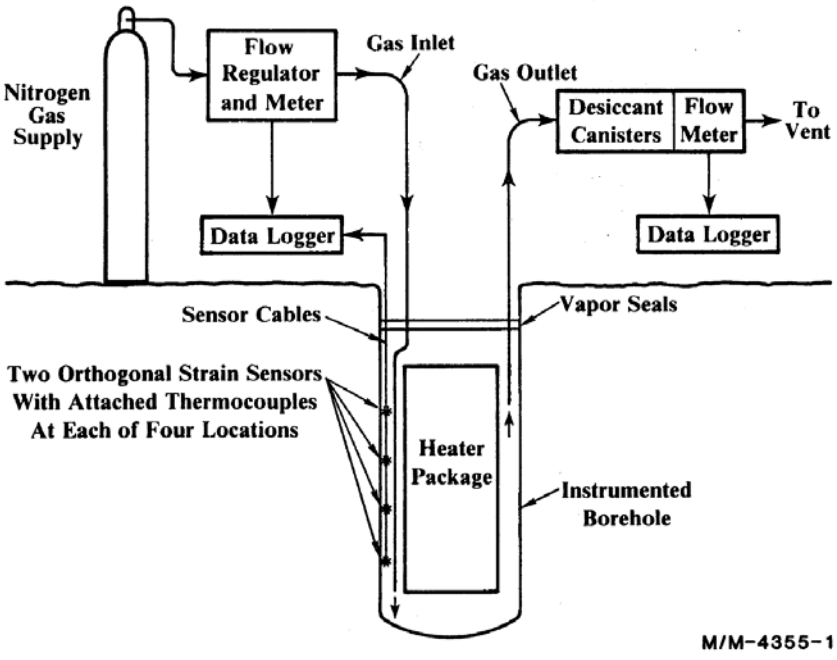

Figure 5-11. Schematic diagram of the experimental setup (Novak 1986).

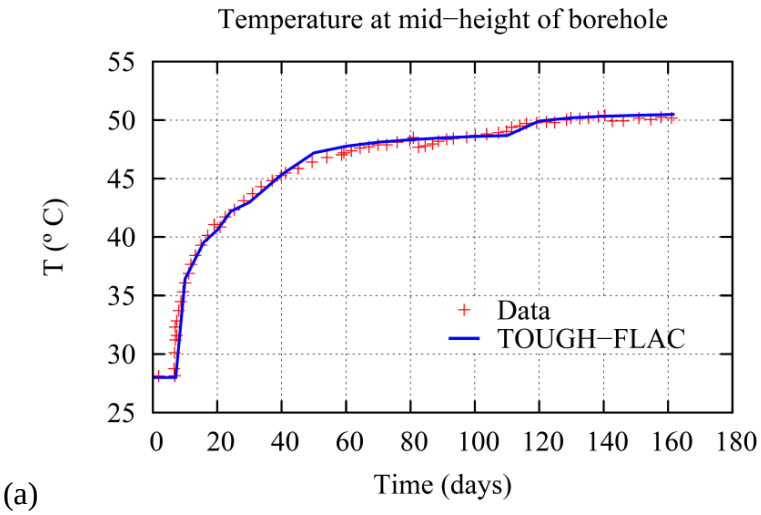

(a)

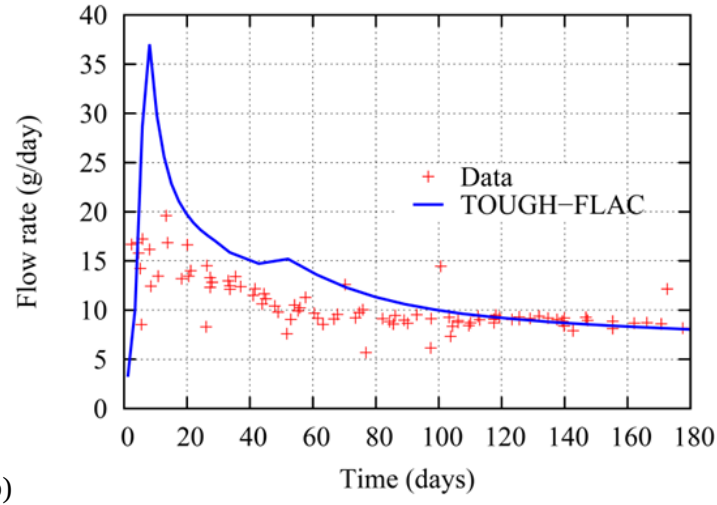

(b)

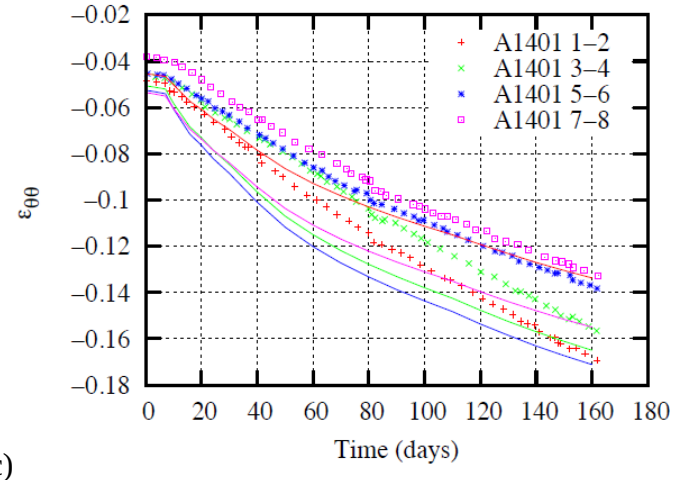

(c)

Figure 5-12. TOUGH-FLAC simulated and measured THM responses at the WIPP Room A1 brine-migration experiment. (a) Temperature at heater surface, (b) inflow, and (c) tangential strain at the mid-heater elevation. Measurements from Novak (1986).

5.2.2 Summary and Relevance to Long-term Isolation

Our study of the 1980s Room A1 brine-migration experiment at WIPP confirmed previous findings that the measured inflow could be explained by Darcy flow in a connected inter-crystalline pore network. The experiments inflow into heated boreholes at WIPP (Room A1 and B) in bedded salt showed the inflow rate depends on the heat load by roughly increasing the rate of inflow by one order of magnitude when wall temperature increases from maximum of 50°C to maximum above 100°C. Over less than a 1 year of heating at Room B with wall borehole finally approaching 120°C, a total inflow volume of 22 liters was recorded. Our numerical modeling of Room A1 indicated that the inflow could be explained by release of brine adjacent to the borehole flowing through increased permeability in the disturbed zone. Although the inflow could be explained by Darcy flow and not by transport of fluid inclusions, the movement of fluid inclusions to grain boundaries might contribute to the source of brine. The predictions of the brine-release and inflow into emplacement caverns are very important for the long-term performance as water and brine can accelerate the corrosion of container materials. Similar heated borehole experiments could help to clarify the true mechanisms of brine-migration around a heat source and this should if possible be instrumented with monitoring surrounding the borehole.

5.3 Pressure-induced dilatant fluid percolation

TOUGH-FLAC has the capability of modeling fluid percolation triggered by high fluid pressure through dilation of the pore-space between salt crystals. Here we first present the results of modeling dilatant fluid migration in a laboratory experiment used for parametrization of relationships between fluid overpressure and permeability in natural salt. Thereafter, we present modeling of the generic repository case under gas generation to illustrate the potential effect of such dilatant permeability enhancement on fluid migration. Pressure-induced dilatant fluid percolation is also relevant for migration of water and brine into the emplacement tunnel, which will affect moisture content within the backfill, and thereby affect corrosion of container material and rate of compaction of the backfill.

5.3.1 Model parametrization and validation against laboratory experiments

In FY2012, the first validation example simulated with TOUGH-FLAC for Salt R&D was related to an infiltration test conducted at TUC involving forced fluid injection into a salt sample (Rutqvist et al. 2012). Fluid infiltration (or percolation) process may occur if the pore pressure locally exceeds the minimum compressive principal stress (Popp and Minkley 2010; Wolters et al. 2012). Such a scenario is feasible in a repository for heat-generating nuclear waste in rock salt given the thermal pressurization of fluids within the very-low permeability host rock and the convergence-induced pore pressure increase. Gas generation from the waste packages may also trigger fluid permeation within the host rock.

The forced fluid infiltration test was conducted on a cylindrical rock salt sample from a German salt mine (Wolters et al. 2012). The sample was 350 mm long, had a diameter of 150 mm and was initially unsaturated. A 100 mm long and 50 mm diameter borehole was drilled along the core axis, see Figure 5-13a. A fluid containing a fluorescent tracer was injected through the borehole, while the upper and lateral surfaces of the sample were no-flow boundaries (the downstream boundary was kept at atmospheric pressure). The test lasted 6 days and was held at

room temperature (about 25 °C) in a triaxial cell, with an axial stress of 20.5 MPa and a confining pressure of 20 MPa. The fluid was injected in the borehole at a constant pressure of 21 MPa. After the test, the rock salt sample was sliced axially and put under ultraviolet light; this caused the tracer in the injected fluid to fluoresce. The delimited area in Figure 5-13b represents the extension of the fluorescent, infiltrated area within the rock salt sample. Figure 5-13c displays the infiltrated area predicted by TOUGH-FLAC modeling at the end of the test (i.e., the area in which $\Delta PFl \geq 0$).

The TOUGH-FLAC run was carried out in axisymmetric conditions. The initial permeability of the salt sample was 10^{-22} m^2, but the permeability if $\Delta PFl \geq 0$ the permeability would increase according to a function illustrated in Figure 5-14. Using such a function a good agreement between modeling and experimental data was obtained as shown in Figure 5-15.

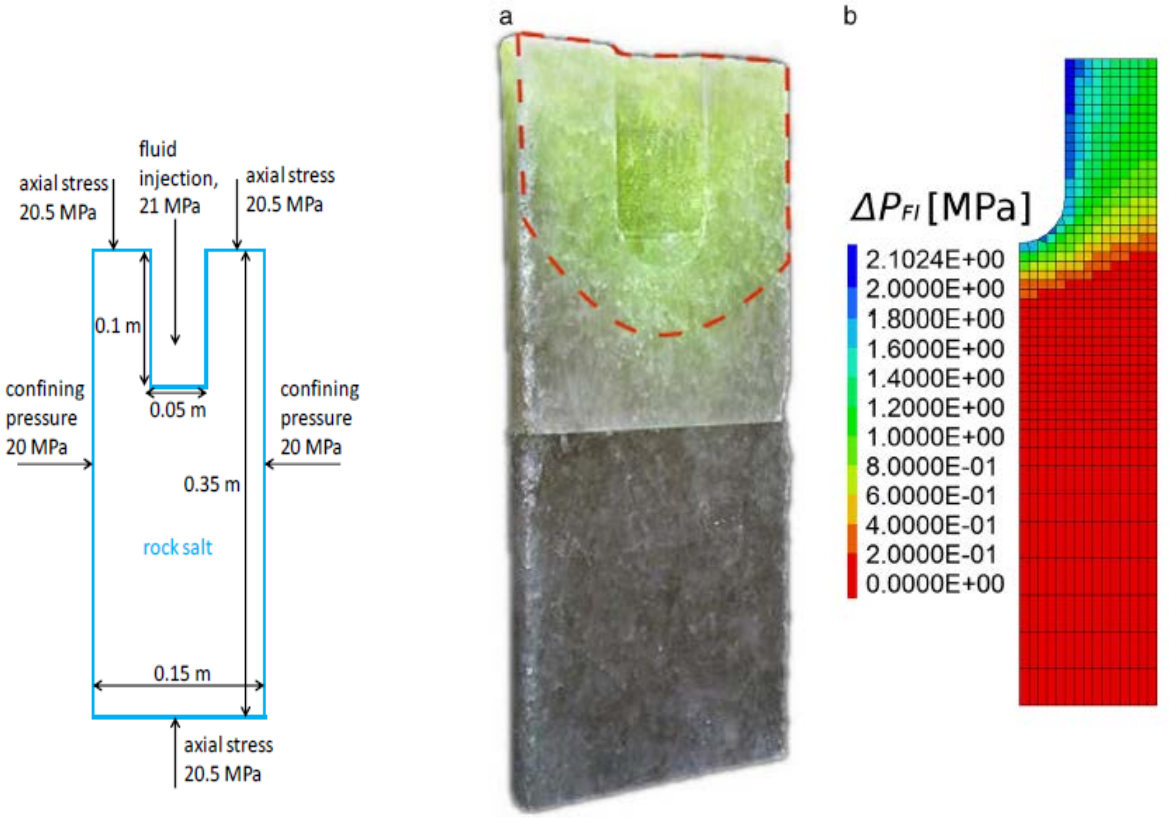

(a) (b) (c)

Figure 5-13. TOUGH-FLAC modeling of pressure-induced fluid percolation experiment. (a) Experimental setup, (b) experimental results showing the extent of fluid migration, and (c) modeling results of overpressure distribution focused within the dilated pore system (Rutqvist et al. 2012; Blanco-Martin et al. 2015a).

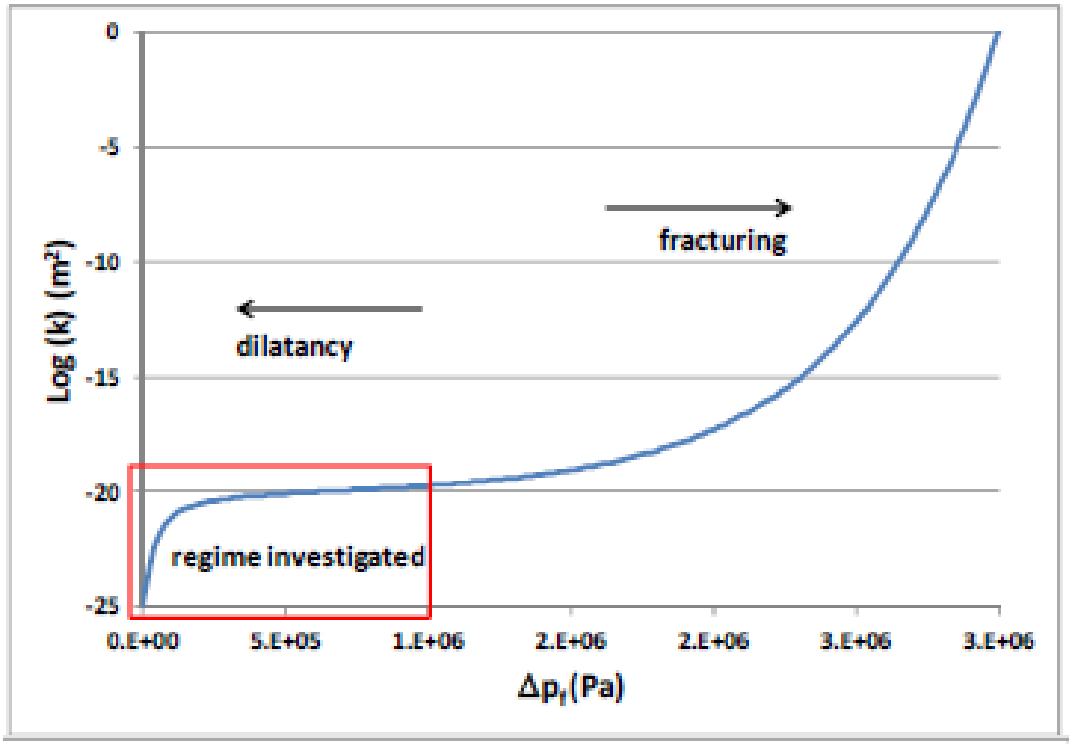

Figure 5-14. Relationship between permeability and fluid overpressure (fluid pressure less least principal stress magnitude) used in the modeling of pressure-induced fluid percolation (Rutqvist et al. 2012; Blanco-Martin et al. 2015a).

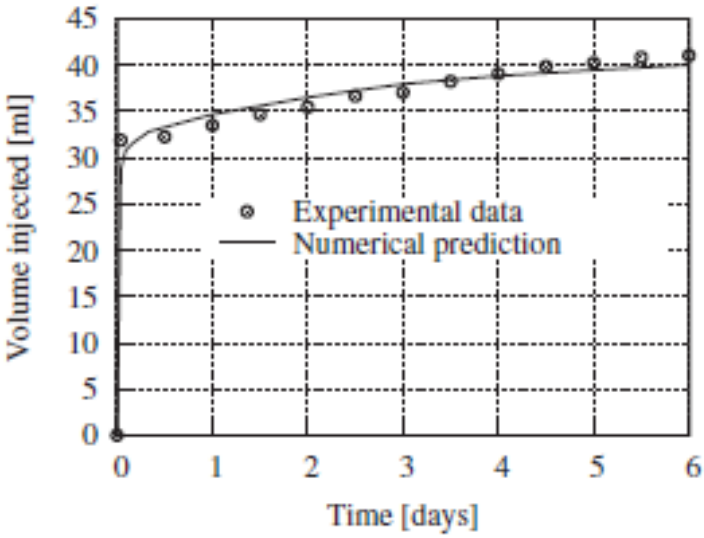

Figure 5-15. TOUGH-FLAC modeling and experiment data of cumulative injection volume in the pressure-induced percolation experiments on rock salt (Blanco-Martin et al. 2015a).

5.3.2 THM Modeling of long-term dilatant fluid percolation

Using such a model with a percolation threshold for $\Delta PFl \geq 0$, a number of simulations of the long-term THM behavior have illustrated how the pore pressure in the host rock and backfill can reach a maximum value approximately equal to the least principal *in situ* stress. For example in the long-term modeling presented in Blanco-Martin et al. (2015a), the pore-pressure increased as a results of thermal pressurization and compaction of the back-fill and stay high for up to 1000 years. In Blanco-Martin et al. (2015b), the effect of gas generation from the waste package on the barriers integrity was studied.

The basic model geometry is the same as the one shown in Figure 5-7. The material properties were also the same as those given in the above example, but with the original properties for host rock and crushed salt geomechanics determined from laboratory experiments. In this simulation considering constant gas generation at the waste package, the gas pressure increases and after about 10 years exceeds the initial stress of 14 MPa at the depth of the emplacement drift (Figure 5-16a). Over the long-term, because we assumed a constant gas generation, the pressure remains at 14 MPa all the time to the end of the simulation at 100,000 years. Backfill porosity has reached low values by the time the pore pressure increases (Figure 5-16b). Figure 5-17 shows how the over pressure propagates away from the drift to finally at 100,000 years extend about 70 m, which in the model was still within the bedded salt layer.

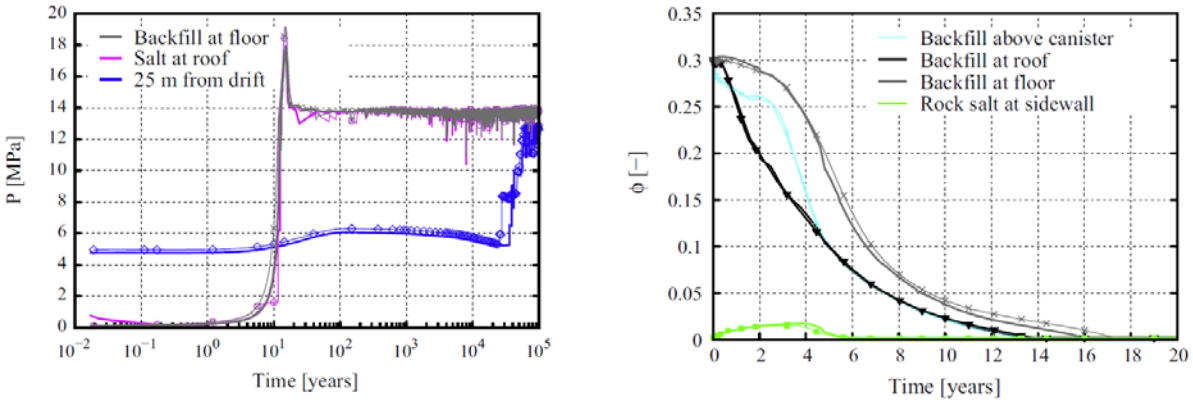

(a) (b)

Figure 5-16. TOUGH-FLAC modeling of long-term THM processes around during overpressure created by gas generation at the waste package. (a) gas pressure evolution in the backfill and salt host rock and (b) porosity evolution in the backfill showing sealing after about 18 years (Blanco-Martin et al. 2015b).

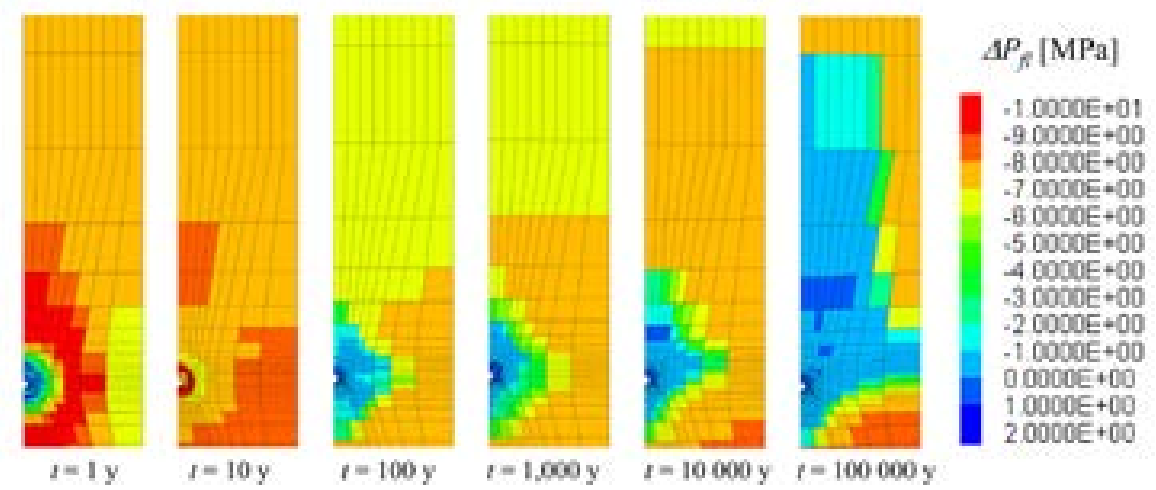

Figure 5-17. TOUGH-FLAC modeling of pressure-induced gas percolation as a result of overpressure created by gas generation at the waste package. (Blanco-Martin et al. 2015b).

5.3.3 Summary and Relevance to Long-term Isolation

Our modeling simulations clearly show that dilatant fluid migration in salt host rock is important over the long-term not only related to gas generation, but also relevant for migration of water and brine into the emplacement tunnel. In the model simulations, the constitutive relations for dilatant permeability enhancement are based on laboratory experiments on large cores conducted at TUC which have been modeled with TOUGH-FLAC for model validation. This is also relevant for migration of water and brine into the emplacement tunnel, which will affect moisture content within the backfill and thereby affect corrosion of container material and rate of compaction of the backfill which depends on water content. Though dilatant water and gas flow has been studied in the laboratory, dedicated field experiments with modeling would help to reduce the uncertainties associated with application of dilatant flow models in the field.

5.4 Halite dissolution and precipitation

As described in Section 4.1, TOUGH-FLAC was recently enhanced by considering the flow of brine and halite precipitation/dissolution effects. In this section we present the result of modeling of the laboratory experiment to validate TOUGH-FLAC for modeling porosity changes associated with salt precipitation/dissolution. We then investigated the long-term effects of halite precipitation and dissolution on the repository performance using the generic salt repository model. Salt precipitation/dissolution affects porosity and permeability of the porous salt (Olivella et al. 1996, 2011; Rege and Fogler 1989), which might impact the multiphase and heat transport behavior in the crushed backfill and host rock, including the evolution of moisture content in the backfill, which in turn could impact the rate of backfill compaction.

5.4.1 Model validation against laboratory experiment

In the FY2015 milestone report we presented details of the TOUGH2-EWASG model verification and validation related to salt precipitation/dissolution (Rutqvist et al. 2015). Here we briefly present the results of the simulation of a thermal test on crushed salt performed by Olivella et al. (2011). In the experiments, a thermal gradient was applied on several crushed salt

samples. The samples (cylindrical) were 100 mm long and had a diameter of 50 mm. The crushed salt grain size was about 1-2 mm. The temperature in the hot end was fixed at 85 °C and 5 °C were imposed in the cold end. The duration of each test was 65 days.

Figure 5-18 shows a comparison between experimental data and numerical results obtained by TOUGH2-EWASG. As the figure shows, the results are quite satisfactory. We highlight that the discrepancies observed in the cold end may be due to the fact that macro voids were observed in some samples due to water condensation and halite dissolution (Olivella et al. 2011).

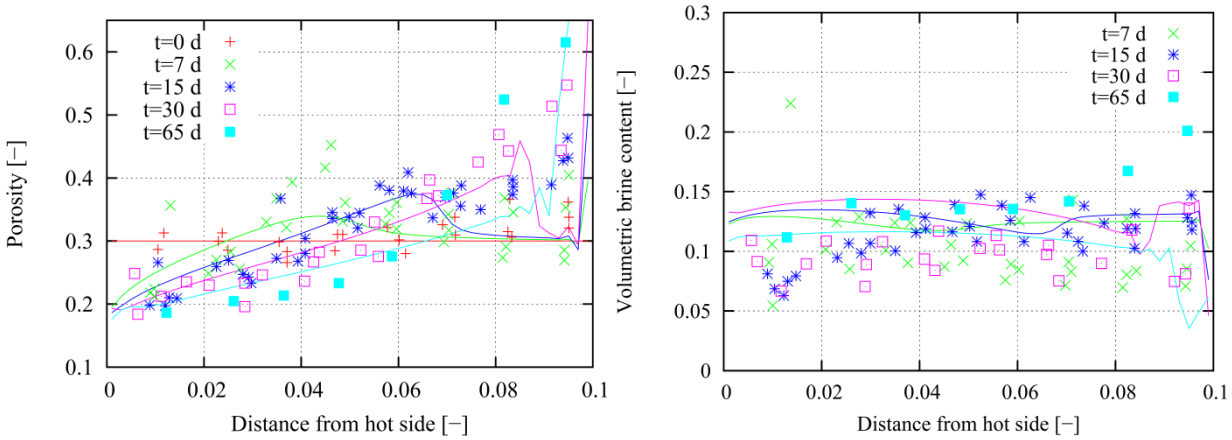

Figure 5-18. Thermal test on crushed salt performed by Olivella et al. (2011): comparison between measurements (points) and TOUGH-EWASG (solid lines).

5.4.2 Modeling long-term effects of halite precipitation and dissolution

After having validated EWASG against another code (CODE_BRIGHT) and measurements, we investigated the long-term effects of halite precipitation and dissolution on the repository performance using the generic salt repository model. In this case, permeability changes related to fluid infiltration and thermo-mechanically induced damage (host rock), as well as permeability changes related to compaction and fluid infiltration (crushed salt backfill) account for the presence of a solid phase in the pores. In other words, the permeability is calculated accounting for the effective porosity. The effect of halite precipitation on porosity was described in Equation (4.5). Then, the permeability is correlated to effective porosity based in experimental data (Bechthold et al. 2004) according to

$$k_{\text{crushed salt}} = 5.6810^{-11}\phi^{4.36} \tag{5.3}$$

where ϕ [-] is the current crushed salt porosity and $k_{\text{crushed salt}}$ [m^2] is the current crushed salt permeability. We note that Equation (5.3) is based on porosity data in the range 1.5-40 %.

In regards to backfill consolidation, our preliminary results suggest that there are no major differences when halite dissolution and precipitation effects are accounted for, at least in terms of time frame and final porosities reached (Rutqvist et al. 2015). This is based on the fact that the calculated crushed salt reconsolidation takes about 20 years to complete, which is consistent with previous THM coupled simulations in which halite dissolution and precipitation effects were not

accounted. Regarding the natural salt host rock, the processes that affect its tightness during the first years develop in a similar way when halite dissolution and precipitation are considered (thermo-mechanical damage in the EDZ and activation of healing processes as the backfill reconsolidation occurs). After seven years, the EDZ is sealed and the initial tightness of the rock restored.

Figure 5-19 shows the secondary permeability of the host rock after 10 years in two situations: when halite solubility is accounted for or disregarded. We note, at 10 years pore pressure has increased significantly in the host rock close to the drift due to the very low permeability of the formation, its saturated conditions and the high thermal expansion coefficient of the pore fluids relative to the host rock (thermal pressurization of the pore fluids). If the pore pressure locally exceeds the minimum compressive principal stress, fluid permeation occurs and a secondary permeability develops. This secondary permeability is shown in Figure 5-19. Therefore, two effects are represented in the figure: fluid permeation (present when halite solubility is accounted for or disregarded), and halite solubility. Indeed, as temperature decreases over time, both the pore pressure and the solubility of halite decrease, resulting in permeability decrease towards the characteristic value of undisturbed natural salt. Our results suggest the effects of halite solubility on permeability vanish after 100-200 years.

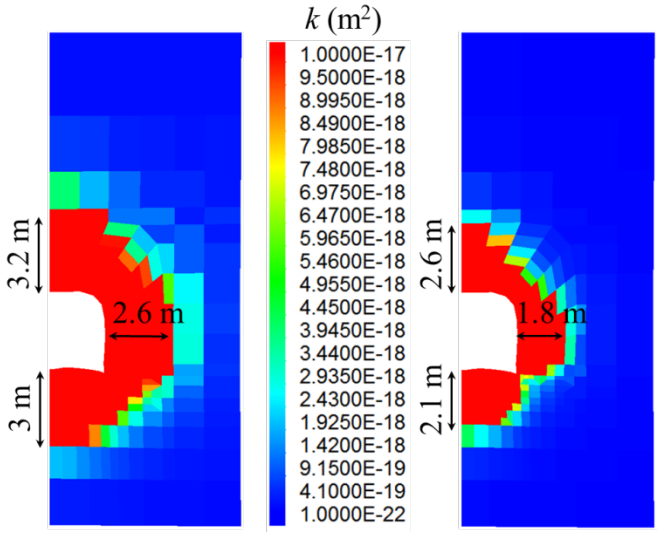

Figure 5-19. Generic Salt Repository in 2D (with solubility constraints): comparison of the area affected by secondary permeability (after 10 years) when halite solubility is accounted for (left) or disregarded (right).

5.4.3 Summary and Relevance to Long-term Isolation

The preliminary calculations conducted to date suggest that the backfill reconsolidation process is not affected noticeably when halite dissolution/precipitation is accounted for (in particular, the time for full reconsolidation and final porosities reached). Concerning the natural salt, the most important effect is related to the increasing solubility of halite with temperature, which affects the effective porosity. Assuming that porosity changes due to chemical effects influence permeability, our simulation results suggest that the extension of the area affected by a secondary permeability is greater when dissolution/precipitation is considered. However, these results are

preliminary and should be validated against experimental evidence. The timeframe during which chemical effects have a noticeable impact is dependent upon the heat power released from the waste packages, and extend between 10 and 100-200 years in the cases considered to-date. Field experiments with detailed monitoring of porosity distribution and evolution could help to confirm these findings.

INTENTIONALLY LEFT BLANK

6. A PORE SCALE MODEL FOR MIGRATION OF BRINE INCLUSIONS IN SALT CRYSTALS IN THERMAL GRADIENTS

In this section, we discuss the development of a pore scale model to simulate the migration of brine inclusions in salt crystals in thermal gradients. We begin by discussing the need for understanding brine migration under thermal gradients and current numerical modeling approaches. We present the necessity for a pore scale approach for understanding brine migration in salt formations. We then develop the mass and momentum conservation equations for brine inclusion migration in salt crystals, reactive transport equations, and a discussion of the implementation of these equations in the Chombo-Crunch pore scale code. We use the code to simulate the experiment results presented in Caporuscio et al. (2013).

6.1 Background

In the 1970s and 1980s, substantial brine-migration research for nuclear waste disposal were, at the time, focused primarily on brine inclusion migration caused by thermal gradients (e.g., Anthony and Cline 1971; Jenks and Claiborne 1981; Roedder and Chou 1982; Yagnik 1983; Olander 1984). These previous investigations show that when a temperature gradient is applied to an all-liquid inclusion, migration is driven by solubility differences. Because the solubility of salt increases with temperature, salt will dissolve at the interface closest to the heat source (the "hot" face), diffuse through the brine as a result of solution composition and temperature gradients, and precipitate at the interface furthest from the heat source (the “cold” face). This is brought about because the thermal conductivity of the salt is higher than that of the brine, which produces a higher temperature gradient within the liquid than the applied gradient to the solid (Yagnik 1983). Thus, the inclusions tend to migrate toward the heat source.

Numerical models for brine migration in thermal gradients use single- or dual-continuum approaches (Olivella et al. 1994; Kuhlman and Malama 2013; Rutqvist et al. 2014). In these approaches, the porous medium is conceptualized as a continuum, i.e., each point in space is assigned bulk properties that characterize this continuum (e.g., porosity, permeability) using the representative elemental volume (REV) concept. In contrast, in the pore scale approach, each point in space is assigned either to the solid or fluid phases; thus, there is no need to consider bulk properties for the porous medium. Rather, the size and shape of brine inclusions, and thus the solid-fluid interfaces are considered explicitly. Pore scale modeling constrained by pore scale observations (e.g., Caporuscio et al. 2013) can provide a useful tool to inform constitutive relationships applicable at the continuum scale.

6.2 Recent Pore Scale Observations

Caporuscio et al. (2013) examined brine inclusion migration in single salt crystals and salt aggregates as a function of thermal gradients. They found that brine in liquid-only inclusions and liquid/gas inclusions migrated toward the heat source when the salt crystals were subjected to thermal gradients. They found that brine inclusion migration velocity depended on the magnitude of the thermal gradient within the inclusion, the temperature of the hot face of the inclusion, the size of the inclusion, and the chemical composition of the brine. As a result of the continued dissolution precipitation process the chemical composition of the brine changes as the brine migrates up the thermal gradient. Near the heat source the brine composition becomes dominated by NaCl whereas away from the heat source a magnesium rich salt is precipitated.

These experiments reported by Caporuscio et al. (2013) are used here as conceptual basis for the development of our pore scale model and has focused on calibration of reactive parameters to match observed migration rates in these experiments. Here we focus on the migration of single-phase inclusions, i.e., for temperatures under 160°C.

6.3 Conceptual Model

The model developed here conceptualizes the simulation domain as being composed of salt and brine (Figure 6-1). The fluid–solid boundary ($\Gamma(\boldsymbol{x})$) is represented by a level set of a function $\phi(\boldsymbol{x}, t)$ such that:

$$\Gamma = \{x | \phi(\boldsymbol{x}, t) = c\} \tag{6.1}$$

where c is a constant, and the level-set function ϕ is greater than c for brine, and less than c for the solid phase (salt). A thermal gradient is prescribed along the X axis. As a result of the temperature gradient, a difference is established in the solubility of salt between the hot and cold faces of the inclusion. This drives dissolution at the hot face and precipitation at the cold face. As a result, the shape of the inclusion changes, and concentration gradients are established within the inclusion. These gradients result in saturation index gradients that continue to drive dissolution and precipitation.

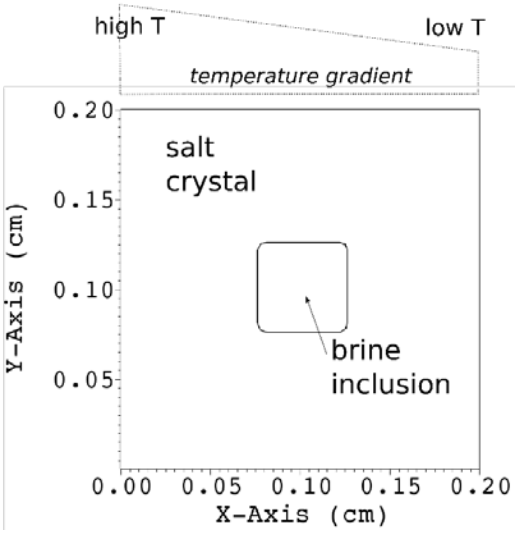

Figure 6-1. (a) Conceptual diagram that is the basis of the pore scape model. Spatial dimensions of the inclusion (0.5x0.5 mm) is derived from the experiments of Caporuscio et al. (2013).

6.4 Governing Equations

The Navier–Stokes equations are used to accurately describe single-phase flow of water in the inclusion via the conservation of momentum and mass, respectively:

$$\rho\left(\frac{\partial \mathbf{u}}{\partial \mathrm{t}} + (\mathbf{u}\cdot\nabla)\mathbf{u}\right) = -\nabla p + \mu\nabla^2\mathbf{u} \tag{6.2}$$

$$\nabla\cdot\mathbf{u} = 0 \tag{6.3}$$

where the left-hand side of Equation (6.2) describes the inertial forces, and the right-hand side includes the pressure gradient (∇p) and the viscous forces, with **u** being the fluid velocity, ρ the fluid density, and μ the dynamic viscosity. Inertial forces have their origin in the convective acceleration of the fluid as it flows through the tortuous pore space. Viscous forces originate in the friction between water molecules and are responsible for the dissipation of energy.

Transport and reaction of dissolved species in the brine are described by the following conservation equation:

$$\frac{\partial}{\partial t}\left(\rho M_{\mathrm{H_2O}} c_i\right) + \nabla\cdot\left(\mathbf{u}\rho M_{\mathrm{H_2O}} c_i - D_i\nabla\left(\rho M_{\mathrm{H_2O}} c_i\right)\right) = R_i \tag{6.4}$$

where c_i is the molal concentration of species i in solution (mol $kg^{-1}H_2O$), M_{H_2O} is the mass fraction of water (kg H_2O kg^{-1}), D_i is the diffusion coefficient (m^2 s^{-1}) and R_i is the reaction term (mol m^3 s^{-1}). The temperature dependence of the diffusion has been accounted for using the Einstein-Stokes equation.

Surface reactions are expressed as a boundary condition at the solid–fluid boundaries (**Γ**):

$$-D_i\left(\nabla\rho M_{\mathrm{H_2O}} c_i\right) = \xi_{im} r_m \tag{6.5}$$

where r_m is the surface reaction rate (expressed in units of mass per unit time per unit surface) and ξ_{im} is the stoichiometric coefficient of the *i*-th component in each surface reaction *m*.

For the dissolution–precipitation of salt mineral, the transition state theory law is employed:

$$r_m = k_m \exp\left[-\frac{E_a}{RT}\right]\prod a_i^n\left[1 - \exp\left(m_2\left(\frac{\Delta G}{RT}\right)^{m_3}\right)\right] \tag{6.6}$$

where k_m is the intrinsic rate constant (mol m^{-2} reactive surface s^{-1}), E_a is the activation energy (kcal mol^{-1}), $\prod a_i^n$ is a product representing the inhibition or catalysis of the reaction by various ions in solution raised to the power n, with a_i being the activity of species *I*, ΔG is the Gibbs free energy (kcal) with m_1, m_2, and m_3 being three parameters that affect the affinity dependence, R is the ideal gas constant (kcal K^{-1} mol^{-1}), and T is the temperature (K).

Dissolution and precipitation of salt minerals such as halite change the geometry of the brine inclusion. Mathematically, dissolution and/or precipitation can be formulated as a moving boundary, or Stefan problem. Assuming uniform dissolution–precipitation of a single-mineral

solid phase (m) (e.g., halite), the velocity of the moving solid–fluid interface (u_n^Γ) can be described by:

$$u_n^\Gamma = \mathbf{u}^\Gamma \cdot \boldsymbol{n} = V_m \, r_m \tag{6.7}$$

where V_m is the molar volume of the mineral. Equation (6.7) is solved along with Equations (6.2) to (6.6).

6.5 Numerical Formulation

The governing equations were implemented in the Chombo-Crunch code, which uses an embedded boundary-algebraic multigrid formulation based on a finite volume discretization (Molins et al. 2012, 2014; Trebotich et al. 2014). The pore scale model developed here thus employs the so-called direct numerical simulation approach with the use of conventional discretization methods to solve flow, transport, and geochemical equations. An operator splitting approach is used to couple flow, transport, reactions and brine-salt interface evolution. Solid-fluid interfaces are represented as embedded boundaries within each of the grid cells. The resulting cut cells are discretized by a finite volume method that accounted for the partial volumes occupied by both fluid and solid, and for the interfacial area between fluid and solid. Conservation equations are solved using a predictor-corrector projection method. A higher-order upwind method with a van Leer flux limiter is applied to advection terms in a semi-implicit Crank-Nicolson approach to minimize numerical dispersion. The movement of the interface is calculated using the approach outlined in Miller and Trebotich (2012). In this approach, the space-time discretization of divergence theorem is used to capture the time evolution of the brine-salt interface.

6.6 Model Setup and Parameters

A two-dimensional domain, 4x2 mm in size, is discretized using 128x32 cells. A brine inclusion, 0.5x0.5 mm in size is placed initially in the right side of the domain. The dimensions of the brine inclusion were obtained from the experiment reported in Figure 38 of Caporuscio et al. (2013) (Figure 6-1). A solution in equilibrium with respect with halite at 150°C is given as initial condition inside the inclusion. After time zero, a linear gradient of temperature is prescribed across the boundary such that the left boundary is in agreement with values in Figure 16 of Caporuscio et al. (2013) (Figure 6-2). Temperature in the left (‘hot’) boundary is 150°C and in the right boundary is 126°C. Both values are below 160°C, noted to be the temperature above which two-phase inclusions were observed (Caporuscio et al. 2013).

The solid phase was assumed to be composed of a single mineral, halite (NaCl). The rate of halite dissolution and precipitation was $10^{-0.21}$ mol/m2/s at 25°C (Palandri and Kharaka 2004), the activation energy was 7.4 KJ/mol; and equilibrium constant was interpolated between $10^{1.5780}$ at 100°C and $10^{1.4499}$ at 150°C. Transport of two components, Na+ and Cl-, with the corresponding diffusion coefficients sourced from Yuan-Hui and Gregory (1974).

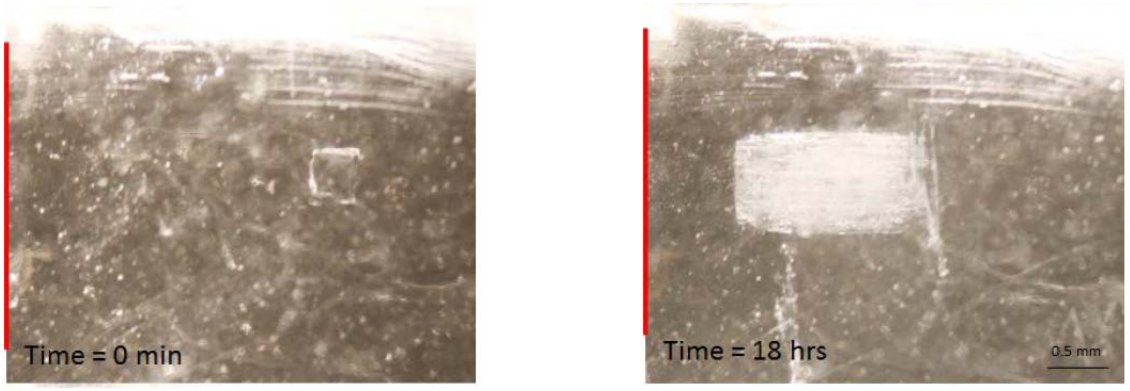

Figure 6-2. Still images showing the evolution of a single phase brine inclusion in a thermal gradient during a steady state migration. The left image was taken at the start of the heating and the right image was taken after 18 hours (taken from Caporuscio et al. 2013).

6.7 Results

Initial simulations with base values for the parameters significantly underestimated migration rates compared to those observed in Caporuscio et al. (2013). Consequently, a number of simulations were performed to study the sensitivity of model results to model parameters and obtain a good match to experimental results. In particular, reaction rate constants and diffusion coefficients were varied over an order of magnitude. The solution was not sensitive to variations of the rate constant, with migration rates almost unaffected by arbitrary changes in the value. This indicated that the rate of migration is controlled by the transport processes within the inclusion. This was confirmed increasing the diffusion coefficients significantly improved the match to observed migration rates.

Figure 6-3 shows simulation results at 18 hours for a simulation that yielded a reasonable match between the observed migration of the experiment by Caporuscio et al. (2013): 2.1 mm of simulation migration compared to observed 1.7 mm. Gradients in the degree of saturation of the brine with respect to halite drive the migration of the inclusion up the temperature gradient. The degree of supersaturation and undersaturation required to drive migration of the brine inclusion is found to be very small, i.e., $O(10^{-4})$.

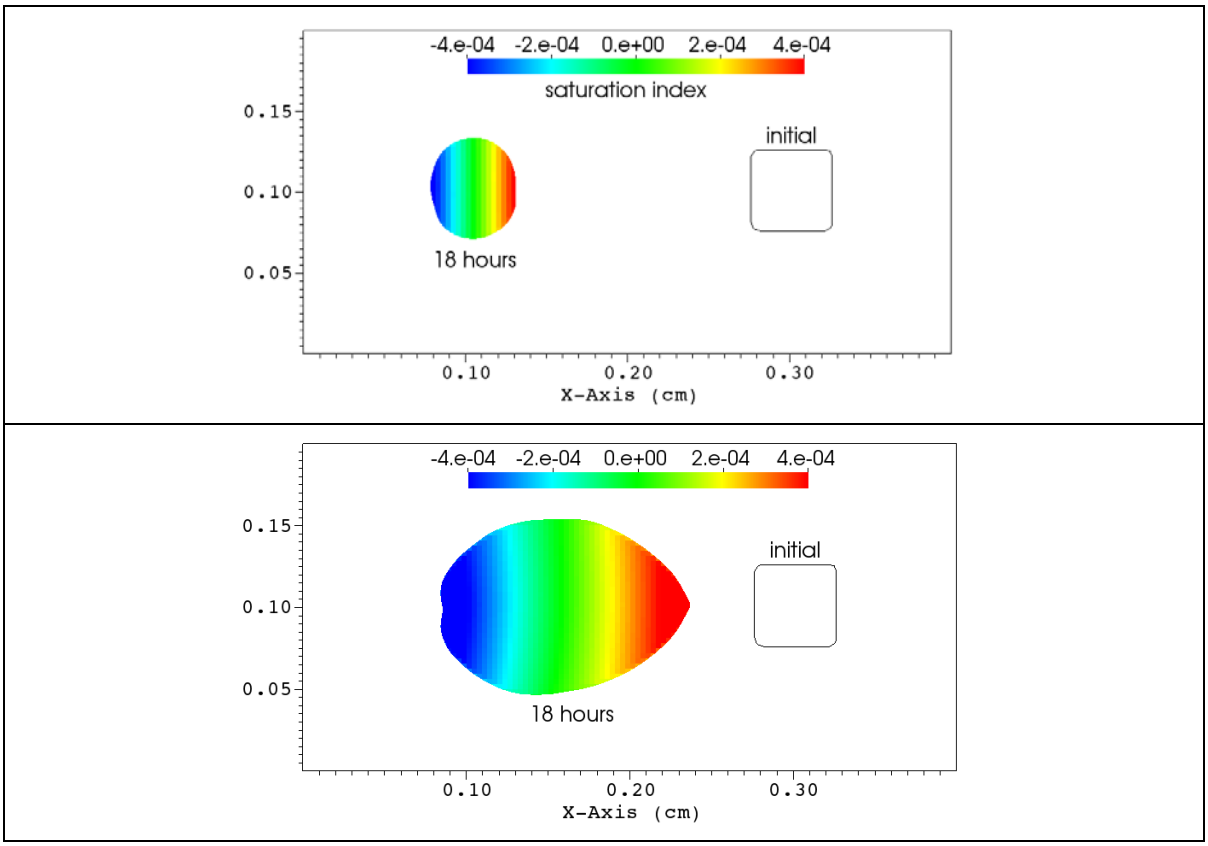

Figure 6-3. Saturation index of halite inside the brine inclusion simulation at 18 hours in relation to the initial location of the inclusion for (top) a simulation that assumes the dissolving and precipitating phase have the same properties and (bottom) a simulation that assumes that the precipitate has a smaller molar volume than the dissolving phase. Negative saturation indices indicate under saturated conditions and drive dissolution, while positive values drive precipitation.

The shape and volume of the inclusion (Figure 6-3, top), however, differs significantly from that observed in the experiments (Figure 6-2). In particular, the shape of the inclusion becomes more rounded and the width of the inclusion increases less than observed (simulated 6.3 mm versus 8.3 mm). More significantly the length of the inclusion in the direction of migration decreases rather than increasing as in the experiments. Previous modeling yielded similar results, in which the volume of the inclusion did not significantly change and the inclusion evolved to more rounded shapes (Chen et al. 2013).

Caporuscio et al. (2013) noted that near the heat source the brine composition becomes dominated by NaCl whereas away from the heat source a magnesium rich salt is precipitated. An additional simulation was conducted in this work to explore the effect of assigning different properties to the precipitating phase (Figure 6-3, bottom). In particular, the molar volume of the precipitate was arbitrarily reduced in half. As a result, the trailing edge of the inclusion migrated at a slower rate, and the volume of the inclusion increases. The trailing edge migrated 0.9 mm in contrast to the observed 0.7 mm, and the leading edge 1.9 mm compared to 1.67 mm. The shape is still considerably different. However, the evolution of the inclusion to a rounded shape is likely a short coming in the current state-of-the-art pore scale modeling, where any mineral

surface is assigned the same reactive properties regardless of their orientation.

6.8 Discussion and outlook

The rate of migration is limited by transport processes within the inclusion rather than reaction processes, in particular, as halite dissolution is a relatively fast reaction. As a result, capturing transport processes correctly is critical. Specifically, improved calibration of transport parameters and especially it'sn dependence on temperature is identified as a future line of work in order to improve our mechanistic understanding of brine inclusions in temperature gradients using pore scale modeling. In spite of the uncertainty of the parameters in the simulations presented here, a remarkably good agreement was found between the observed and simulated migration rates.

Simulation results presented here confirm the importance of the chemical composition of the brine in the migration of brine inclusion as identified by Caporuscio et al. (2013). Assigning a smaller molar volume to the precipitate was necessary to successfully capture the increasing inclusion volume as it migrated toward the heat source.

Improvements in pore scale modeling are still required to account for the crystalline structure of minerals, which feed to physical evolution pore structures.

Intentionally Left Blank

7. DEVELOPMENT OF CONTINUUM MODEL FOR SIMULATING BRINE MIGRATION IN SALT FORMATIONS

This section summarizes new development of a continuum model that will be implemented into TOUGH-FLAC to enable modeling of brine-inclusion migration into the coupled THM modeling framework.

7.1 Introduction

Usually bedded or domal salt, as a porous media contains a mixture of fluids in both liquid and gaseous phases in pores, and brine inclusions mostly in the form of liquid located within salt crystals. The nuclear waste generates heat establishing a thermal gradient in the salt. Under such a thermal gradient, brine-filled inclusions can migrate up the gradient and accumulate brine around the heat source (i.e., the stored nuclear waste), that may slowly corrode and degrade the waste package (Olander et al. 1980; Olander et al. 1981a, b; Roedder and Belkin 1980). The brine inclusions can migrate up the gradient because salt dissolves at the hot face of the inclusion, diffuses through the brine by molecular and thermal diffusion, and then crystalizes at the cold face. Therefore, it is important to analyze the migration of brine inclusions under thermal gradients to properly evaluate the performance of nuclear wastes storage in a salt repository.

A number of laboratory and *in situ* experiments were conducted for understanding the salt behavior and mechanism of brine migration associated with heat-generating waste storage in salt. (Kuhlman et al. 2012; Callahan et al. 2012; Kuhlman and Malama 2013; Kuhlman and Sevougian 2013). In the 1950s and 1960s, laboratory tests focused on understanding the linear Darcy flow in porous salt cores (Reynolds and Gloyna 1960; Gloyna and Reynolds 1961). From the 1970s to the mid-1980s, extensive experimental studies examined brine migration in salt at scales ranging from centimeters to meters in the laboratory and *in situ* in mine settings (Bradshaw and McClain 1971; Machiels et al. 1981; Yagnik 1982, 1983; Krause and Brodsky 1987; Nowak 1986; Nowak and McTigue 1987a; Rothfuchs et al. 1988).

Various numerical models were developed for coupled hydro-thermal-mechanical analysis under salt repository conditions, as reviewed by Kuhlman (2014), such models include a finite element code by Ratigan (1984), CODE_BRIGHT (Olivella et al. 1994), FEMH (Zyvoloski et al. 2011), and TOUGH-FLAC (Blanco-Martin et al. 2015a). However, none of these models are currently capable of modeling brine migration due to advective, diffusive and thermal forces, including release to the grain boundaries (or even transporting to other grains). Therefore, a model which can thoroughly consider such processes and their impact on the overall brine migration is desired.

In this study, we will first give a short overview of dual-continuum models and the potential advantages of the dual-continuum models in the following Section 7.2. Then we will develop a dual-continuum model for salt migration by constructing a dual-continuum conceptual model and derive the govern equations in Section 7.3. In Section 7.4, we develop a simplified finite volume method code for preliminary analysis of salt migration. The dual-continuum will be implemented in TOUGH2 and TOUGH-FLAC and compared with the current simplified FVM model, as introduced in Section 7.5.

7.2 A short overview of dual-continuum models

For transient problems such as advection, diffusion, or heat conduction, the computational domain may contain heterogeneities with very large contrasts of properties, or driven and dominated by very different sources. The basic equations can be described by the following equation:

$$\alpha \frac{\partial u_1}{\partial t} + \beta \frac{\partial u_2}{\partial t} = f(u_1) + g(u_2) \tag{7.1}$$

where u_1 and u_2 are the field variables, possibly with very different properties such as α and β, or governed by different principles represented by functions $f(u_1)$ and $g(u_2)$. Equation (7.1) can represent the mass balance, energy balance, and so on.

When the two types of material domains are governed by the same law and can be averaged through certain laws, Equation (7.1) can be simplified as:

$$\gamma \frac{\partial \bar{u}}{\partial t} = h(\bar{u}) \tag{7.2}$$

where γ, $\bar{u}$ and $h(\bar{u})$ are averaged values corresponding to those from Equation (7.1). Equation (7.2) is known as equivalent continuum model, as shown in Figure 7-1a.

When the contrast of material properties or the governing principles are very different between these two material domains, the dual-continuum concept provides an effective approach for such a problem.

One type of dual-continuum model for flow and transport analysis is known as the dual-porosity model. In the dual-porosity model, both of the two continua have porosities, but one may not necessarily be permeable, such as the model by Warren and Root (1963) and Birkholzer and Rouvé (1994). In such a model Equation (7.1) can be broken into the following two equations:

$$\begin{cases} \alpha \frac{\partial u_1}{\partial t} + \beta \frac{\partial u_2}{\partial t} = g(u_2) \\ \alpha \frac{\partial u_1}{\partial t} = L(u_1, u_2) \end{cases} \tag{7.3}$$

where $L(u_1, u_2)$ represented a simplified relationship between the two fields as a coupling term. In such a scheme, the field performance of the first continuum is not considered, while its coupling with the second continuum is considered, as shown in Figure 7-1b.

Another type of dual-continuum model for flow and transport analysis is known as dual-permeability model. In such a model, both of the two continua are active and they interact with each other by coupling terms, such as the model developed by Birkholzer and Rouvé (1994). Equation (7.1) is then broken into the following two equations:

$$\begin{cases} \alpha \frac{\partial u_1}{\partial t} = f(u_1) + C(u_1, u_2) \\ \beta \frac{\partial u_2}{\partial t} = g(u_2) - C(u_1, u_2) \end{cases} \tag{7.4}$$

where $C(u_1, u_2)$ represents the coupling between the two continua. Therefore, the perspective field performance as well as the interaction of the two media are considered, as depicted in Figure 7-1c. Such a way to transfer the original problem in Equation (7.1) to Equation (7.4) is very similar to a sequential coupling scheme for analyzing coupled hydro-mechanical processes in porous media. When the coupling between the two media is very strong, the coupling term $C(u_1, u_2)$ should be carefully derived, which may dramatically affect the accuracy and stability of the solution. Birkholzer and Rouvé (1994) discussed and compared existing dual-continuum approaches and provided a detailed derivation of coupling terms based on solid physical explanation for transport problems.

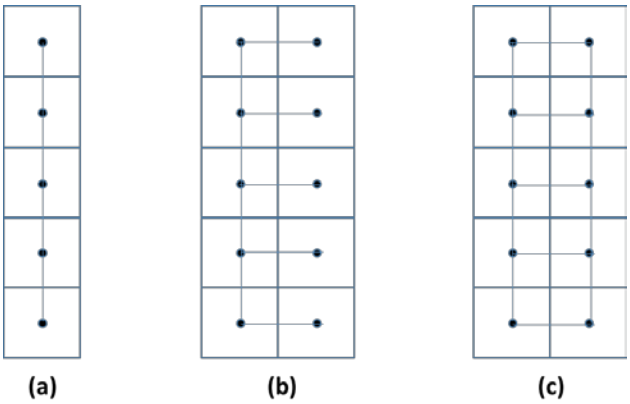

Figure 7-1. Schematic of 1D models as (a) single continuum, (b) dual-porosity, and (c) dual-permeability (Doughty 1999).

However, the field gradient may be very high in one of the two media. Without using fine mesh in the entire domain, first-order models are not precise enough to describe an abrupt change in that medium. Therefore, increased-order models were developed to address such a problem. As shown in Figure 7-2, several types of increased-order models are listed.

Figure 7-2a shows the MINC model used in TOUGH2 (Pruess and Narasimhan 1985), where the rock matrix continuum is discretized into several grids. These grids share the same center, and the interaction with each other can be simplified into several 1D flux exchange terms in different directions. Therefore, such a model is very effective based on the original first-order model in TOUGH2. Figure 7-2b shows another model named explicit discretization method (EDM) reported by Wu and Pruess (1988). EDM is computationally more expensive due to explicit equi-dimensional discretization requiring finer mesh compared with MINC. Moreover, the conformity between the rock matrix and fractures is problematic. As reported by Wu and Pruess (1988), compared with EDM, MINC gives more accurate solution for water imbibition. Figure 7-2c shows another formulation to consider immobile continuum regions (such as rock matrix) consisting of N blocks connected to each mobile continuum region (such as a fracture), described as multi-rate mass transfer (MRMT) formulation by Silva et al. (2009). The fundamental equation of the immobile blocks is represented by the second equation in Equation (7.3). And $L(u_m, u_{im,j}) = \alpha_j(u_m - u_{im,j})$, representing the interaction among the mobile and the *j*th immobile blocks. With the derived analytical solution of $u_{im,j}$, u_m can be numerically solved.

Such a scheme does not explicitly refine the mesh in the immobile blocks, instead, the usage of several immobile regions enhances the approximation orders by producing piecewise-linear approximation. Therefore, non-linear, high-gradient problems can be solved.

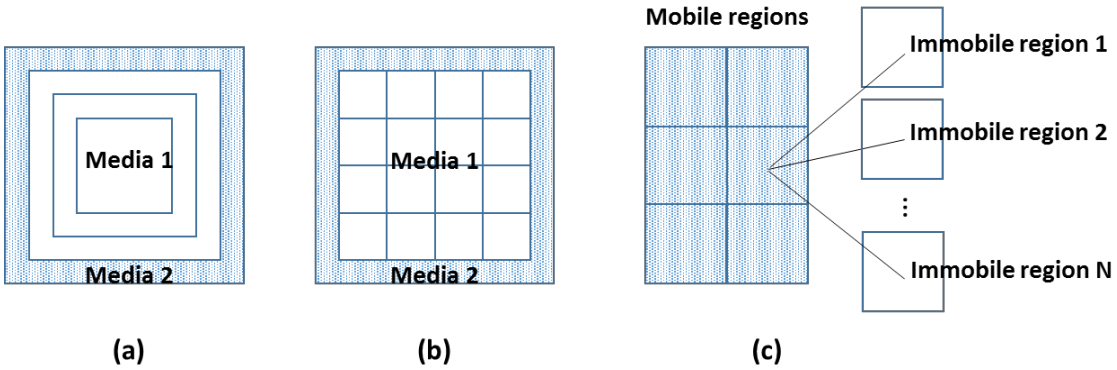

Figure 7-2. Schematic of dual-continuum-concept-based increased-order models

A dual-continuum model provides a good way to consider two media with different properties and field activities, and can be further extended for high-gradient problems, in this study we develop a dual-continuum model for salt migration.

7.3 A dual-continuum model for analyzing salt migration

7.3.1 Conceptual model and simplification

For porous water and brine migration in salt, we assume two types of continuum: the interconnected pores as the primary continuum and the salt grains as the secondary continuum. In the whole dual-continuum system, two components are considered, i.e., salt and water. The salt could be in dissolved or solid phase, considering dissolution and precipitation processes, and water could be in liquid or gaseous phase, considering vaporization or condensation. These two components exist in the two continua. A schematic of the dual-continuum model is shown in Figure 7-3.

The following simplifications and assumptions are made for the model:

(1) The only component in the gaseous phase is assumed to be water vapor. There may be a small amount of dry air and dissolved air contained in the pores, but the specific components may differ from case to case, with a negligible amount. Therefore, to simplify the model, in this study we only consider the water vapor, without additional components.

(2) No gas is considered within the salt grains. In rare cases when the brine inclusions contain gaseous bubbles, water evaporates at the hot side of these bubbles, migrate down to the cold side and condense. As these bubbles occur and disappear locally within the inclusions and are not naturally originated, they are not envisioned to play an important role for brine-inclusion migration. Therefore, in this study we assume no gas in the salt grains.

(3) No mechanical effects are considered. The coupled hydro-mechanical effects, such as the direct coupling in terms of deformation effects on the mass balance, and the indirect coupling in terms of deformation effects on the material properties are not considered for this study.

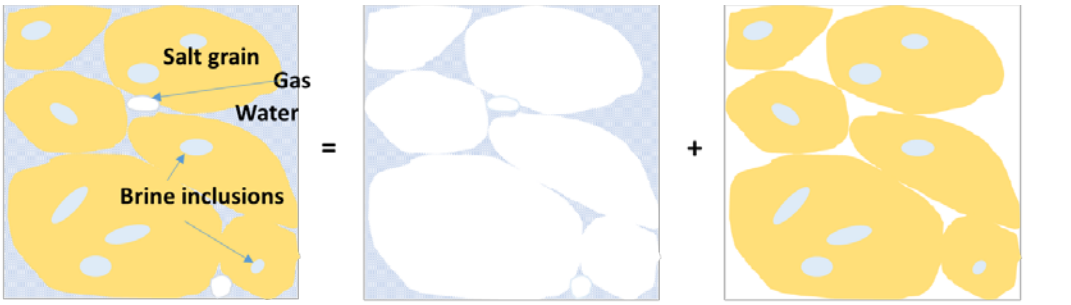

Components	In primary continuum	In secondary continuum
Salt	Salt (solid or dissolved)	Salt (solid or dissolved)
Water	Water (liquid and gas)	Water (liquid)

Figure 7-3. Schematic of the dual-continuum model for salt migration

7.3.2 Dual-continuum model governing equations

With above assumptions, the constitutive behavior listed in Table 7-1 will be considered in the new model.

Table 7-1 Constitutive laws used in the dual-continuum model

Components	Primary continuum	Secondary continuum	Coupling
Salt	Darcy`s law Fick`s law	Brine migration law	Brine migration-related salt migration flux as a sink/source
Water	Darcy`s law Fick`s law	Brine migration law	Brine migration flux as a sink/source

The mass balance of the salt in interconnected pore space is expressed as:

$$\frac{\partial(X_l^s \rho_l S_l \varphi)}{\partial t} = \nabla \cdot (X_l^s \mathrm{q}_l + \mathrm{F}_l^s) + X_s^s q_{inclusion} + q_{source}^s \tag{7.5}$$

where X_l^s is the mass fraction of salt in the liquid in the pores, ρ_l is the density of the liquid in pores, S_l is the saturation of the liquid, φ is the porosity, $X_s^s q_{migration}$ is the brine-migration

induced salt source in the pores (which will be introduced later), and q^s_{source} is the salt source in the pores, together with

$$\mathrm{q}_l = -\rho_l \frac{k k_{rl}}{\mu_l}(\nabla \mathrm{P}_l - \rho_l \mathrm{g}) \tag{7.6}$$

$$\mathrm{F}^s_l = -\varphi \tau_0 \tau_l \rho_l d^s_l \nabla X^s_l \tag{7.7}$$

representing the Darcy's law for advective flux and Fick's law for diffusive flux, respectively. In Equations (7.6) and (7.7), k is the absolute permeability of the interconnected pore space, k_{rl} is the liquid relative permeability, μ_l is the viscosity, $\mathbf{P_l}$ is the liquid fluid pressure, **g** is the gravitational acceleration, $\tau_0\tau_l$ represents the tortuosity (including a porous medium dependent factor τ_0 and a coefficient that depends on liquid saturation) and d^s_l is the molecular diffusion coefficient of salt in the liquid.

The mass balance of the salt in salt grains is expressed as:

$$\frac{\partial[(1-\varphi)X^s_s \rho_s]}{\partial \mathrm{t}} = \nabla \cdot (X^s_s \mathrm{v}_{inclusion}) - X^s_s q_{inclusion} \tag{7.8}$$

where X^s_s is the mass fraction of salt in the salt grains and $\mathbf{v}_{inclusion}$ is the brine inclusion velocity.

The mass balance of water in the interconnected pore space is expressed as:

$$\frac{\partial(X^w_l \rho_l S_l \varphi + X^w_g \rho_g S_g \varphi)}{\partial \mathrm{t}} = \nabla \cdot \left(X^w_l \mathrm{q}_l + \mathrm{q}_g + \mathrm{F}^w_l + \mathrm{F}^w_g\right) + X^w_s q_{inclusion} + q^w_{source} \tag{7.9}$$

where X^w_l is the mass fraction of water in the liquid, X^w_g is the mass fraction of water in the gas, ρ_g is the density of the gas in pores, S_g is the saturation of the gas, $X^w_s q_{migration}$ is the brine-migration induced water source in the pores (which will be introduced later), and q^w_{source} is the water source, together with

$$\mathrm{q}_g = -\rho_g \frac{k k_{rg}}{\mu_g}\left(\nabla \mathrm{P}_g - \rho_g \mathrm{g}\right) \tag{7.10}$$

$$\mathrm{F}^w_l = -\varphi \tau_0 \tau_l \rho_l d^w_l \nabla X^w_l \tag{7.11}$$

$$\mathrm{F}^w_g = -\varphi \tau_0 \tau_g \rho_g d^w_g \nabla X^w_g \tag{7.12}$$

representing the Darcy's law for advective flux in gas and Fick's law for diffusive flux in liquid and gaseous water, respectively. In Equation (7.10), k_{rg} is the gas relative permeability, μ_g is the viscosity of the gas, P_g is the gaseous fluid pressure, and d^w_l and d^w_g are the molecular diffusion coefficients of water in the liquid and gaseous phase, respectively.

The mass balance of water in the salt grains is:

$$\frac{\partial[(1-\varphi)X^w_s \rho_s]}{\partial \mathrm{t}} = \nabla \cdot (X^w_s \mathrm{v}_{inclusion}) - X^w_s q_{inclusion} \tag{7.13}$$

In Equations (7.5), (7.8), (7.9) and (7.13), the brine inclusion migration velocity $\mathbf{v}_{inclusion}$ and migration-induced sink/source $q_{inclusion}$ were derived by Anthony and Cline (1971) and used by Ratigan (1984) and Olivella et al. (1994). We follow their expressions as below:

$$\mathrm{v}_{inclusion} = -\rho_s \sigma (1-\varphi) D \nabla \mathrm{T} \tag{7.14}$$

$$q_{inclusion} = \frac{|\mathbf{v}_{inclusion}|}{d} \tag{7.15}$$

where ρ_s is the density of the salt, σ is the soret coefficient ($℃^{-1}$), D is the diffusivity of the brine, d is the ratio of the crystal volume to the crystal surface area.

Among the above equations, the following relationship should be satisfied:

$$\mathrm{P}_l = \mathrm{P}_g + \mathrm{P}_{capillary} \tag{7.16}$$

$$S_l + S_g = 1 \tag{7.17}$$

$$X_g^w = 1 \tag{7.18}$$

$$X_l^s + X_l^w = 1 \tag{7.19}$$

$$X_s^s + X_s^w = 1 \tag{7.20}$$

The energy balance in the whole system is:

$$\frac{\partial[(1-\varphi)\rho_s C_s T + \rho_g S_g \varphi u_g + \rho_l S_l \varphi u_l]}{\partial \mathrm{t}} = \nabla \cdot \mathrm{H} + f_{heat} \tag{7.21}$$

where u_g and u_l are the specific internal energy in gas and liquid, f_{heat} is the heat source, and

$$\mathrm{H} = -\lambda \nabla \mathrm{T} + h_l \mathrm{q}_l + h_g \mathrm{q}_g \tag{7.22}$$

where λ is the thermal conductivity, h_l and h_g are the specific enthalpy in liquid and gas, respectively.

Combining the above equations, we have the governing equations to describe the coupled hydro-thermal processes driven by advective, diffusive and thermal forces in the salt as well as in the interconnected pore space in the dual-continuum system.

7.4 Finite volume method model development of salt migration

7.4.1 Model description

Instead of using TOUGH2, we first develop a numerical model based on the finite volume method (FVM) for a simplified case, assuming only liquid flow occurs in the interconnected pore space. The primary variables are the unknowns of the equations and secondary parameters, which change with primary variables are listed in Table 7-2.

Table 7-2. Primary variables and secondary parameters used in the developed FVM

Primary variables	**Secondary parameters**
Mass fraction of water in the pores, X_l^w	Porosity, φ
Mass fraction of water in the salt grains, X_s^w	Density of pore fluid, ρ_l
Temperature, T	Density of salt grains, ρ_s
Fluid pressure, P_l	Liquid viscosity, μ_l

To solve the problem governed by Equations (7.5) to (7.22), we discretize a model with rectangular FV cells as shown in Figure 7-4. We use $u_n(x, y)$ to uniformly represent the primary variables, where x and y denote the coordinates of the center of the cells and n denotes the number of the cell, respectively. Different from the common FVM, the $u_n(x, y)$ on a cell n is:

$$\mathrm{u}_n(x,\ y) = \mathrm{u}_{n0} + \mathrm{u}_{n1}x + \mathrm{u}_{n2}y + \mathrm{u}_{n3}x^2 + \mathrm{u}_{n4}y^2 + \mathrm{u}_{n5}xy + \cdots \tag{7.23}$$

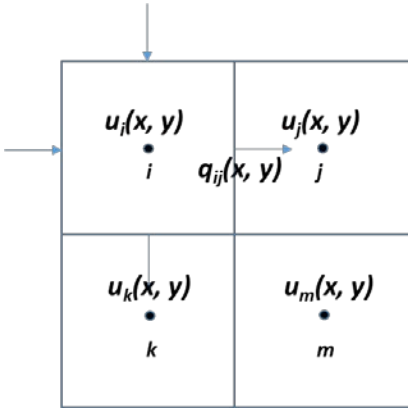

Figure 7-4. Schematic of discretization in the finite volume method

Equation (7.23), represents a first variable in cell n with an arbitrary order, consisting of a zero-order u_{n0} (representing a constantly distributed value on the entire cell n), a linear distribution with $\mathrm{u}_{n0} + \mathrm{u}_{n1}x + \mathrm{u}_{n2}y$ (representing a linearly distributed value on the entire cell n as a function of location), and a second-order distribution with $\mathrm{u}_{n0} + \mathrm{u}_{n1}x + \mathrm{u}_{n2}y + \mathrm{u}_{n3}x^2 + \mathrm{u}_{n4}y^2 + \mathrm{u}_{n5}xy$ (representing a second-order distributed value on the entire cell n as a function of location). In common FVM with first-order approximation, usually $\mathrm{u}_n(x,\ y) = \mathrm{u}_{n0}$ is used. However, the concept of dual-continuum makes it flexible to

increase approximation order for a certain primary variable possibly having high gradient while using constant values for other variables. Assuming a linear average, the gradient between two cells *i* and *j* is:

$$q_{ij}(x,\ y) = \frac{u_i(x,y) - u_j(x,y)}{d_{ij}} \tag{7.24}$$

where d_{ij} denotes the distance between the cells *i* and *j*. In this model, we first use constants for all the primary variables. Therefore, the formulation of mass balance written as

$$\int_{\Omega_n} m(t)dV = \int_{\Gamma_n} \nabla u d\Gamma + g(u) \tag{7.25}$$

can be transferred to:

$$m_n(t)V_n = \Sigma u_n s_{mn} + g(u) \tag{7.26}$$

Where V_n and s_{mn} are the volume of cell n and surface area of the cell *n* connected to cell *m*, respectively.

The equations are linearized by taking the mass fraction of salt and water in pores at the previous-time step, as coefficients of the pressure gradient. Then we use LU decomposition solver to solve this problem. With the linearization, the current model can be extended to fully coupled hydro-thermo-mechanical analysis. By introducing the mechanical equilibrium equation including pore pressure effects on effective stress and thermal expansion, and by considering the deformation effect on mass balance, the fully coupled THM analysis will be ready soon and used for comparison with TOUGH2 results.

7.5 Implementation in TOUGH2

The above FVM model does not consider gaseous phase in the pores, nor the phase change. In TOUGH2, we are going to develop the model based on the EWASG (Equation-of-State for Water, Salt and Gas) developed by Battistelli et al. (1997) for modeling salt migration. The fundamentals, including the establishment of the equations, the discretization and the solving of the nonlinear equations were introduced by Pruess et al. (1999). The EWASG, considering salt as an independent component with its dissolution and precipitation can be readily considered. Based on this, we just need to introduce the thermally-induced brine migration part. Further, approximation order needs to be improved, especially for mass fraction of the brine in salt grains, which may change fast under thermal gradient.

Compared with the developed FVM model, TOUGH2 can consider the gaseous phase in the pores and the corresponding phase transition. On the other hand, TOUGH2 uses Newton-Raphson iteration method to achieve the linear equations and several solvers are available to choose depending on the condition of the equations. Therefore, it is very desirable to develop the salt migration model based on the well-built TOUGH2 simulator. This work will be done in the next step and the results can be compared with the current FVM results.

7.6 Conclusions and perspectives

Salt migration under the effects of thermal gradients may have a significant impact on the integrity of the disposed nuclear waste in salt formations. In this study, we did a preliminary

study to develop a dual-continuum model for this problem. We set up the conceptual model and derived the governing equations first. Then, in order to study such a phenomenon, we developed a finite volume method code for salt migration and single-phase water flow under advective, diffusive and thermal effects. We verified with a few simple examples. This FVM code can be further extended to THM analysis by including the mechanical equilibrium equations, considering the couplings among thermal, hydraulic and mechanical fields.

On the other hand, based on the dual-continuum model, an increased-order TOUGH2 model can be developed with full consideration of two-phase flow and phase transition.

8. RELEVANCE TO LONG-TERM WASTE ISOLATION AND LINKS TO PA MODEL

The UFD Salt R&D program is approaching a shift in FY2017 towards a phased underground field testing program bringing together current UFD Salt R&D activities at Sandia, Los Alamos, and Lawrence Berkeley National Laboratories. This would start with the design of an intermediate field addressing the long-term waste isolation and performance issues in a salt media. In light of such proposed field testing, a number of findings and their relevance to the long-term waste isolation can be summarized as extracted from Section 4 above:

Drift compaction and sealing: Our modeling of TSDE experiment showed that previous laboratory calibrated parameters of creep parameters are not valid for very low deviatoric stress that prevails *in situ* and therefore the time required for complete drift convergence and sealing could be underestimated. Using creep parameters calibrated against the TSDE *in situ* convergence data, the time to complete compaction and sealing of the backfill in a generic repository extended from tens of years to hundreds of years. Further, our modeling of backfill compaction indicated some deviations in the calculated and measured stress evolution within the backfill. This may be due to that the constitutive model for backfill is not adequate to accurately capture the stress evolution, especially at high temperatures. Predictions of the compaction of the backfill and sealing are very important for the long-term performance assessment and therefore *in situ* experiments addressing creep at low deviatoric stress gradient and backfill compaction properties at high temperature would be very useful for reducing the uncertainties of such predictions.

Thermally induced brine-release and migration: Our study of the 1980s Room A1 brine-migration experiment at WIPP confirmed previous findings that the measured inflow could be explained by Darcy flow in a connected inter-crystalline pore network. The experiments inflow into heated boreholes at WIPP (Room A1 and B) in bedded salt showed that the inflow rate depends on the heat load, increasing the rate of inflow by one order of magnitude when wall temperature increases from maximum of 50°C to maximum above 100°C. Over less than a year of heating at Room B with wall borehole finally approaching 120°C, a total inflow volume of 22 liters was recorded. Our numerical modeling of Room A1 indicated that the inflow could be explained by the release of brine adjacent to the borehole flowing through increased permeability in the disturbed zone. Although the inflow could be explained by Darcy flow and not by transport of fluid inclusions, the movement of fluid inclusions to grain boundaries might contribute to the source of brine. The predictions of the brine-release and inflow into emplacement caverns are very important for long-term performance as water and brine can accelerate the corrosion of container materials and leach radioactive materials from waste forms. Similar heated borehole experiments could help to clarify the true mechanisms of brine-migration around a heat source and this should, if possible, be instrumented with monitoring surrounding the borehole.

Pressure induced dilatant fluid percolation: A number of our simulations of the long-term THM responses around emplacement tunnels containing heat releasing waste have shown some significant thermal pressurization with pore-pressure exceeding the pressure required for dilatant fluid migration. This has also been modeled related to simulated gas release from the waste package. In the model simulations, the constitutive relations for dilatant permeability enhancement are based on laboratory experiments on large cores conducted at

TUC which have been modeled with TOUGH-FLAC for validation. This is also relevant for migration of water and brine into the emplacement tunnel, which will affect moisture content within the backfill and thereby affect corrosion of container material and rate of compaction of the backfill which depends on water content. Though dilatant water and gas flow has been studied in the laboratory, dedicated field experiments with modeling would help to reduce the uncertainties associated with application of dilatant flow models in the field.

Halite precipitation and dissolution: Preliminary calculation results conducted to-date suggests the backfill reconsolidation process is not affected noticeably when halite dissolution/precipitation is accounted for (in particular, the time for full reconsolidation and final porosities reached). Concerning the natural salt, the most important effect is related to the increasing solubility of halite with temperature, which affects the effective porosity. Assuming porosity changes due to chemical effects influence permeability, our simulation results suggest that the extension of the area affected by a secondary permeability is greater when dissolution/precipitation is considered. However, these results are preliminary and should be validated based on experimental evidence. The time frame during which chemical effects have a noticeable impact is dependent upon the heat power released from the waste packages, and extend between 10 and 100-200 years in the cases considered to-date. Field experiments with detailed monitoring of porosity distribution and evolution could help to confirm these findings.

The above four items were presented by LBNL at a meeting between UFD Salt R&D partners on June 6, 2016, held for the planning of a phases field testing program to be started in FY2017. It was decided to focus the efforts on an initial small-diameter heater test to be conducted at the WIPP site. Such an experiment is very much in-line with the items related to thermally-induced brine-release and inflow, also TOUGH-FLAC will be upgraded with continuum modeling of brine inclusions will be one of the models used to support the design of such an experiment. Moreover, a small-diameter experiment might include several, if not all, of the above four items to various degrees. It will be important to properly design monitoring to be able measure these effects in the field.

The modeling of the small-diameter borehole experiment will also provide some validation of the model to be used for input into the PA model. These are very complex processes, including advanced constitutive models, and very time consuming calculations. For potential input into the PA model we first conclude that TOUGH-FLAC with salt constitutive THM models provides a tool for calculating the evolution of the crushed salt backfill and the host rock, including the disturbed rock zone (DRZ) from just after emplacement to over 100,000 years. Using TOUGH-FLAC, the analysis for coupling to the PA model might be conducted in a 2D cross-section of one emplacement drift or alternative a 3D model focused on the near field of an emplacement tunnel or a few emplacement tunnels in different parts of a repository and for different FEPs such as nominal case or such as for cases of extensive gas generation. The input required for such analysis is the site-specific geometry, heat source, THM properties of buffer and host rock, and THM conditions (such as in situ stress). The output to the PA model would be the changes in flow properties (e.g., permeability and porosity) in the Engineered Barrier System and near-field, including the buffer, and DRZ, and also to inform PA related to local flow created by coupled THM processes.

9. CONCLUSIONS

Leveraging on existing LBNL modeling capabilities, and by a very fruitful international collaboration with the Technical University of Clausthal (TUC), Germany, we have, within a few years, been able to develop and validate an advanced state-of-the-art numerical simulation tool for modeling of coupled THM processes in salt and have demonstrated its applicability to nuclear waste isolation. The DOE UFD campaign and LBNL greatly benefit from TUC's experience in salt geomechanics and modeling of salt TM processes using FLAC^{3D}. Equally, TUC benefits from LBNL's expertise in modeling multiphase and heat transport processes at high temperature with TOUGH2 as well as LBNL's experience with the TOUGH-FLAC simulator for the modeling coupled THM processes in nuclear waste isolation.

In FY2016 we conducted further verification, validation, and applications of the TOUGH-FLAC code and published the results in an international journal in collaboration with TUC. We completed code validation against the Asse Mine TSDE experiment, and published the results in a peer-reviewed journal paper:

- Blanco-Martín et al. (2016) "Thermal–hydraulic–mechanical modeling of a large-scale heater test to investigate rock salt and crushed salt behavior under repository conditions for heat-generating nuclear waste" in *Computers and Geotechnics*.

The modeling of the TSDE resulted in updated creep deformation parameters for salt rock, parameters that are difficult to determine in laboratory. Using these parameters, we updated the long-term THM modeling investigating the effect on the drift closure and sealing.

We conducted model validation against a 1980s *in situ* brine-migration experiment at the WIPP site, Room A1. In modeling the Room A1 brine-migration experiment we found good agreement with measured inflow measurements showing that the mechanisms of brine-migration towards the heat source in that case was indeed Darcy flow enhanced by thermal pressurization.

We conducted new model verification against analytical solutions related hydro-mechanical couplings, under small- and large-strain calculations. These verifications were conducted with the purpose of verification of the sequential coupling algorithm between TOUGH and FLAC^{3D} under strong pore-volume coupling. This is relevant for calculating pore-pressure changes when the porous media is mechanically squeezed, such as when excavating a tunnel or when crushed salt backfill is compacted in a repository tunnel.

We have in FY2016 completed pore-scale modeling of salt inclusion migration with comparison to laboratory experiments at LANL and developed a modeling approach for continuum modeling of brine inclusion movements. With the addition of brine inclusion modeling into the continuum framework of TOUGH-FLAC, a complete and comprehensive model will be available for applications to brine-migration under high temperature. Though the aforementioned Room A1 brine-migration experiment in bedded salt could be modeled without considering brine-inclusion migration, such processes might be more important in domal salt. Moreover, a comprehensive model containing all potentially relevant processes are necessary for identifying potential knowledge gaps and to investigate what are the potentially most relevant processes for short-term as well as for the long-term performance assessment.

The UFD Salt R&D program is approaching a shift from FY2017 towards a phased underground field testing program bringing together current UFD Salt R&D activities at different national laboratories. This would start with the design of an intermediate field addressing the long-term waste isolation and performance issues in a salt media. In light of such proposed field testing, a number of findings related to the long-term waste isolation in salt host media were summarized in the previous section related to:

- Drift compaction and sealing
- Thermally induced brine-release and migration
- Pressure induced dilatant fluid percolation
- Halite precipitation and dissolution

Our current understanding from coupled THM modeling is that the first three items—drift closure and sealing, thermally induced brine-release and migration, and pressure-induced dilatant fluid percolation—are most relevant for the long-term performance, whereas halite precipitation and dissolution did not affect our long-term results very significantly. The main effect of halite precipitation was that the extension of the area affected by a secondary permeability around the emplacement tunnel is greater when dissolution/precipitation is considered. There are still some uncertainties related to how long it will take for drift compaction and sealing, and field experiments such as the TSDE experiment at Asse Mine, which are extremely important in validating drift closure models.

The DOE UFD Salt R&D program has now decided to focus the efforts on an initial small-diameter heater to be conducted at the WIPP site. Such an experiment is very much in-line with the item related to thermally-induced brine-release and migration. TOUGH-FLAC will be upgraded with continuum modeling of brine inclusions will be one of the models used to support the design of such an experiment. By adding additional monitoring in the near field of such test, many other aspects of heating a previously undisturbed salt host rock can be studied. Thus, the pre-test modeling will be important to design such monitoring. The modeling of this experiment will also be an opportunity for developing a framework for pre-test modeling, post-test model evaluation, and inter-model comparison. This framework would be developed for the small-scale tests and carried forward into the design and execution of larger scale tests in the future.

In FY2017, LBNL will conduct coupled THM modeling to explicitly support UFD's phased salt field test campaign that is planned to start with a small-diameter borehole thermal test within the next five years. LBNL will conduct pretest THM modeling to support the design of the proposed small-diameter borehole thermal test and for inter-comparison with models from Sandia and Los Alamos National Laboratories. LBNL will apply the new continuum brine-migration modeling approach for intergranular and intragranular brine migration developed and presented in this milestone report. The continuum brine migration modeling approach will be implemented into the TOUGH2 simulator as well as linked to the FLAC^{3D} geomechanics. This will allow macroscopic modeling of brine release and transport near the small diameter heat source coupled with creep compaction at high temperatures. The modeling will also include salt dissolution/precipitation and explore changes in electric conductivity for monitoring. Other laboratory and field data including literature data may also be used for model validation. Additional pore-scale modeling would be useful to shed more light on the underlying

mechanisms of brine-inclusion migration that could feed the development and application of the continuum brine-inclusion modeling at field scale. In addition LBNL will continue the fruitful collaboration with TUC and Professor Lux's team, and may perform further benchmark exercises regarding the disposal of heat-generating nuclear waste in saliferous formations (natural salt host rock and crushed salt backfill).

Intentionally Left Blank

10. ACKNOWLEDGMENTS

Funding for this work was provided by the Used Fuel Disposition Campaign, Office of Nuclear Energy, of the U.S. Department of Energy under Contract Number DE-AC02-05CH11231 with Lawrence Berkeley National Laboratory.

Intentionally Left Blank

11. REFERENCES

Abousleiman, Y., Cheng, A.H.-D., Cui, L., Detournay, E., Roegiers, J.-C., 1996. Mandel's problem revisited. Géotechnique, 46(2), 187-195.

Anthony, T.R. and Cline, H.E., 1971. The thermal migration of liquid droplets through solids, Journal of Applied Physics, 42:3380–3387.

Battistelli, A., Calore, C. and Pruess, K. 1997. The simulator TOUGH2/EWASG for modelling geothermal reservoirs with brines and a non-condensible gas. *Geothermics* 26(4): 437-464.

Battistelli, A. 2012. Improving the treatment of saline brines in EWASG for the simulation of hydrothermal systems. In *Proceedings TOUGH Symposium 2012, Berkeley, 17-19 September 2012*.

Bechthold, W., Rothfuchs, T., Poley, A., Ghoreychi M, Heusermann S, Gens A et al. Backfilling and Sealing of Underground Repositories for Radioactive Waste in Salt (BAMBUS Proj). Eur Atomic Energy Community, 1999. Rep EUR19124 EN.

Bechthold, W., Smailos, E., Heusermann, S., Bollingerfehr, W., Bazargan Sabet, B., Rothfuchs, T., Backfilling and Sealing of Underground Repositories for Radioactive Waste in Salt (BAMBUS II Proj). Eur Atomic Energy Community, 2004. Rep EUR20621 EN.

Benz, T., 2007. Small-strain stiffness of soils and its numerical consequences. Ph.D. thesis: University of Stuttgart (Germany).

Birkholzer, J.T. and Rouvé, G., 1994. Dual-continuum modeling of contaminant transport in fractured formations, In: Computational Methods in Water Resources X, A. Peters et al. (eds.), Kluwer Academic Publishers, Amsterdam, The Netherlands.

Blanco-Martín, L., Rutqvist, J., Birkholzer, J.T. Long-term modelling of the thermal-hydraulic-mechanical response of a generic salt repository for heat-generating nuclear waste. *Engineering Geology*, 193, 198–211 (2015a).

Blanco-Martín, L., Wolters, R., Rutqvist, J., Lux, K.-H., Birkholzer, J.T. Comparison of two simulators to investigate thermal-hydraulic-mechanical processes related to nuclear waste isolation in saliniferous formations. Computers and Geotechnics, 66, 219–229 (2015b).

Blanco-Martín, L., Wolters, R., Rutqvist, J., Lux, K.-H., Birkholzer, J.T. Thermal–hydraulic–mechanical modeling of a large-scale heater test to investigate rock salt and crushed salt behavior under repository conditions for heat-generating nuclear waste. *Computers and Geotechnics*, 77, 120–133 (2016).

Booker, J.R. and Savvidou, C. 1985. Consolidation around a point heat source. International Journal for Numerical and Analytical Methods in Geomechanics, 9, 173-184.

Bradshaw, R.L. and McClain, W.C. Project Salt Vault: A demonstration of the disposal of high-activity solidified wastes in underground salt mines. ORNL-4555, Oak Ridge National Laboratory, Oak Ridge, TN, 1971.

Callahan, G.D. and DeVries, K.L. 1991. *Analyses of Backfilled Transuranic Waste Disposal Rooms*. Report SAND-91-7052: RE/SPEC Inc. (Prepared for Sandia National Laboratories), Rapid City, SD (USA).

Callahan, G.D., Guerin, D.C., Levitt, D.G., Newell, D.L., Robinson, B.A., and Van Sambeek, L.L. (2012). Salt Repository Synthesis Data of Non-Delaware Basin and International Programs for the Storage/Disposal of Nuclear Waste. FCRD-UFD-2012–000312, U.S. DOE, Used Fuel Disposition Campaign.

Camphouse, R.C., Gross, M., Herrick, C.G., Kicker, D.C., and Thompson, B. 2012. Recommendations and Justifications of Parameter Values for the Run-of-Mine Salt Panel Closure System Design Modeled in the PCS-2012 PA. Final memo: Sandia National Laboratories, Albuquerque, NM (USA).

Caporuscio, F.A., Boukhalfa, H., Cheshire, M.C., Jordan, A.B., and Ding, M. 2013. Brine migration experimental studies for salt repositories, LA-UR-13-27240, Los Alamos National Laboratory, Los Alamos, NM.

Carter, J., Luptak, A. and Gastelum, J. 2011. *Fuel Cycle Potential Waste Inventory for Disposition*. Report FCR&D-USED-2010-000031 Rev 5: Prepared for US DOE Used Nuclear Fuel (USA).

Cinar, Y., Pusch, G., Reitenbach, V. 2006. Petrophysical and Capillary Properties of Compacted Salt. Transp. Porous Med. 64, 199–228. doi: 10.1007/s11242-005-2848-1.

Chen, L., Q. Kang, B. A. Robinson, Y.-L. He, and W.-Q. Tao (2013), Pore-scale modeling of multiphase reactive transport with phase transitions and dissolution-precipitation processes in closed systems, Phys. Rev. E, 87(4), 43306, doi:10.1103/PhysRevE.87.043306.

Coussy, O. 2004. *Poromechanics*. 1st ed. Chichester: John Wiley and Sons.

DBE. 2001 Numerische Untersuchungen zum Konvergenzverhalten eines Einzelhohlraumes. DBE Technology GmbH, Rep 22341011.

Dean, R.H., Gai, X., Stone, C.M., Minkoff, S.E. 2006 A comparison of techniques for coupling porous flow and geomechanics. SPE J 2006;11(1):132–40.

Doughty, C. 1999. Investigation of conceptual and numerical approaches for evaluating moisture, gas, chemical, and heat transport in fractured unsaturated rock. J. Contam. Hydrol. 38 (1– 3), 69– 106.

Gloyna, E.F. and Reynolds, T.D. 1961 Permeability measurements of rock salt. Journal of Geophysical Research, 66(11):3913–3921.

Hou, Z. 2003. Mechanical and hydraulic behaviour of rock salt in the excavation disturbed zone around underground facilities. International Journal of Rock Mechanics and Mining Sciences 40, 725-738. doi:10.1016/S1365-1609(03)00064-9.

Hou, Z. and Lux, K.-H. 1998. Ein neues Stoffmodell für duktile Salzgesteine mit Einbeziehung von Gefügeschädigung und tertiärem Kriechen auf der Grundlage der Continuum-Damage-Mechanik. Geotechnik 21(3), 259–263.

Hou, Z., Lux, K.-H. and Duesterloh, U., 1998. Bruchkriterium und Fließmodell für ductile Salzgesteine bei kurzzeitiger Beanspruchung. Glueckauf-Forschungshefte 59(2), 59–67.

Hou, Z. and Lux, K.-H., 1999. A constitutive model for rock salt including structural damages as well as practice-oriented applications. In: Proceedings of the Fifth Conference on the Mechanical Behaviour of Salt, Bucharest, Romania, pp. 151–169.

Hou, Z. and Lux, K.-H., 2000. Ein Schädigungsmodell mit Kriechbruchkriterium für duktile Salzgesteine auf der Grundlage der Continuum- Damage-Mechanik. Bauingenieur 75(13), 300–307.

Itasca. 2011 FLAC^{3D} (Fast Lagrangian Analysis of Continua in 3 Dimensions), Version 5.0. Minneapolis: Itasca Consulting Group.

Jenks, G.H., and Claiborne, 1981. Brine migration in salt and its implications in the geologic disposal of nuclear waste, ORNL-5818, Oak Ridge National Laboratory, Oak Ridge, TN.

Jové-Colón, C., Greathouse, J.A., Teich-McGoldrick, S., Cygan, R.T. , Hadgu, T., Bean, J.E., Martínez, M.J., Hopkins, P.L., Argüello, J.G. and Hansen, F.D., 2012. *Evaluation of Generic EBS Design Concepts and Process Models: Implications to EBS Design Optimization*. Report FCRD-USED-2012-000140: Sandia National Laboratories, Albuquerque, NM (USA).

Kachanov, LM. 1986. Introduction to Continuum Damage Mechanics. 1st ed. Dordrecht: Martinus Nijhoff Publishers.

Kelly, W. 1985. Brine migration in salt, Topical Report 8505060429, Nuclear Regulatory Commission, Washington, DC.

Kim, J., Tchelepi, H.A., Juanes, R., 2011. Stability and convergence of sequential methods for coupled flow and geomechanics: fixed-stress and fixed-strain splits. Comput. Methods Appl. Mech. Eng. 200 (13-16), 1591–1606. http://dx.doi.org/10.1016/j.cma.2010.12.022.

Kim, J., Sonnenthal, E., Rutqvist, J. 2012 A modeling and sequential numerical algorithms of coupled fluid/heat flow and geomechanics for multiple porosity materials. International Journal of. Numerical. Methods in Engineering. 92, 425–456.

Kim, J., Tchelepi, H.A., Juanes, R., 2013. Rigorous coupling of geomechanics and multiphase flow with strong capillarity. SPE J. 18 (6), 1123–1139.

Krause, W.B. and Brodsky, N.S. 1987 Intracrystalline brine inclusion motion for Palo Duro unit 5 salt from the Mansfield no. 1 borehole in Oldham County, Texas. BMI/ONWI-663, Office of Nuclear Waste Isolation, Columbus, Ohio.

Kuhlman, K.L., and Malama, B. 2013. Brine flow in heated geologic salt, SAND2013-1944, Sandia National Laboratory, Albuquerque, NM.

Kuhlman, K.L. 2014. S*ummary Results for Brine Migration Modeling Performed by LANL, LBNL and SNL for the UFD Program*. Report FCRD-UFD-2014-000071: Sandia National Laboratories (Prepared for US DOE UFD), Albuquerque, NM (USA).

Kuhlman, K.L. and Sevougian, S.D. 2013. Establishing the technical basis for disposal of heatgenerating waste in salt. FCRD-UFD-2013–000233, US Department of Energy Used Fuel Disposition Campaign, Albuquerque, NM (USA).

Kuhlman, K. L., Wagner, S., Kicker, D., Kirkes, R., Herrick, C., Guerin, D. 2012. Review and evaluation of salt R&D data for disposal of nuclear waste in salt. FCRD-UFD-2012–000380, US Department of Energy Used Fuel Disposition Campaign, Carlsbad, NM (USA)..

Lerche, S. 2012 Kriech- und Schädigungsprozesse im Salinargebirge bei mono- und multizyklischer Belastung. Ph.D. Dissertation, TU Clausthal.

Leverett, M.C., 1941. Capillary behaviour in porous solids. Petroleum Transactions, AIME(192), 152-169.

Lux, K-H. 1984 Gebirgsmechanischer Entwurf und Felderfahrung im Salzkavernenbau: Ein Beitrag zur Entwicklung von Prognosemodellen für den Hohlraumbau im duktilen Salzgebirge. 1st ed. Stuttgart: Ferdinand Enke Verlag.

Machiels, A.J., Yagnik, S., Olander, D.R., Kohli, and R. 1981, The mechanism of intragranular migration of brine inclusions in salt. Transaction of the American Nuclear Society, V38: pp 169-170.

Mandel, J. 1953. La consolidation des sols (étude mathématique). Géotechnique 3(7), 287-299.

Miller, G.H. and Trebotich D. 2012 "An Embedded Boundary Method for the Navier-Stokes Equations on a Time-Dependent Domain", Communications in Applied Mathematics and Computational Science, 7(1):1-31,

Minkley, W. and Popp, T. 2010. Final Disposal in Rock Salt- Geomechanical Assessment of the Barrier Integrity. Proceedings of the 44th U.S. Rock Mechanics Symposium, Salt Lake City, Utah, USA, June 27-June 30, 2010: American Rock Mechanics Association ARMA, Paper No. 492.

Molins, S., Trebotich, D., Steefel, C.I., Shen, C. (2012) An investigation of the effect of pore scale flow on average geochemical reaction rates using direct numerical simulation. Water Resour Res 48: WR03527

Molins, S., Trebotich, D., Yang, L., Ajo-Franklin, J.B., Ligocki, T.J., Shen, C., Steefel, C.I. (2014) Pore-scale controls on calcite dissolution rates from flow-through laboratory and numerical experiments. Environ Sci Technol 48:7453–7460

Nowak, E.J. 1986. Preliminary results of birne migration studies in the Waste Isolation Pilot Plant (WIPP). Report SAND-86-0720: Sandia National Laboratories, Albuquerque, NM (USA).

Nowak, E.J. and McTigue, D.F. 1987a. Interim results of brine transport studies in the Waste Isolation Pilot Plant (WIPP). Report SAND -87-0880: Sandia National Laboratories, Albuquerque, NM (USA).

Nowak, E.J. and McTigue, D.F. 1987b. Brine transport studies in bedded salt of the waste isolation pilot plant. Report SAND -87-1274c: Sandia National Laboratories, Albuquerque, NM (USA).

Nutt, M. 2011. Used Fuel Disposition Campaign Disposal Research and Development Roadmap (FCR&D-USED-2011-000065 REV0), U.S. DOE Used Fuel Disposition Campaign.

Olander, D.R., Machiels, A.J., Balooch, M.; Muchowski, E., Yagnik, S.K. 1980 Thermomigration of brine inclusions in sodium chloride single crystals" Trans. Am. Nucl. Soc.; V34: pp 352-353.

Olander, D.R., Machiels, A.J., Yagnik, S.K. 1981a, Thermomigration of two-phase inclusions in salt, Trans. Am. Nucl. Soc.;, V35: pp 168-169.

Olander, D.R.; Machiels, A.J.; Muchowski, E. 1981b, Migration of Gas-liquid inclusions in single crystals of potassium and sodium chlorides, Nuclear Science and Engeneering, V79 (2): pp 212-227.

Olander, D.R., 1984. A study of thermal-gradient induced migration inclusions in salt: Final report, BMI/ONWI-538, Regents of the University of California, Oakland, CA.

Olivella, S., Carrera, J., Gens, A., Alonso, E.E. 1994. Nonisothermal multiphase flow of brine and gas through saline media, Transport in Porous Media, 15:271–293.

Olivella, S., Carrera, J., Gens, A., Alonso, E.E. 1996. Porosity Variations in Saline Media Caused by Temperature Gradients Coupled to Multiphase Flow and Dissolution/Precipitation. Transp Porous Med 25:1-25.

Olivella, S., Castagna, S., Alonso, E.E. and Lloret, A. 2011. Porosity variations in saline media induced by temperature gradients: experimental evidences and modelling. Transp Porous Med 90:763-777.

Palandri, J. and Kharaka, Y. (2004). A compilation of rate parameters of water-mineral interaction kinetics for application to geochemical modeling, U.S. GEOLOGICAL SURVEY OPEN FILE REPORT (OF 2004-1068).

Popp, T., Kern, H., Schulze, O. 2001. Evolution of dilatancy and permeability in rock salt during hydrostatic compaction and triaxial deformation. J Geophys Res;106(B3):4061-78. doi: 10.1029/2000JB900381.

Popp, T. and Minkley, W. 2010. Salt barrier integrity during gas pressure build-up in a radioactive waste repository – Implications from lab and field investigations. Proceedings of the 44th U.S. Rock Mechanics Symposium, Salt Lake City, Utah, USA, June 27-June 30, 2010: American Rock Mechanics Association ARMA, Paper No. 492.

Pruess, K. and Narasimhan, T.N. 1985. A practical method for modeling fluid and heat flow in fractured porous media, Society of Petroleum Engineers Journal, 25: 14-26.

Pruess, K., Oldenburg, C., and Moridis, G. 1999. TOUGH2 user's guide, version 2. Berkeley: Lawrence Berkeley Natl Lab; 2012 [Rep LBNL-43134].

Pruess, K., Oldenburg, C., and Moridis, G. 2012. TOUGH2 user's guide, version 2.1. Berkeley: Lawrence Berkeley Natl Lab; 2012 [Rep LBNL-43134 (revised)].

Ratigan, J.L. 1984. A finite element formulation for brine transport in rock salt, International journal for numerical and analytical methods in geomechanics, 8: 225-241.

Rege, S.D. and Fogler H.S. 1989. Competition among flow, dissolution and precipitation in porous media. AIChE J. 35(7):1177-1185.

Reynolds, T.D. and Gloyna, E.F. 1960 Reactor fuel waste disposal project: Permeability of rock salt and creep of underground salt cavities. TID-12383, Atomic Energy Commission Division of Technical Information, Oak Ridge, TN.

Roedder, E. and Belkin, H.E. 1980. Thermal gradient migration of fluid inclusions in single crystals of salt from the Waste Isolation Pilot Plant (WIPP), Scientific Basis for Nuclear Waste Management, Vol. 2 (1980) Edited by Clyde J.M. Northrup, Jr., Plenum Publishing Corporation, New York, NY.

Roedder, E, and Chou, L.M. 1982. A critique of "Brine migration in salt and its implications in the geologic disposal of nuclear waste," Oak Ridge National Laboratory Report 5818, by G.H. Jenks and H.C. Claiborne, USGS Open-File Report 82-1131.

Rothfuchs, T., Wieczorek, K., Feddersen, H.K., Stupendahl, G., Coyle, A.J., Kalia, H., and Eckert, J. 1988 Brine migration test, Asse salt mine, Federal Republic of Germany: Final report. GSF-Bericht 6/88, Office of NuclearWaste Isolation (ONWI) and Gesellschaft f¨ur Strahlenund Umweltforschung M¨unchen (GSF), Munich, Germany.

Rutqvist, J. 2011 Status of the TOUGH-FLAC simulator and recent applications related to coupled fluid flow and crustal deformations. Computers & Geosciences, 37, 739–750.

Rutqvist, J., Blanco Martín, L., and Houseworth, J. 2012. THM Coupled Process Modeling with TOUGHFLAC to Evaluate the Fate and Transport of Water in a Salt-Based Repository. Report FCRD-UFD-2012-000297.

Rutqvist, J., Blanco Martín, L., Mukhopadhyay, S., Houseworth, J. Birkholzer, J. 2014 Modeling Coupled THMC Processes and Brine Migration in Salt at High Temperatures, LBNL-6718E, Lawrence Berkeley National Laboratory.

Rutqvist, J., Blanco Martin, L., Molins S., Trebotich D., and Birkholzer J. 2015 Modeling Coupled THMC Processes and Brine Migration in Salt at High Temperatures. Prepared for U.S. Department of Energy, Used Fuel Disposition, FCRD-UFD-2015-000366, LBNL-191216, Lawrence Berkeley National Laboratory.

Rutqvist, J., Wu, Y.S., Tsang, C.F. and Bodvarsson, G. 2002. A Modeling Approach for Analysis of Coupled Multiphase Fluid Flow, Heat Transfer, and Deformation in Fractured Porous Rock. *Int. J. Rock Mech. Min. Sci*. 39: 429-442.

Rutqvist, J., Blanco Martin, L., Kim, J. and Birkholzer, J.T. 2013. Modeling Coupled THMC Processes and Brine Migration in Salt at High Temperatures. Report FCRD-UFD-2013-000262.

Rycroft, C.H. 2009 Voro++: a three-dimensional Voronoi cell library in C++. http://math.lbl.gov/voro++/.

Silva, O., Carrera, J., Dentz, M., Kumar, S., Alcolea, A., Willmann, M. 2009. A general real-time formulation for multi-rate mass transfer Problems, Hydrology and earth system sciences, 13: 1399- 1411.

Sjaardema, G.D. and Krieg, R.D. 1987. A Constitutive Model for the Consolidation of WIPP Crushed Salt and Its Use in Analyses of Backfilled Shaft and Drift Configurations. Report SAND-87-1977: Sandia National Laboratories, Albuquerque, NM (USA).

Terzaghi, K. 1943. Theoretical soil mechanics. John Wiley & Sons, New York, NY, 510 pp.

Trebotich, D., Adams, M.F., Molins, S., Steefel, C.I., and Shen, C. 2014. High-resolution simulation of pore-scale reactive transport processes associated with carbon sequestration. Comput Sci Engin 16(6):22–31

van Genuchten, M.T. 1980. A closed-form equation for predicting the hydraulic conductivity of unsaturated soils. Soil Sci. Soc. Am. J. 44(5), 892-898.

Wang, Y. 2011. Research & Development (R&D). Plan for Used Fuel Disposition Campaign (UFDC). Natural System Evaluation and Tool Development, U.S. DOE Used Fuel Disposition Campaign.

Warren, J.E. and Root, P.J. 1963 The Behavior of Naturally Fractured Reservoirs, Soc. Pet. Eng. J., Transactions, AIME, 228, 245-255, September.

Wolters, R., Lux K-H, Düsterloh U. 2012 Evaluation of Rock Salt Barriers with Respect to Tightness: Influence of Thermomechanical Damage, Fluid Infiltration and Sealing/Healing. In: Proc 7th Int Conf Mech Behav Salt (SaltMech7), Paris, p. 425-34.

Wu, Y.-S. and Pruess, K. 1988. A multiple-porosity method for simulation of naturally fractured petroleum reservoirs, SPE Reservoir Engineering, 3:327-336.

Yagnik, S.K. 1982. Thermal gradient migration of brine-inclusions in salt crystals. PhD Thesis, University of California Berkeley. LBL-14752.

Yagnik, S.K. 1983. Interfacial stability of migrating brine inclusions in alkali halide single crystals supporting a temperature gradient, Journal of Crystal Growth, 62:612-626.

Yuan-Hui, L. and Gregory, S. 1974, Diffusion of ions in sea water and in deep-sea sediments, Geochimica et Cosmochimica Acta, 38(5), 703–714, doi:10.1016/0016-7037(74)90145-8.

Zyvoloski, G.A., Robinson, B.A., Dash, Z.V., Kelkar, S., Viswanathan, H.S., Pawar, R.J., Stauffer, P.H. 2011 Software Users Manual (UM) for the FEHM Application Version 3.1–3.X. Los Alamos National Laboratory, Los Alamos, NM.